Relating the finite-volume spectrum and the two-and-three-particle S-matrix for relativistic systems of identical scalar particles

Raúl A. Briceño,[1,*] Maxwell T. Hansen,[2,†] and Stephen R. Sharpe[3,‡]

[1] *Thomas Jefferson National Accelerator Facility, 12000 Jefferson Avenue, Newport News, VA 23606, USA*
[2] *Institut für Kernphysik and Helmholz Institute Mainz, Johannes Gutenberg-Universität Mainz, 55099 Mainz, Germany*
[3] *Physics Department, University of Washington, Seattle, WA 98195-1560, USA*

(Dated: January 16, 2017)

Working in relativistic quantum field theory, we derive the quantization condition satisfied by coupled two- and three-particle systems of identical scalar particles confined to a cubic spatial volume with periodicity L. This gives the relation between the finite-volume spectrum and the infinite-volume $\mathbf{2} \to \mathbf{2}$, $\mathbf{2} \to \mathbf{3}$ and $\mathbf{3} \to \mathbf{3}$ scattering amplitudes for such theories. The result holds for relativistic systems composed of scalar particles with nonzero mass m, whose center of mass energy lies below the four-particle threshold, and for which the two-particle K-matrix has no singularities below the three-particle threshold. The quantization condition is exact up to corrections of the order $\mathcal{O}(e^{-mL})$ and holds for any choice of total momenta satisfying the boundary conditions.

Keywords: finite volume

I. INTRODUCTION

Over the last few decades, enormous progress has been made in determining the properties of hadrons directly from the fundamental theory of the strong force, quantum chromodynamics (QCD). A key tool in such investigations is lattice QCD (LQCD) in which correlation functions defined on a discretized, finite Euclidean spacetime are calculated numerically using importance-sampling techniques. State-of-the-art LQCD calculations of stable hadronic states use dymanical up, down, strange and even charm quarks, with physical quark masses, and include isospin breaking both from the mass difference of the up and down quarks and also from the effects of quantum electrodynamics (QED). For recent reviews, see Refs. [1–3].

Using LQCD to investigate hadronic resonances that decay via the strong force is significantly more challenging. Resonances do not correspond to eigenstates of the QCD Hamiltonian and thus cannot be studied by directly interpolating a state with the desired quantum numbers. Instead, resonance properties are encoded in scattering and transition amplitudes, and only by extracting these observables can one make systematic, quantitative statements. In fact, it is not *a priori* clear that one can extract such observables using LQCD. Confining the system to a finite volume obscures the meaning of asymptotic states and restricting to Euclidean momenta prevents one from directly applying the standard approach of LSZ reduction. In addition, since one can only access numerically-determined Euclidean correlators with nonvanishing noise, analytic continuation to Minkowski momenta is, in general, not a well-posed problem.

For two-particle states, it is by now well known that scattering amplitudes can be constrained indirectly in LQCD, by first extracting the discrete finite-volume energy spectrum. The approach follows from seminal work by Lüscher [4, 5] who derived a relation between the finite-volume energies and the elastic two-particle scattering amplitude, for a system of identical scalar particles. Since then, this relation has been generalized to accommodate non-zero spatial momentum, $\vec{P}$, in the finite-volume frame and also to describe more complicated two-particle systems, including non-identical and non-degenerate particles as well as particles with intrinsic spin [6–14]. This formalism has been applied in many numerical LQCD calculations to determine the properties of low-lying resonances that decay into a single two-particle channel [15–20], including most recently the first study of the lightest hadronic resonance, the $\sigma/f_0(500)$ [21]. The extension to systems with multiple coupled two-particle channels [7, 10–13], has led to the first LQCD results for resonances at higher energies, where more than one decay channel is open [22–26].

Thus far, however, no LQCD calculations have been performed for resonances that have a significant branching

*e-mail: rbriceno@jlab.org
†e-mail: hansen@kph.uni-mainz.de
‡e-mail: srsharpe@uw.edu

fraction into three or more particles. This is largely because the formalism needed to do so, the three-particle extension of the relations summarized above, is still under construction. Early work in this direction includes the non-relativistic studies presented in Refs. [27] and [28]. More recently, in Refs. [29] and [30], two of the present authors derived a three-particle quantization condition for identical scalar particles using a general relativistic quantum field theory (subject to some restrictions described below). Since these articles are the starting point for the present work, we briefly summarize their methodology.[1]

Reference [29] studied a three-particle finite-volume correlator and determined its pole positions, which correspond to the finite-volume energies, in terms of an infinite-volume scattering quantity. This was done by deriving a skeleton expansion, expressing each finite-volume Feynman diagram in terms of its infinite-volume counterpart plus a finite-volume residue, summing the result into a closed form and then identifying the pole locations. The resulting expression for the finite-volume energies depends on a non-standard infinite-volume scattering quantity—the divergence-free K-matrix, denoted $\mathcal{K}_{\text{df},3}$. A drawback of this result is that $\mathcal{K}_{\text{df},3}$, as well as other quantities in the quantization condition, depends on a smooth cutoff function (denoted H_3 below), although the energies themselves are independent of this cutoff. Thus the relation to the infinite-volume scattering amplitude is not explicit.

The second publication, Ref. [30], resolved this issue by deriving the relation between $\mathcal{K}_{\text{df},3}$ and the standard infinite-volume three-to-three scattering amplitude $\mathcal{M}_3$. We comment that, like the two-to-two scattering amplitude, $\mathcal{M}_2$, the three-particle scattering amplitude must satisfy constraints relating its real and imaginary parts that are dictated by unitarity. These constraints are built into quantum field theory, and can be recovered order-by-order in a diagrammatic expansion. In the two-particle case, both the definition of the S-matrix and the diagrammatic analysis can be used to show that $[\mathcal{M}_2]^{-1} \propto \cot\delta - i$ where the scattering phase shift δ (and the proportionality constant) are real. In the three-particle sector, unitarity takes a much more complicated form but enters through the condition that $\mathcal{K}_{\text{df},3}$ is a real function on three-particle phase space. The relation to $\mathcal{M}_3$ then automatically produces the required unitarity properties, in addition to removing the scheme dependence.

As mentioned above, the results of Refs. [29, 30] were obtained under some restrictions. The finite spatial volume was taken to be cubic (with linear extent L), with periodic boundary conditions on the fields, and the particles were assumed to be spinless and identical (with mass m). The more important restrictions concerned the class of interactions considered. These were assumed to satisfy the following two properties.

1. They have a $\mathbb{Z}_2$ symmetry such that $\mathbf{2} \leftrightarrow \mathbf{3}$ transitions are forbidden, i.e. only even-legged vertices are allowed.

2. They are such that the two-particle K-matrix, appearing due to subprocesses in which two particles scatter while the third spectates, is smooth in the kinematically available energy range.

Given these restrictions, a relation was found between the three-particle finite-volume energies (with any allowed total three-momentum, $\vec{P}$, in the finite-volume frame) and the three-to-three scattering amplitude. This relation is valid up to exponentially suppressed corrections scaling as e^{-mL}, which we assume are negligible also here.

In this work we remove the first of the two major restrictions. We consider theories without a $\mathbb{Z}_2$ symmetry, so that all vertices are allowed in the field theory. We continue to impose the second restriction. This leads to a relativistic, model-independent quantization condition that can be used to extract coupled two- and three-particle scattering amplitudes from LQCD. We otherwise use the set-up of the previous studies. In particular we assume a theory of identical scalar particles in a periodic, cubic box. Given past experience in the two-particle sector, we expect that these technical restrictions will be straightforward to remove. We also expect that the generalization to multiple two- and three-body channels will be straightforward. We defer consideration of these cases until a later publication.

The generalization that we derive here is a necessary step towards using LQCD to study resonances that decay into both two- and three-particle states. A prominent example is the Roper resonance, $N(1440)$, the lowest lying excitation of the nucleon. This state is counterintuitive from the perspective of quark models, as it lies below the first negative parity excited state. The Roper resonance is estimated to decay to $N\pi$ with a branching fraction of $55-75\%$ and otherwise to $N\pi\pi$, with other open channels highly suppressed. Similarly, nearly all of the recently discovered XYZ states have significant branching fractions into both two- and three-particle final states (see Refs. [33, 34] for recent reviews). These states exhibit the rich phenomenology of non-perturbative QCD and it is thus highly desirable to have theoretical methods to extract their properties directly from the underlying theory.

This article derives two main results: the relation between the discrete finite-volume spectrum and the generalized divergence-free K-matrix, given in Eq. (79), and the relation between the K-matrix and the coupled two- and three-particle scattering amplitudes, given compactly in Eq. (85) and more explicitly throughout Sec. III. These results

[1] We also note that additional checks of the quantization condition have been given in Refs. [31, 32].

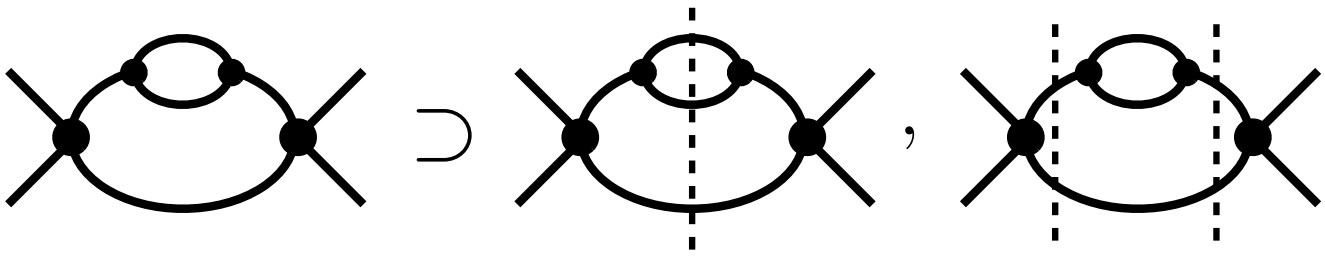

FIG. 1: An example of a Feynman diagram contributing to the finite-volume correlator. Above the three-particle threshold, this diagram has cuts due to both two- and three-particle states, as shown on the right-hand side. The three-particle cut runs through a self-energy bubble, meaning that such diagrams must be explicitly displayed (rather than subsumed into a dressed propagator) in order to properly identify all finite-volume effects.

generalize those of Refs. [29] and [30], respectively. The first, Eq. (79), has a form reminiscent of the coupled two-particle result [7, 10–13]. The finite-volume effects are contained in a diagonal two-by-two matrix with entries F_2 in the two-particle sector and F_3 in the three-particle sector. Aside from minor technical changes, these are the same finite-volume quantities that arise in the previously derived two- and three-particle quantization conditions [4, 5, 8, 12–14, 29, 30]. The coupling between channels is captured by the generalized divergence-free K-matrix. This contains diagonal elements, mediating two-to-two and three-to-three transitions, as well as off-diagonal elements that encode the two-to-three transitions.

To obtain both results from a single calculation, we use a matrix of finite-volume correlators, $\mathcal{M}_L$, chosen so that it goes over to the corresponding matrix of infinite-volume scattering amplitudes when the $L \to \infty$ limit is taken appropriately. This differs from the type of correlator used in Ref. [29], but is the direct generalization of that considered in Ref. [30].

The results of this work, like those given in Refs. [4, 5, 8, 12–14, 29, 30], are derived by analyzing an infinite-set of finite-volume Feynman diagrams and identifying the power-law finite-volume effects. The central complication new to the present derivation comes from diagrams such as that of Fig. 1, in which a two-to-three transition is mediated by a one-to-two transition together with a spectator particle. The cuts on the right-hand side of the figure indicate that this diagram gives rise to finite-volume effects from both two- and three-particle states. As we describe in detail below, a consequence of such diagrams is that we cannot use standard fully-dressed propagators in two-particle loops, but instead need to introduce modified propagators built from two-particle-irreducible (2PI) self-energy diagrams. In addition, we must keep track of the fact that the two- and three-particle states in these diagrams share a common coordinate. This makes it more challenging to separate the finite-volume effects arising from the two- and three-particle states in diagrams such as that of Fig. 1.

To address this complication, and other technical issues that arise, we use here an approach for studying the finite-volume correlator that differs from the skeleton-expansion-based methods of Refs. [4, 5, 8, 12–14, 29, 30]. In particular, we construct an expansion using a mix of fully-dressed and modified two- and three-particle irreducible propagators, which are connected via the local interactions of the general QFT. We then identify all power-law finite-volume effects using time-ordered perturbation theory (TOPT). We also introduce smooth cutoff functions, H_2 and H_3, that only have support in the vicinity of the two- and three-particle poles respectively. A key simplification of this construction is that, in disconnected two-to-three transitions such as that shown in Fig. 1, the two- and three-particle poles do not contribute simultaneously. This is an extension of the result that an on-shell one-to-two transition is kinematically forbidden for stable particles.

After eliminating such disconnected two-to-three transitions we are left with a series of terms built from two- and three-particle poles, summed over the spatial momenta allowed in the periodic box, and with all two-to-three transitions mediated by smooth functions. To further reduce these expressions, we apply the results of Refs. [4, 5, 8, 29, 30], to express the sums over poles as products of infinite-volume quantities and finite-volume functions. The modifications that we make to accommodate two-to-three transitions affect the exact forms of these poles, so that some effort is required to extend the previous results to rigorously apply here. With these modified relations we are able to derive a closed form for the finite-volume correlator and to express its pole positions in terms of a quantization condition.

The remainder of this work is organized as follows: In the following section we derive the quantization condition relating the discrete finite-volume spectrum to the generalized divergence-free K-matrix. After giving the precise definition of the finite-volume correlator, $\mathcal{M}_L$, and introducing various kinematic variables, we divide the bulk of the derivation into four subsections. In Sec. II A we apply standard time-ordered perturbation theory to identify all of

the two- and three-particle states that lead to important finite-volume effects. However, due to technical issues, the form reached via the standard approach is not useful for the subsequent derivation. Thus, in Sec. II B, we provide an alternative procedure that displays the same finite-volume effects in a more useful form. This improved derivation is highly involved and we relegate the technical details to Appendix B. With the two- and three-particle poles explicitly displayed, in Sec. II C we complete the decomposition of finite- and infinite-volume quantities by extending and applying various relations derived in Refs. [4, 5, 8, 29, 30]. Again, many technical details are collected in Appendix C. Finally, in Sec. II D, we identify the poles in $\mathcal{M}_L$ and thereby reach our quantization condition.

To complete the derivation, in Sec. III we relate the generalized divergence-free K-matrix to the standard infinite-volume scattering amplitude. Our derivation here closely follows the approach of Ref. [30] but is complicated by the mixing of two- and three-body states. After deriving an expression for $\mathcal{M}_L$ in terms of the K-matrix in Sec. III A, we then invert the relation in Sec. III B. Given a parametrization of the scattering amplitude, this allows one to determine the K-matrix and thus predict the finite-volume spectrum in terms of a given parameter set. Having given the general relation between finite-volume energies and coupled two- and three-particle scattering amplitudes, in Sec. IV we study various limiting cases that simplify the general results. We conclude and give an outlook in Sec. V.

We include four appendices. In addition to the two mentioned above, Appendix A describes a specific example of the smooth cutoff functions, H_2 and H_3, that are used to simplify the results in various ways, in particular by removing disconnected two-to-three transitions, while Appendix D derives properties of the divergence-free K-matrix that follow from the parity and time-reversal invariance of the theory.

II. DERIVATION OF THE QUANTIZATION CONDITION

In this section we derive the main result of this work, a relation between the discrete finite-volume energy spectrum of a relativistic quantum field theory and that theory's physically-observable, infinite-volume scattering amplitudes in the coupled two- and three-particle subspace. We restrict attention to theories with identical massive scalar particles, whose physical mass is denoted m. As we explain in more detail below, we must also assume that the two-particle K-matrices, appearing due to two-particle subprocesses in the three-to-three scattering amplitude, are only sampled at energies where they have no poles.

The main result of this work, given in Eq. (79) below, is a quantization condition of the form

$$\Delta^{[\mathcal{M}]}(E, \vec{P}, L) = 0\,. \tag{1}$$

Here $\vec{P}$ is the total three-momentum of the system, and L is the linear extent of the periodic, cubic spatial volume. The superscript $\mathcal{M}$ indicates that the quantization condition depends on the infinite-volume scattering amplitudes of the theory. For fixed values of $\vec{P}$ and L, solutions to Eq. (1) occur at a discrete set of energies $E = E_1, E_2, E_3, \cdots$. These give the finite-volume energy levels of the system, up to exponentially suppressed corrections of the form e^{-mL} that we neglect throughout.

We begin our derivation by introducing various kinematic variables. Since in general we work in a "moving frame", with total energy-momentum $(E, \vec{P})$, the energy in the center-of-mass (CM) frame is

$$E^* = \sqrt{E^2 - \vec{P}^2}\,. \tag{2}$$

If the energy-momentum is shared between two particles, we denote the momentum of one by $\vec{p}$, and that of the other by $\vec{b}_p = \vec{P} - \vec{p}$. We add primes to these quantities if there are multiple two-particle states. If the particles are on shell, we denote their energies as ω_p and ω_{Pp}, respectively, with

$$\omega_p = \sqrt{\vec{p}^2 + m^2} \quad \text{and} \quad \omega_{Pp} = \sqrt{(\vec{P} - \vec{p})^2 + m^2} = \sqrt{\vec{b}_p^{\,2} + m^2}\,. \tag{3}$$

If both particles are on shell, then when we boost to the CM frame, their energy-momentum four-vectors become $(\omega_p^*, \vec{p}^*)$ and $(\omega_p^*, -\vec{p}^*)$, respectively, with $\omega_p^* = E^*/2$ and $p^* \equiv |\vec{p}^*| = q^*$, where

$$q^* = \sqrt{E^{*2}/4 - m^2}\,. \tag{4}$$

Thus the only remaining degree of freedom, with $(E, \vec{P})$ fixed, is the direction of CM frame momentum $\hat{p}^*$. Throughout this work we use $\hat{p}^*$ to parametrize an on-shell two-particle state.

A similar description applies when three particles share the total energy-momentum. The generic names we use for their momenta are $\vec{k}$, $\vec{a}$ and $\vec{b}_{ka} = \vec{P} - \vec{k} - \vec{a}$. If these particles are on shell, their energies are denoted ω_k, ω_a and

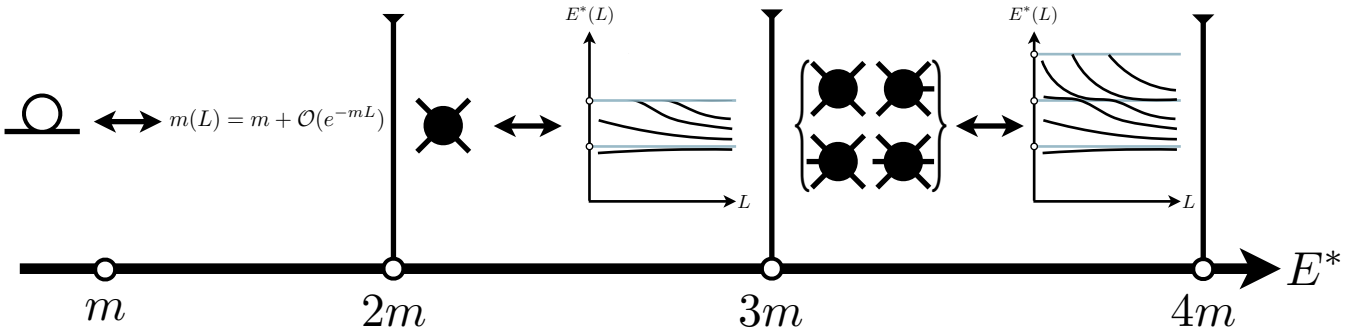

FIG. 2: Summary of the range of center-of-mass frame energy, E^*, accommodated, and the scattering channels open in the various regions.

ω_{Pka}, respectively, with

$$\omega_{Pka} = \sqrt{(\vec{P} - \vec{k} - \vec{a})^2 + m^2} = \sqrt{\vec{b}_{ka}^{\,2} + m^2}\,. \tag{5}$$

We will often consider the situation in which one of the particles, say that with momentum $\vec{k}$, is on shell (and is referred to as the "spectator"), while the other two may or may not be on shell (and are called the "nonspectator pair"). In this situation, if we boost to the CM frame of the nonspectator pair, the energy of this pair in this frame is denoted $E^*_{2,k}$, and is given by

$$E^*_{2,k} = \sqrt{(E - \omega_k) - (\vec{P} - \vec{k})^2}\,. \tag{6}$$

If we further assume that all three particles are on shell, then the four-momenta of the nonspectator pair boost to their CM frame as $(\omega_a, \vec{a}) \to (\omega^*_a, \vec{a}^*)$, $(\omega_{Pka}, \vec{b}_{ka}) \to (\omega^*_a, -\vec{a}^*)$, where $\omega_{a^*} = E^*_{2,k}/2$ and $a^* \equiv |\vec{a}^*| = q^*_k$, with

$$q^*_k = \sqrt{E^{*2}_{2,k}/4 - m^2}\,. \tag{7}$$

Thus the degrees of freedom for three on-shell particles with total energy-momentum $(E, \vec{P})$ fixed can be parametrized by the ordered pair $\vec{k}, \hat{a}^*$—i.e. a spectator momentum and the direction of the nonspectator pair in their CM frame.

The quantization condition derived in this work is valid for CM energies in the range[2]

$$m < E^* < \min[4m, m + M_p]\,. \tag{8}$$

Here M_p is the energy of the lowest lying pole in the two-particle K-matrix (in the two-particle CM frame). In practice we expect the region of practical utility to run from just below the two-particle threshold at $E^* = 2m$, where there may be bound states, up to energies below the quoted upper limit. We caution that at energies below but near the upper limit, i.e. at $E^* = \min[4m, m + M_p] - \kappa^2/m$ with $\kappa \ll m$, neglected corrections of the form $e^{-c\kappa L}$ [with c a constant of $\mathcal{O}(1)$] can become important. This indicates the transition into the new kinematic region where four-particle states (or K-matrix poles) must be included.

To explain the kinematic range quoted in Eq. (8), we work though the different regimes in E^*. The following discussion is summarized schematically in Fig. 2. In the range $m < E^* < 3m$, the infinite-volume system is described

[2] Strictly speaking, the quantization condition is valid also for $E^* < m$, but we do not expect this to be of practical interest as there are, in general, no finite-volume states in this region. The quantization condition will have a solution for $E^* = m + \mathcal{O}(e^{-mL})$, corresponding to a single-particle pole, but the exponentially suppressed finite-volume corrections in the position of this pole will be incorrect. This is because we do not systematically control such corrections. This is in contrast to finite-volume corrections to the mass of a two-particle bound state, which are proportional to $e^{-\kappa L}$, with κ the binding momentum. These are correctly reproduced by the quantization condition.

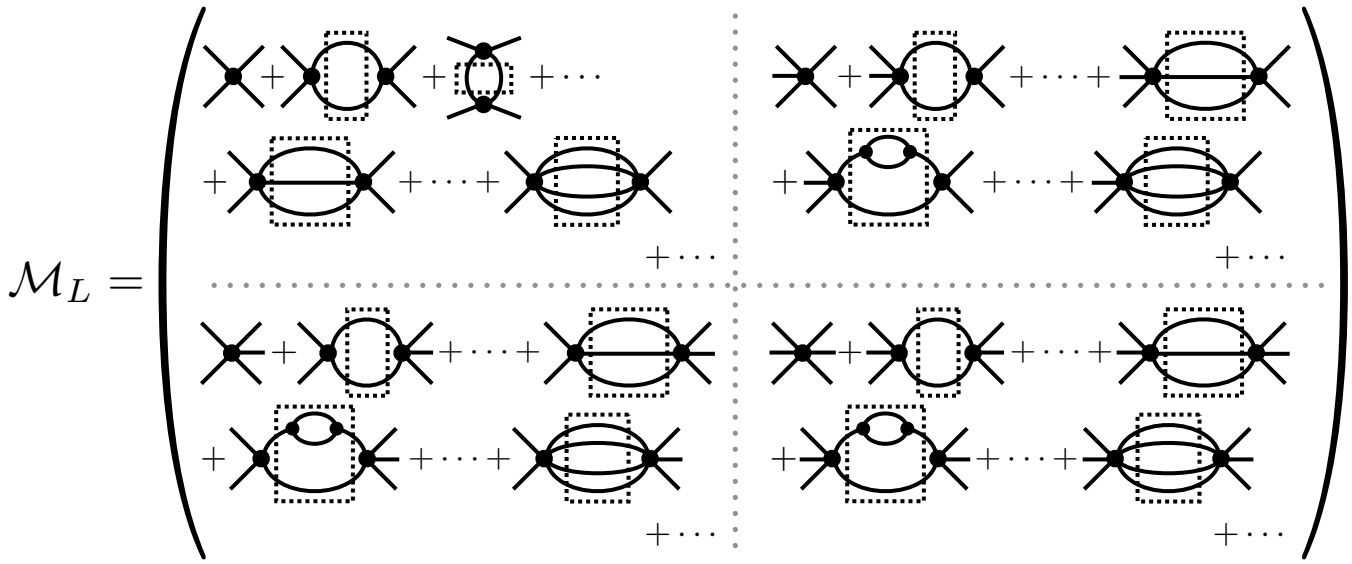

FIG. 3: Examples of diagrams contributing to $\mathcal{M}_L$. External lines are amputated and evaluated on shell. Dashed boxes indicate that spatial loop momenta are summed over the finite-volume set.

solely by the two-to-two scattering amplitude, and in finite volume this amplitude is sufficient to determine the spectral energies. This is done with the quantization condition of Lüscher [4, 5], and its generalizations.

The major new result of the present work is to provide the quantization condition for $3m < E^* < 4m$. (For ease of discussion we assume first that the two-particle K-matrix is smooth for the energies considered.) In this region, both two- and three-particle states can go on-shell, and the dynamics of the infinite-volume system are governed by the coupled two- and three-particle scattering amplitudes. Thus, one would expect that these same amplitudes determine the finite-volume spectrum. In this work we demonstrate that this is in fact the case and give the detailed form of the resulting quantization condition. Above $4m$, four-particle states become important. We do not include the effects of these and are thus limited by the four-particle production threshold. In fact, depending on the dynamics of the system, contributions from four-particle states might become important below threshold, as already discussed above.

Finally, we note that within the three-to-three scattering amplitude, two-to-two scattering can occur as a subprocess with the third particle spectating. If the spectator is at rest in the three-particle CM frame, then the two-to-two amplitude is sampled at the highest possible two-particle CM frame energy, $E^* - m$. However, in our derivation of the quantization condition, we assume that the two-particle K-matrix is a smooth function of the two-particle energies sampled. Thus, if the K-matrix *does* have a pole at some two-particle CM energy M_p, then our result only holds when $E^* - m < M_p \Longrightarrow E^* < m + M_p$. This explains the additional restriction in Eq. (8). Since there are expected to be large finite-volume effects in the vicinity of $E^* \sim m + M_p$ that have not been taken into account in the present formalism, in practice one should restrict attention to energies below this kinematic point.

We now introduce the key object used in our derivation of the quantization condition, a matrix of finite-volume correlators denoted $\mathcal{M}_L$:

$$\mathcal{M}_L \equiv \begin{pmatrix} \mathcal{M}_{L,22} & \mathcal{M}_{L,23} \\ \mathcal{M}_{L,32} & \mathcal{M}_{L,33} \end{pmatrix} . \tag{9}$$

$\mathcal{M}_{L,ij}$ is defined to be the sum of all amputated, on-shell, connected diagrams with j incoming and i outgoing legs, evaluated in finite volume. This is illustrated in Fig. 3. The restriction to finite volume implies that all spatial loop momenta are summed, rather than integrated, with the sum running over $\vec{q} = 2\pi\vec{n}/L$, where $\vec{n}$ is a vector of integers.[3] The entries in $\mathcal{M}_L$ depend on the coordinates introduced above that parametrize either two or three on-shell particles.

[3] We sometimes refer to the set of all such momenta as the "finite-volume set".

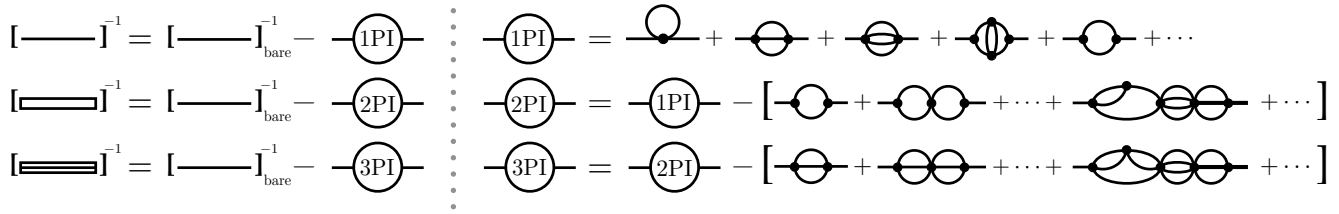

FIG. 4: Summary of the three types of propagators used in our construction of Feynman diagrams: fully-dressed (or 1PI-dressed), 2PI-dressed and 3PI-dressed.

In particular

$$\mathcal{M}_{L,22} \equiv \mathcal{M}_{L,22}(\hat{p}'^*; \hat{p}^*)\,, \tag{10}$$

$$\mathcal{M}_{L,23} \equiv \mathcal{M}_{L,23}(\hat{p}'^*; \vec{k}, \hat{a}^*)\,, \tag{11}$$

$$\mathcal{M}_{L,32} \equiv \mathcal{M}_{L,32}(\vec{k}', \hat{a}'^*; \hat{p}^*)\,, \tag{12}$$

$$\mathcal{M}_{L,33} \equiv \mathcal{M}_{L,33}(\vec{k}', \hat{a}'^*; \vec{k}, \hat{a}^*)\,. \tag{13}$$

These are extensions of the quantities $\mathcal{M}_{2,L}$ and $\mathcal{M}_{3,L}$ introduced in Ref. [30]. Indeed, the latter correspond, respectively, to $\mathcal{M}_{L,22}$ and $\mathcal{M}_{L,33}$ in a theory having a $\mathbb{Z}_2$ symmetry (in which case $\mathcal{M}_{L,23} = \mathcal{M}_{L,32} = 0$).

It is clear from their definition that the $\mathcal{M}_{L,ij}$ are finite-volume versions of the infinite-volume scattering amplitudes. Indeed, as discussed in Sec. III, if the limit $L \to \infty$ is taken in an appropriate way, $\mathcal{M}_L$ goes over to the infinite-volume scattering matrix. Because of this, we loosely refer to the entries of $\mathcal{M}_L$ as "finite-volume scattering amplitudes", recognizing that this is an imprecise description since there are no asymptotic states for finite L.

As defined, the external momenta of $\mathcal{M}_L$ (including $\vec{P}$) must lie in the finite-volume set. In this case $\mathcal{M}_L$ is a bona fide finite-volume correlation function whose poles occur at the energies of the finite-volume spectrum, a property that is crucial for our derivation of the quantization condition. In order to relate $\mathcal{M}_L$ to its infinite-volume counterpart, however, we will need to extend its definition so as to allow arbitrary external momenta. As discussed in Ref. [30], this extension is straightforward using the diagrammatic definition. In every loop, the external momentum is routed such that only one loop momentum lies outside the finite-volume set. A consistent choice of which momenta lie outside this set can be made.

In many of the previous studies concerned with deriving such quantization conditions (see for example Refs. [8, 13, 29]) it is standard to first construct a skeleton expansion that expresses the finite-volume correlator as a series of diagrams built from Bethe-Salpeter kernels connected by fully dressed propagators. The utility of this approach is that it explicitly displays the loops of particles that can go on shell, and it turns out that only these long-distance loops lead to the power-law finite-volume effects that we are after. It also leads to a final expression where all quantities can be defined in terms of relativistically covariant amplitudes constructed from Feynman diagrams.

In the present case, however, we find it simpler to follow a somewhat different approach, based more extensively on time-ordered perturbation theory (TOPT). This avoids the necessity of introducing a large number of different Bethe-Salpeter kernels. Instead of using a skeleton expansion, we start from an all-orders diagrammatic expansion for $\mathcal{M}_L$ in terms of an arbitrary collection of contact interactions, including all possible derivative structures. At this stage, the only place where we group diagrams together into composite building blocks is in the propagators. Here we take all propagators to be fully dressed with two classes of exceptions. The first applies to propagators appearing in a two-particle loop carrying the total energy-momentum $(E, \vec{P})$. Then, instead of standard fully-dressed propagators defined via the one-particle irreducible (1PI) self-energy diagrams, we use a modified propagator defined via the *two*-particle irreducible (2PI) self energy (see Fig. 4). This is necessary because if one of the particles in the two-particle loop splits into two, then this leads to a three-particle state that carries the total energy and momentum and can thus go on shell. We refer to such propagators as "2PI-dressed". The second exception occurs for diagrams in which a single propagator carries the total energy-momentum. Such a propagator must be built from self energies that are *three*-particle irreducible (3PI) (see Fig. 4). This is done so that all two- and three-particle intermediate states are kept explicit, and we call the resulting propagator "3PI-dressed". The possibility of self-energy diagrams leading to on-shell three-particle states is, in fact, one of the central complications of this work.

A second non-standard aspect of our construction, closely related to the use of 2PI and 3PI propagators, is our use of a "diagram-by-diagram" renormalization procedure. All diagrams are regulated in the ultraviolet (UV) using a regulator that we do not need to explicitly specify. Counterterms are then broken into an infinite series of terms

designed to cancel the UV divergences of each individual diagram, as well as certain finite pieces. We then define each diagram to be implicitly accompanied by its counterterm so that the divergence is canceled immediately. In fact, this construction is only crucial for self-energy diagrams. Let D_i^R denote the renormalized ith self-energy diagram in some labeling scheme $i = 1, 2, \cdots$. We then require that the counterterms are chosen such that

$$D_i^R(m^2) = 0\,, \qquad \frac{d}{dp^2} D_i^R(p^2)\bigg|_{p^2=m^2} = 0\,, \tag{14}$$

implying that each self-energy diagram scales as $(p^2 - m^2)^2$ near the pole. This ensures that the 1PI, 2PI, 3PI and bare propagators all coincide at the one-particle pole. This choice is not strictly necessary, since our final result is renormalization scheme independent, but it greatly simplifies the analysis.

A. Identification of two-and three-particle poles: naive approach

In this section we use TOPT to give an expression for $\mathcal{M}_L$ in which all the two- and three-particle poles are explicit. However, the resulting expression turns out to be difficult to use to determine the volume dependence, due to technical issues related to self-energy insertions. This is why we call the approach taken here naive. The technical issues are resolved in the following section, and its accompanying appendix, but we think that it is useful pedagogically to separate the basic structure of the derivation, along with the needed notation, from the technicalities.

We give a brief recap of the essential features of TOPT in Appendix B 5. In essence, one evaluates all energy integrals in a Feynman diagram, arriving at sum of terms, each of which depends only on spatial momenta. This works equally well in finite volume, since we are taking the time direction to be infinite and so energy remains continuous. Each term corresponds to a particular time-ordering of vertices, between which are intermediate states, each coming with an energy denominator. An example of such a time-ordered diagram is shown in Fig. 5. In an abuse of notation we refer to the intermediate states as "n-cuts" if they contain n particles.

In an amputated diagram, the factor associated with an n-cut is proportional to

$$\mathcal{C}_n \propto \frac{1}{n!} \left(\prod_{i=1}^{n} \frac{1}{2\omega_i} \right) \frac{1}{E - \sum_{i=1}^{n} \omega_i}\,, \tag{15}$$

where ω_i is the on-shell energy of the i'th particle in the cut. The $1/n!$ is the symmetry factor for identical particles, and the factors of $1/(2\omega_i)$ result from on-shell propagators. The key point is that, other than the factors appearing in Eq. (15) associated with the intermediate states, all contributions to a TOPT diagram are smooth, nonsingular functions of the momenta. Thus, for the kinematic range we consider [given in Eq. (8)] the only singularities in the diagrams arise from two- and three-cuts, and have the respective forms

$$\frac{1}{E - \omega_p - \omega_{Pp}} \quad \text{and} \quad \frac{1}{E - \omega_k - \omega_a - \omega_{Pka}}\,. \tag{16}$$

Our aim here is to obtain an expression for $\mathcal{M}_L$ in which all such factors are explicit.

If a summed momentum does not enter one of these two pole structures at least once, then we infer that for this coordinate the summand is a smooth function of characteristic width m. For such a smooth function $s(\vec{k})$, the difference between the sum and corresponding integral is exponentially suppressed:

$$\left[\frac{1}{L^3} \sum_{\vec{k}} - \int_{\vec{k}} \right] s(\vec{k}) = \mathcal{O}(e^{-mL})\,, \tag{17}$$

Here the sum runs over the finite-volume set and $\int_{\vec{k}} = \int d^3k/(2\pi)^3$. It follows that we may replace sums with integrals in all coordinates that do not enter two- and three-particle poles. This applies for loops with all n-cuts having $n \geq 4$, and so we are left with the finite-volume dependence arising only from loops involving two- and three-cuts. This procedure is illustrated in Fig. 5.

Following this procedure and organizing all terms leads to the following result

$$\mathcal{M}_L = A \sum_{j=0}^{\infty} [\mathcal{C}A]^j - \widetilde{I} = A(1 - \mathcal{C}A)^{-1} - \widetilde{I}\,. \tag{18}$$

Each of the quantities on the right-hand side is a 2×2 matrix, like $\mathcal{M}_L$. The notation is highly compact, and is explained in detail below. The basic content of the equation is, however, simple to state: $\mathcal{M}_L$ can be written as a

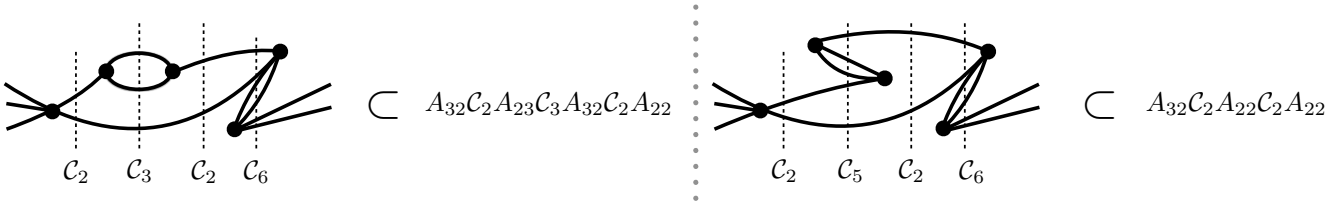

FIG. 5: Examples of TOPT diagrams contributing to $\mathcal{M}_{L,32}$. The vertical dashed lines indicate intermediate states, which come with the n-cut factor $\mathcal{C}_n$. For the sake of clarity, we have not distinguished between the different types of propagators, an issue that is discussed at length in the text. We also do not show the diagrams containing counterterms that are associated with these diagrams. These two diagrams are both time-orderings of the same underlying Feynman diagram, and yet contribute to different parts of the result (18), as indicated by the expressions right of the figures.

sum of terms built from alternating insertions of smooth functions, collected into the matrix A, and two- and three-particle poles, collected into the matrix $\mathcal{C}$. A contains all time-orderings lying between adjacent two- or three-cuts, and includes n-cuts with $n \geq 4$. The same matrix A always appears between any pair of factors of $\mathcal{C}$ or external states, because the same set of time-orderings always appears. The elements of A are the analog of the Bethe-Salpeter kernels in the standard skeleton expansion approach.

The last term in Eq. (18) is the subtraction, $\widetilde{I}$. This arises because of the presence of disconnected terms in A. That such terms are present is easily seen from Fig. 5. In the left-hand diagram, the contribution to A_{23} is disconnected, since it involves a particle that runs between the $\mathcal{C}_2$ and $\mathcal{C}_3$ without interacting. Similarly the right-most A_{32} obtains a disconnected contribution. The other two contributions (to the left-most A_{32} and to A_{22}) are connected. In the right-hand figure the contribution to A_{22} is disconnected. Disconnected contributions are characterized by containing one or two Kronecker-deltas setting initial and final momenta equal, each multiplied by factors of $2\omega L^3$. When such disconnected contributions are combined in $A + A\,\mathcal{C}A + \cdots$, some of the resulting TOPT diagrams are themselves disconnected. This is most obvious for the leading term, i.e. A itself. Since $\mathcal{M}_L$ is, by definition, fully connected, such terms must be removed by hand, and $\widetilde{I}$ is simply defined to be the sum of all disconnected contributions in $A[1 - \mathcal{C}A]^{-1}$.

It will turn out that we do not need a more detailed expression for $\widetilde{I}$. What will be important, however, is that $\widetilde{I}$ only has diagonal entries,

$$\widetilde{I} \equiv \begin{pmatrix} \widetilde{I}_{22} & 0 \\ 0 & \widetilde{I}_{33} \end{pmatrix} . \tag{19}$$

This is because off-diagonal disconnected pieces in $\mathcal{M}_L$ necessarily involve a $1 \to 2$ or $2 \to 1$ transition in which all external legs are on shell, and this is not kinematically possible for stable particles. We stress, however, that A itself does contain off-diagonal disconnected contributions, because its external legs are in general not on shell.

An important property of A is that all loops contained within it are integrated, rather than summed. For the connected component of A, this implies that it is an infinite-volume object (albeit not Lorentz invariant). This holds also for the disconnected part, up to the volume dependence in the explicit factors of L^3 and Kronecker-deltas mentioned above.

We now give precise definitions of the quantities entering Eq. (18), beginning with $\mathcal{C}$. Like all quantities in Eq. (18), $\mathcal{C}$ is a two-by-two matrix on the space of two- and three-particle scattering channels. In contrast to $\mathcal{M}_L$ and A, $\mathcal{C}$ (and also I, as we have explained above) is diagonal

$$\mathcal{C} \equiv \begin{pmatrix} \mathcal{C}_{2;p';p} & 0 \\ 0 & \mathcal{C}_{3;k'a';ka} \end{pmatrix} . \tag{20}$$

The diagonal entries are matrices defined on the space of off-shell finite-volume momenta. For example $\mathcal{C}_2$ has two indices of the form $\vec{p} \in (2\pi/L)\mathbb{Z}^3$. We abbreviate this with the subscript $p';p$ as shown. The definition is

$$\mathcal{C}_{2;p';p} \equiv -\delta_{p'p} \frac{1}{2} \frac{1}{L^3} \frac{1}{2\omega_{Pp} 2\omega_p (E - \omega_p - \omega_{Pp})} , \tag{21}$$

which we recognize as containing the energy denominator of Eq. (15), as well as other factors. These additional factors are (i) $\delta_{p'p}$, which equals 1 for $\vec{p}\,' = \vec{p}$, and 0 otherwise, and is present because the cut does not change loop momenta; (ii) $1/L^3$, which is always associated with a loop sum; (iii) a symmetry factor of $1/2$ because the two intermediate

particles are identical; and (iv) the overall minus sign, which arises from keeping track of powers of i in the Feynman propagators and vertices before decomposing into TOPT diagrams. Similarly, the three-cut factor is

$$\mathcal{C}_{3;k'a';ka} \equiv -\delta_{k'k}\delta_{a'a}\frac{1}{6}\frac{1}{L^6}\frac{1}{2\omega_a 2\omega_k 2\omega_{Pka}(E-\omega_a-\omega_k-\omega_{Pka})}\,, \tag{22}$$

where the indices include two finite-volume momenta,[4] with ka standing for $\{\vec{k},\vec{a}\}$.

The definition of the matrix A depends on it location in the product. If it appears between two factors of $\mathcal{C}$, A is defined as a matrix on the same space as $\mathcal{C}$:

$$A = \begin{pmatrix} A_{22;p';p} & A_{23;p';ka} \\ A_{32;k'a';p} & A_{33;k'a';ka} \end{pmatrix} \qquad \text{(between two factors of } \mathcal{C})\,. \tag{23}$$

If the A lies at the left-hand end of the chains in Eq. (18), so that it only abuts a $\mathcal{C}$ on the right, then it has finite-volume indices on the right but on-shell momenta on the left:

$$A = A(\hat{p}'^*;\vec{k}',\hat{a}'^*) \equiv \begin{pmatrix} A_{22;p}(\hat{p}'^*) & A_{23;ka}(\hat{p}'^*) \\ A_{32;p}(\vec{k}',\hat{a}'^*) & A_{33;ka}(\vec{k}',\hat{a}'^*) \end{pmatrix} \qquad (\mathcal{C} \text{ only on the right})\,. \tag{24}$$

This is mirrored if $\mathcal{C}$ only appears to the left

$$A = A(\hat{p}^*,\vec{k},\hat{a}^*) \equiv \begin{pmatrix} A_{22;p'}(\hat{p}^*) & A_{23;p'}(\vec{k},\hat{a}^*) \\ A_{32;k'a'}(\hat{p}^*) & A_{33;k'a'}(\vec{k},\hat{a}^*) \end{pmatrix} \qquad (\mathcal{C} \text{ only on the left})\,. \tag{25}$$

Finally, the $j=0$ term in Eq. (18) contains no factors of $\mathcal{C}$ and is evaluated only with on-shell momenta

$$A = \begin{pmatrix} A_{22}(\hat{p}'^*;\hat{p}^*) & A_{23}(\hat{p}'^*;\vec{k},\hat{a}^*) \\ A_{32}(\vec{k}',\hat{a}'^*;\hat{p}^*) & A_{33}(\vec{k}',\hat{a}'^*;\vec{k},\hat{a}^*) \end{pmatrix} \qquad (\mathcal{C}-\text{independent term})\,. \tag{26}$$

The various definitions of A are all closely related and can all be determined from a "master function",

$$A(\vec{p}',\vec{k}',\vec{a}';\vec{p},\vec{k},\vec{a}) = \begin{pmatrix} A_{22}(\vec{p}';\vec{p}) & A_{23}(\vec{p}';\vec{k},\vec{a}) \\ A_{32}(\vec{k}',\vec{a}';\vec{p}) & A_{33}(\vec{k}',\hat{a}';\vec{k},\vec{a}) \end{pmatrix}\,, \tag{27}$$

by applying various coordinate-space restrictions. The master function depends on unrestricted momenta. It is obtained from the fully off-shell matrix form of A, Eq. (23), by continuing the momenta away from finite-volume values. As discussed earlier, this continuation impacts the integrands inside A in a well-defined and smooth way. For a two-particle state only one momentum, $\vec{p}$, is specified. We then define two restrictions of this coordinate. To restrict to on-shell momenta we require that $\vec{p}$ is such that $E=\omega_p+\omega_{Pp}$. This leaves only a directional degree of freedom, denoted $\hat{p}^*$. Alternatively, to restrict to finite-volume momenta we require $\vec{p}\in(2\pi/L)\mathbb{Z}^3$, and represent the momentum as an index, p. For a three-particle state we begin with two momenta $\vec{k}$, $\vec{a}$. The restriction to on-shell states is effected by requiring $E=\omega_k+\omega_a+\omega_{ka}$, leading to the degrees of freedom $\vec{k},\hat{a}^*$. The restriction to finite-volume momenta, $\vec{k},\vec{a}\in(2\pi/L)\mathbb{Z}^3$, is denoted with the index pair ka.

This notation allows one to easily construct various finite-volume sums. To give a concrete example we write out the term from Eq. (18) that is linear in $\mathcal{C}$:

$$A(\hat{p}''^*,\vec{k}'',\hat{a}''^*)\mathcal{C}A(\hat{p}^*,\vec{k},\hat{a}^*) = \sum_{p'}[A_{22;p'}(\hat{p}''^*)+A_{32;p'}(\vec{k}'',\hat{a}''^*)]\mathcal{C}_{2;p';p'}[A_{22;p'}(\hat{p}^*)+A_{23;p'}(\vec{k},\hat{a}^*)] \tag{28}$$

$$+\sum_{k',a'}[A_{23;k'a'}(\hat{p}''^*)+A_{33;k'a'}(\vec{k}'',\hat{a}''^*)]\mathcal{C}_{3,k'a';k'a'}[A_{32;k'a'}(\hat{p}^*)+A_{33;k'a'}(\vec{k},\hat{a}^*)]\,, \tag{29}$$

$$=-\frac{1}{2}\frac{1}{L^3}\sum_{\vec{p}'}\frac{[A_{22}(\hat{p}''^*;\vec{p}')+A_{32}(\vec{k}'',\hat{a}''^*;\vec{p}')][A_{22}(\vec{p}';\hat{p}^*)+A_{23}(\vec{p}';\vec{k},\hat{a}^*)]}{2\omega_{Pp'}2\omega_{p'}(E-\omega_{p'}-\omega_{Pp'})} \tag{30}$$

$$-\frac{1}{6}\frac{1}{L^6}\sum_{\vec{k}',\vec{a}'}\frac{[A_{23}(\hat{p}''^*;\vec{k}',\vec{a}')+A_{33}(\vec{k}'',\hat{a}''^*;\vec{k}',\vec{a}')][A_{32}(\vec{k}',\vec{a}';\hat{p}^*)+A_{33}(\vec{k}',\vec{a}';\vec{k},\hat{a}^*)]}{2\omega_{Pk'a'}2\omega_{k'}2\omega_{a'}(E-\omega_{k'}-\omega_{a'}-\omega_{Pk'a'})}\,. \tag{31}$$

---

[4] Here we are choosing $\vec{k}$ and $\vec{a}$ to lie in the finite-volume set, so that, if the external momenta do not lie in this set, the remaining momentum $\vec{b}_{ka}$ also lies outside the set. The apparent asymmetry in this choice is removed by the fact that the entries of A are symmetric under particle exchange.

The simplest contribution is the product of two A_{22} factors

$$A\mathcal{C}A \supset -\frac{1}{2}\frac{1}{L^3}\sum_{\vec{p}'}\frac{A_{22}(\hat{p}''^*;\vec{p}')A_{22}(\vec{p}';\hat{p}^*)}{2\omega_{Pp'}2\omega_{p'}(E-\omega_{p'}-\omega_{Pp'})}\,. \tag{32}$$

The external momenta $\hat{p}''^*$ and $\hat{p}^*$ are fixed and the internal coordinate $\vec{p}'$ is summed over all finite-volume values.

Disconnected terms in A complicate the determination of the volume dependence of $\mathcal{M}_L$. Indeed the analysis of Ref. [29] was largely concerned with understanding the impact of such contributions. Thus we would like to remove them to the extent possible. This turns out to be possible for the off-diagonal disconnected parts of A, as we now explain.

We begin by recalling that finite-volume dependence arises when one of the intermediate states goes on shell. As already noted in the discussion of $\widetilde{I}$, however, it is not kinematically possible for both a two- and a three-particle state to be simultaneously on shell if one of the particles has a common momentum. This implies that any disconnected component in A_{23} or A_{32} cannot simultaneously lead to finite-volume effects from both the adjacent cuts. This suggests adding factors to the pole terms in $\mathcal{C}$ such that this property is built in from the beginning, rather than discovered at the end.

To formalize this idea, we introduce two functions $H_2(\vec{p})$ and $H_3(\vec{k},\vec{a})$. These depend, respectively on the momenta in a two- and three-particle off-shell intermediate state. These functions have four key properties. First, they are smooth functions of the momenta. Second, they are symmetric under interchange of the particles in their respective intermediate states, i.e.

$$H_2(\vec{p}) = H_2(\vec{b}_p)\,, \tag{33}$$

$$H_3(\vec{k},\vec{a}) = H_3(\vec{a},\vec{k}) = H_3(\vec{a},\vec{b}_{ka}) = H_3(\vec{b}_{ka},\vec{a}) = H_3(\vec{k},\vec{b}_{ka}) = H_3(\vec{b}_{ka},\vec{k})\,. \tag{34}$$

Third, they equal unity when all particles in a given intermediate state are on shell. And, finally, they have no common support if one momentum is shared between the two intermediate states. As an equation, the "non-overlap" property is

$$H_2(\vec{p})H_3(\vec{p},\vec{a}) = 0\,. \tag{35}$$

Further discussion of these properties and an explicit example of functions that satisfy them are given in Appendix A. The reason that they can be defined is that there is a separation of $\mathcal{O}(m)$ between the momenta required to have a single particle on-shell and that yielding two on-shell particles.

We now rewrite Eq. (18) using these smooth cutoff functions. Specifically, we separate $\mathcal{C}$ into a singular part, $\mathcal{C}^H$, and a pole-free part, $\mathcal{C}^\infty$,

$$\mathcal{C} = \mathcal{C}^H + \mathcal{C}^\infty\,, \tag{36}$$

where

$$\mathcal{C}^H \equiv \begin{pmatrix} H_2(\vec{p})\mathcal{C}_{2;p'p} & 0 \\ 0 & H_3(\vec{k},\vec{a})\mathcal{C}_{3;k'a'ka} \end{pmatrix}\,, \tag{37}$$

$$\mathcal{C}^\infty \equiv \begin{pmatrix} [1-H_2(\vec{p})]\mathcal{C}_{2;p'p} & 0 \\ 0 & [1-H_3(\vec{k},\vec{a})]\mathcal{C}_{3;k'a'ka} \end{pmatrix}\,. \tag{38}$$

$\mathcal{C}^\infty$ is nonsingular because the factors of $1-H_i$ cancel their respective poles. Substituting Eq. (36) into Eq. (18), and collecting terms according to the power of $\mathcal{C}^H$, we arrive at

$$\mathcal{M}_L = \widetilde{A}\sum_{n=0}^{\infty}[\mathcal{C}^H\widetilde{A}]^n - \widetilde{I}\,, \tag{39}$$

where $\widetilde{A}$ is given by

$$\widetilde{A} = A\sum_{n=0}^{\infty}[\mathcal{C}^\infty A]^n\,. \tag{40}$$

This result (39) is identical in form to Eq. (18), but with the poles now "regulated" by the H functions, and with the kernels suitably modified. The additional terms that have been added to obtain $\widetilde{A}$ from A [i.e. the $n>0$ terms

in the sum in Eq. (40)] all involve sums over intermediate momenta that have nonsingular summands, so that these sums can be replaced by integrals ($1/L^3 \sum_k \longrightarrow \int_{\vec{k}}$). Thus $\widetilde{A}$ remains an infinite-volume, smooth kernel, aside from the above-mentioned Kronecker-deltas accompanied by factors of L^3.

The reason for this reorganization can now be understood. $\widetilde{A} = A + A\mathcal{C}^\infty A + \cdots$ contains disconnected parts, built up from the disconnected parts of A discussed above. However, it is easy to see that the off-diagonal disconnected parts of $\widetilde{A}$ do not contribute to $\mathcal{M}_L$. This is because, if one of the $\widetilde{A}$s in the expansion of Eq. (39) lies between two factors of $\mathcal{C}^H$, then its off-diagonal parts will be multiplied by H_2H_3. But this factor vanishes for any disconnected parts, by construction. The same is true if one or both sides of the $\widetilde{A}$ are at the end of the chain, because then the external particles are on shell.[5] Thus, with no approximation, in Eq. (42) we can drop the disconnected parts of $\widetilde{A}_{23}$ and $\widetilde{A}_{32}$.

Having derived the formula (39) we now explain why it is not yet in a form that allows the determination of the volume dependence of $\mathcal{M}_L$ using the methods of Refs. [8, 29, 30]. The problems are related to self-energy diagrams and the presence of disconnected contributions. We provide here only a brief sketch of the problems, without explaining all the technical details, since in the end we avoid them by using an alternative approach described in the following section.

The first issue arises in self-energy insertions on propagators present in two-particle s-channel loops. An example is provided by the central loop of both diagrams in Fig. 5. The difference between these two diagrams is that the two vertices in the self-energy loop have a different time-ordering, leading to a different sequence of cuts. Focusing on the central region between the two factors of $\mathcal{C}_2$, the left diagram contributes to $A_{23}\mathcal{C}_3A_{32}$, while that on the right contributes directly to A_{22}. When we change A to $\widetilde{A}$ the two time-orderings are recombined as

$$\widetilde{A}_{22} = A_{22} + A_{23}\,\mathcal{C}_3(1-H_3)A_{32} + \cdots\,. \tag{41}$$

The sum over momenta that comes with $\mathcal{C}_3$ can be converted into an integral because it is multiplied by $1-H_3$. Furthermore, since $\widetilde{A}_{22}$ lies between two factors of either $\mathcal{C}_2H_2$ or external on-shell states, we can set H_3 to zero. Thus the two time-orderings are recombined in $\widetilde{A}_{22}$ without any regulator functions. At this point we would like to say that adding these two orderings will lead to the full, Lorentz invariant one-loop self energy, which is proportional to $(p^2-m^2)^2$, given our renormalization conditions. If so, the double zero would cancel the poles in both factors of $\mathcal{C}_2$, so that such diagrams would not in fact lead to finite-volume dependence from the two-particle loop. In this way we would not have to worry about the self-energy insertion, except for its contribution to three-cuts with a factor of H_3.

However, this argument is incorrect. To obtain the full one-loop self energy, one needs to include additional time-orderings in which the vertices in the self-energy loop lie either before or after the bracketing $\mathcal{C}_2$ cuts. Without these, it turns out that the sum of the two diagrams that are included only vanishes as (p^2-m^2), and thus only cancels the poles in one of the $\mathcal{C}_2$ factors. Thus the loop does contribute finite-volume effects. Similarly, additional self-energy insertions on the propagators in the two-particle loop must also be kept. This requires consideration of an infinite class of diagrams that does not arise in the treatments of Refs. [8, 29, 30].

The second issue concerns Feynman diagrams contributing to $\mathcal{M}_L$ that are 1PI in the s-channel, i.e. have all the energy-momentum flowing through a single particle. As noted above, the propagator of this particle must be 3PI. It turns out that this leads to a new type of disconnected contribution to A_{33} that is not a smooth function of the external momenta. This is explained in Appendix B 3. Such contributions cannot be dealt with using the methods of Refs. [8, 29, 30], which rely on the certain smoothness properties of the kernels. Thus the 3PI propagators must be dealt with at the level of Feynman diagrams, before turning to TOPT.

B. Identification of two-and three-particle poles: Improved approach

In this section we sketch the derivation of a replacement for Eq. (39) that has identical form but contains modified kernels B (replacing $\widetilde{A}$), and a modified subtraction I (in place of $\widetilde{I}$):

$$\mathcal{M}_L = B\frac{1}{1-\mathcal{C}B} - I\,, \tag{42}$$

---

[5] In more detail, the argument in this case goes as follows. We are free to multiply the on-shell external states by a factor of H_i (with i the number of particles in the state), since this factor is unity. Thus off-diagonal terms in $\widetilde{A}$ come with a factor of H_2H_3 also here.

The issues described at the end of the previous section do not apply to the new formulation, and the methods of Refs. [8, 29, 30] can be applied to analyze Eq. (42). The derivation is rather technical and lengthy and so is only sketched here. It is explained in detail in Appendix B. The derivation proceeds in multiple steps.

We begin by following the same path as in the previous section, constructing the diagrammatic expansion for $\mathcal{M}_L$ in terms of all possible contact interactions and the three types of dressed propagators. We observe that the latter can be replaced by their infinite-volume counterparts. We also explain why tadpole diagrams can be absorbed into vertices. This is described in more detail in Appendix B 1.

We then deviate from the naive approach in the class of diagrams containing self-energy insertions on propagators in two-particle s-channel loops (see Fig. 9(a)). As described in Appendix B 2, by inserting $1 = H_2(\vec{p}) + [1-H_2(\vec{p})]$ in such loops, we find that self-energies can be ignored for the part with H_2, because they cancel poles and collapse the propagators to local interactions. The $1-H_2$ terms remain, but they do not have any two-particle cuts. This resolves the first complication described at the end of the previous section.

We next resolve the second complication from the previous section involving 3PI-dressed propagators. As described in Appendix B 3, we show that these propagators can be effectively shrunk to point vertices that cannot be cut.

After taking stock of the remaining classes of diagrams in Appendix B 4, we next switch to using TOPT. In Appendix B 5, we explain how TOPT applies to our amputated on-shell correlators involving dressed propagators. We thus reach a result corresponding to Eq. (18) in the naive approach, but with kernels that are better behaved, and with a subtraction only needed for the 33 component.

Next, as explained in Appendix B 6, we separate the cut functions $\mathcal{C}$ as in Eq. (36), and use the identity in (35) to reduce the number of resulting terms. In this and the following section of the appendix we show diagrammatically how the result Eq. (42) arises. The key properties of the kernel are that the B_{22}, B_{23} and B_{32} components contain no disconnected parts, and are smooth, infinite-volume quantities, while B_{33} has disconnected parts corresponding to the two-to-two scattering subprocess. The explicit form of the disconnected part is given in Eq. (C22).

C. Volume dependence of $\mathcal{M}_L$

In this section we use the decomposition of the finite-volume scattering amplitude, given in Eq. (42), to determine the volume dependence of $\mathcal{M}_L$. Our aim is to piggyback on the methods and results of Refs. [8, 29, 30], and it turns out that we can do so to a considerable extent. However, since these works do not use TOPT to decompose finite-volume amplitudes, some effort is needed to map their approach into the one used here.

We begin by reorganizing the series in (42) so as to separate the contributions from the diagonal and off-diagonal elements of B. Specifically, we introduce

$$B_D = \begin{pmatrix} B_{22} & 0 \\ 0 & B_{33} \end{pmatrix} \quad \text{and} \quad B_T = \begin{pmatrix} 0 & B_{23} \\ B_{32} & 0 \end{pmatrix} , \tag{43}$$

such that $B = B_D + B_T$. We then rearrange Eq. (42) into

$$\mathcal{M}_L = B_D + B_T + (B_D + B_T)\Xi \sum_{n=0}^{\infty} [B_T \Xi]^n (B_D + B_T) - I \, , \tag{44}$$

where

$$\Xi \equiv \mathcal{C}^H \frac{1}{1 - B_D \mathcal{C}^H} \equiv \begin{pmatrix} \Xi_{22} & 0 \\ 0 & \Xi_{33} \end{pmatrix} . \tag{45}$$

In this way all off-diagonal entries of B are kept explicit, while the diagonal entries are resummed into the diagonal matrix Ξ. The latter contains all the intermediate-state factors $\mathcal{C}^H$.

The key observation is that Ξ has exactly the form that arises in the analyses of Refs. [8, 29, 30]. More specifically, Ξ_{22} (which contains only two-cuts) arises in Ref. [8], while Ξ_{33} (containing only three-cuts) arises in Refs. [29, 30]. The only subtlety is that the result for Ξ depends on the nature of the B factors on either side, i.e. whether they are B_D or B_T. This dependence arises because B_D (or, more precisely, B_{33}) contains disconnected parts. Physically, these correspond to two-to-two subprocesses, and the form of the result depends on whether such processes occur at the "ends" or not.

To keep track of the different environments of the factors of Ξ, we introduce superscripts indicating which type of B is on either side. For example, $\Xi^{(D,T)}$ implies that there is a B_D on the left and a B_T on the right. We stress

that this is only a notational device, allowing us to make substitutions that depend on the environment (as will be explained below). Using this notation, we further decompose $\mathcal{M}_L$ as

$$\begin{aligned}\mathcal{M}_L = B_D + B_D\Xi^{(D,D)}B_D - I + B_D\Xi^{(D,T)}\sum_{n=0}^{\infty}\left[B_T\Xi^{(T,T)}\right]^n B_T\Xi^{(T,D)}B_D \\ + B_T + B_D\Xi^{(D,T)}\sum_{n=0}^{\infty}\left[B_T\Xi^{(T,T)}\right]^n B_T + B_T\sum_{n=0}^{\infty}\left[\Xi^{(T,T)}B_T\right]^n\Xi^{(T,D)}B_D + B_T\sum_{n=0}^{\infty}\left[\Xi^{(T,T)}B_T\right]^n\Xi^{(T,T)}B_T\,. \quad (46)\end{aligned}$$

Our aim is to determine the appropriate substitutions for the four different types of Ξ factors appearing in this form.

We begin with the diagonal quantity that contains no factors of B_T:

$$X = B_D + B_D\Xi^{(D,D)}B_D - I = B_D\sum_{n=0}^{\infty}\left[\mathcal{C}^H B_D\right]^n - I = \begin{pmatrix} X_{22} & 0 \\ 0 & X_{33}\end{pmatrix}. \quad (47)$$

In terms of the components we have

$$X_{22} = B_{22}\sum_{n=0}^{\infty}\left[\mathcal{C}_2^H B_{22}\right]^n, \quad (48)$$

$$X_{33} = B_{33}\sum_{n=0}^{\infty}\left[\mathcal{C}_3^H B_{33}\right]^n - I_{33}\,. \quad (49)$$

These two quantities are chosen to have very similar forms to the finite-volume amplitudes analyzed previously in Refs. [8] and Refs. [29, 30], respectively, so that we can make use of the results of these works.

We focus first on X_{22}. This is the part of $\mathcal{M}_L$ having two-particle external states and in which, by hand, we allow only two-cuts. X_{22} is not a physical quantity, since three-cuts that are present in $\mathcal{M}_{L,22}$ are removed by hand. The unphysical nature of X_{22} holds both below and above the three-particle threshold at $E^* = 3m$. Above this threshold, this is because we have removed physical three-particle intermediate states. Below this threshold, while there are no on-shell three-particle states, there are virtual contributions to $\mathcal{M}_{L,22}$ that are being dropped. In this regard, we stress that our formalism is designed to work both below and above the three-particle threshold, and thus differs from the analysis one would do when working solely below this threshold. In the latter case, one could study the amplitude taking into account only the two-cuts, and this is indeed the approach used in Ref. [8].

Despite the unphysical nature of X_{22}, it has nevertheless been constructed to have the same form as the physical below-threshold finite-volume amplitude when the latter is analyzed the latter taking into account only two-cuts. In particular, X_{22} is built of alternating smooth quantities (B_{22}) and two-cuts ($\mathcal{C}_2^H$). This allows us to apply the methods of Ref. [8], as explained in Appendix C 1. We show there that

$$X_{22}(E,\vec{P}) = \mathcal{K}_{22,D}(E,\vec{P})\frac{1}{1 + F_2(E,\vec{P})\mathcal{K}_{22,D}(E,\vec{P})}\,, \quad (50)$$

where $\mathcal{K}_{22,D}$ is an unphysical K-matrix discussed below, and F_2 is the moving-frame Lüscher zeta-function[6]

$$F_{2;\ell'm';\ell m}(E,\vec{P}) \equiv \frac{1}{2}\left[\frac{1}{L^3}\sum_{\vec{p}} - \mathrm{PV}\int\frac{d^3p}{(2\pi)^3}\right]\frac{4\pi Y_{\ell'm'}(\hat{p}^*)Y^*_{\ell,m}(\hat{p}^*)}{2\omega_p 2\omega_{Pp}(E-\omega_p-\omega_{Pp})}\left(\frac{p^*}{q^*}\right)^{\ell+\ell'} h(\vec{p})\,. \quad (51)$$

$h(\vec{p})$ is a UV cutoff function, the details of which do not matter, except that it must equal unity when $E = \omega_p + \omega_{Pp}$. Different choices for the cutoff function are given in Refs. [8] and Ref. [29, 30]. "PV" indicates the use of the principal-value prescription for the integral over the pole. For $E^* > 2m$ this is standard (given, for example, by the real part of the $i\epsilon$ prescription), while for $E^* < 2m$ we define PV such that the result is obtained by analytic continuation from above threshold. This corresponds, for example, to the definition given in Refs. [4, 5].

The derivation in Appendix C 1 leads to an explicit expression for $\mathcal{K}_{22,D}$, Eq. (C10). We stress that the appearance of an unphysical amplitude in the quantization condition is analogous to what happens in the three-particle quantization

[6] In Ref. [29] what we call F_2 here is called simply F. Here we reserve F for the slightly different quantity defined in Eq. (59).

condition of Ref. [29], which contains $\mathcal{K}_{\mathrm{df},3}$. This is not a concern, because in the end (Sec. III) we will be able to relate the unphysical quantities to physical scattering amplitudes.

We now turn to the quantity X_{33}, defined in Eq. (49). This is the part of $\mathcal{M}_L$ with three-particle external states that contains only three-cuts. It is unphysical at all energies since the physical amplitude always has two-cuts. Nevertheless, it has the same structure as the finite-volume amplitude considered in Ref. [30], namely $\mathcal{M}_{3,L}$ in the presence of a $\mathbb{Z}_2$ symmetry forbidding even-odd transitions (and thus forbidding two-cuts). Thus we can hope to reuse results from that work. As for X_{22}, however, we cannot do so directly, because the analysis leading to these results uses Feynman diagrams, whereas here we are using TOPT. Since we are dropping cuts by hand, we cannot in any simple way recast the TOPT result (49) into one using Feynman diagrams. Instead, in order to use the results from Ref. [30], we have to redo the analysis of Refs. [29, 30] using TOPT.

In a theory with a $\mathbb{Z}_2$ symmetry we have $B_{23} = B_{32} = 0$, so X_{33} is simply equal to $\mathcal{M}_{3,L}$ and is thus physical. The TOPT derivation given above still applies (and indeed is simplified by the absence of $2 \leftrightarrow 3$ mixing) so the result Eq. (49) for X_{33} still holds. Although B_{33} will differ in detail from that in our $\mathbb{Z}_2$-less theory, its essential properties are the same. In particular, it can be separated into connected and disconnected parts

$$B_{33} = B_{33}^{\mathrm{conn}} + B_{33}^{\mathrm{disc}}\,, \tag{52}$$

with the latter containing all contributions in which two particles interact while the other particle remains disconnected. Determining the finite-volume dependence arising from these disconnected contributions was the major challenge in the analysis of Refs. [29, 30].

Thus we must start with Eq. (49) rather than the Feynman diagram skeleton expansion. This turns out to be a rather minor change. Both approaches have the same sequences of cuts alternating with either connected or disconnected kernels. Working through the derivation of Refs. [29, 30] we find that all steps still go through, the only change being in the precise definition of the kernels. This is a tedious but straightforward exercise that we do not reproduce in detail, although we collect some technical comments on the differences caused by using TOPT in Appendix C 3. The outcome is that the final result, Eq. (68) of Ref. [30], still holds, but with some of the quantities having different definitions. Applying this result to X_{33} in the $\mathbb{Z}_2$-less theory, we find[7]

$$X_{33} = \mathcal{D}_{L,3} + \mathcal{S}_{\mathcal{L},3}\left\{\mathcal{L}_{L,3}^{(u,u)}\mathcal{K}_{\mathrm{df},33,\mathrm{D}}\frac{1}{1+F_3\mathcal{K}_{\mathrm{df},33,\mathrm{D}}}\mathcal{R}_{L,3}^{(u,u)}\right\}\mathcal{S}_{\mathcal{R},3}\,, \tag{53}$$

$$\mathcal{D}_{L,3} = -\mathcal{S}_{\mathcal{L},3}\left\{\mathcal{D}_{L,3}^{(u,u)}\right\}\mathcal{S}_{\mathcal{R},3}\,, \tag{54}$$

$$\mathcal{D}_{L,3}^{(u,u)} = \frac{1}{1+\mathcal{M}_{2,L}G^H}\mathcal{M}_{2,L}G^H\mathcal{M}_{2,L}[2\omega L^3]\,, \tag{55}$$

$$\mathcal{L}_{L,3}^{(u,u)} = \frac{1}{3} - \frac{1}{1+\mathcal{M}_{2,L}G^H}\mathcal{M}_{2,L}F\,, \tag{56}$$

$$\mathcal{R}_{L,3}^{(u,u)} = \frac{1}{3} - \frac{F}{2\omega L^3}\frac{1}{1+\mathcal{M}_{2,L}G^H}\mathcal{M}_{2,L}[2\omega L^3]\,, \tag{57}$$

$$F_3 = \frac{F}{2\omega L^3}\mathcal{L}_{L,3}^{(u,u)} = \mathcal{R}_{L,3}^{(u,u)}\frac{F}{2\omega L^3}\,. \tag{58}$$

Here $\mathcal{S}_{L,3}$ and $\mathcal{S}_{R,3}$ are symmetrization operators acting respectively on the arguments at the left and right ends of expressions within curly braces. They are defined in Eqs. (36) and (37) of Ref. [30].[8] The superscripts involving u are explained in Ref. [29]. $\mathcal{K}_{\mathrm{df},33,\mathrm{D}}$ is an unphysical, three-particle K-matrix that is a smooth function of its arguments, and is given by Eq. (C39). It takes the place of the quantity $\mathcal{K}_{\mathrm{df},3}$ that appears in the theory with a $\mathbb{Z}_2$ symmetry, in an analogous way to the replacement of $\mathcal{K}_2$ with $\mathcal{K}_{22,D}$ in X_{22} described above. F, which is defined in Ref. [29], is similar to F_2, but includes an extra index to account for the third particle:[9]

$$F_{k'\ell'm';k\ell m} = \delta_{k'k}H(\vec{k})F_{2;\ell'm';\ell m}(E-\omega_k, \vec{P}-\vec{k})\,, \tag{59}$$

---

[7] Note that we use an italic L to denote finite-volume, while calligraphic $\mathcal{L}$ and $\mathcal{R}$ denote left and right, respectively.

[8] In Ref. [30] $\mathcal{S}_{L,3}$ and $\mathcal{S}_{R,3}$ were combined into a single symmetrization operator $\mathcal{S}$. Here it is convenient to separate the two operations.

[9] This form of F differs from that defined in Ref. [29] by the choice of UV regulator in the sum-integral difference. Here we use $h(\vec{p})$ [see Eq. (51)], whereas in Ref. [29] a product of two H functions is used. Since both regulators equal unity at the on-shell point, the change in regulator only leads to differences of $\mathcal{O}(e^{-mL})$.

where the additional factor of H arises from the definition of H_3.

The two remaining quantities that need to be defined are $\mathcal{M}_{2,L}$ and G^H. The former is the finite-volume two-particle scattering amplitude below the three-particle threshold, except with an extra index for the third particle

$$\mathcal{M}_{2,L;k'\ell'm';k\ell m} = \delta_{k'k}\left[\mathcal{K}_2(E-\omega_k,\vec{P}-\vec{k})\frac{1}{1+F_2(E-\omega_k,\vec{P}-\vec{k})\mathcal{K}_2(E-\omega_k,\vec{P}-\vec{k})}\right]_{\ell'm';\ell m}. \tag{60}$$

It is important to distinguish this quantity from the two-particle finite-volume scattering amplitude, which we denote as $\mathcal{M}_{22,L}$. A key feature of this result is that it is the physical K-matrix $\mathcal{K}_2$ that appears in this expression (rather than the unphysical $\mathcal{K}_{22,D}$, for example) as long as $E^* < 4m$. This nontrivial result is explained in Appendix C 3. It implies that $\mathcal{D}_{L,3}$, $\mathcal{L}_{L,3}^{(u,u)}$, $\mathcal{R}_{L,3}^{(u,u)}$ and F_3 are the same as those appearing in Refs. [29, 30]. The only unphysical quantity in X_{33} is thus $\mathcal{K}_{\mathrm{df,33,D}}$. We do not have an explicit expression for this rather complicated quantity, but this does not matter as it will be related to the physical scattering amplitudes in Sec. III below.

Finally, we define G^H. This is almost identical to the matrix G defined in Refs. [29, 30] (see, for example, Eq. (A2) of Ref. [29]), except that it contains an additional cutoff function. The necessity of this change is discussed in Appendix C 3, and the explicit form is given in Eq. (C27). This is a minor technical change that has no impact on the general formalism.

The results for X_{22} and X_{33} can be conveniently combined by introducing the matrices

$$\mathcal{D}_L = \begin{pmatrix} 0 & 0 \\ 0 & \mathcal{D}_{L,3} \end{pmatrix}, \quad \mathcal{S}_{\mathcal{L}} = \begin{pmatrix} 1 & 0 \\ 0 & \mathcal{S}_{\mathcal{L},3} \end{pmatrix}, \quad \mathcal{S}_{\mathcal{R}} = \begin{pmatrix} 1 & 0 \\ 0 & \mathcal{S}_{\mathcal{R},3} \end{pmatrix}, \quad \mathcal{F} = \begin{pmatrix} F_2 & 0 \\ 0 & F_3 \end{pmatrix}, \tag{61}$$

$$\mathcal{K}_{\mathrm{df,D}} = \begin{pmatrix} \mathcal{K}_{22,D} & 0 \\ 0 & \mathcal{K}_{\mathrm{df},33,D} \end{pmatrix}, \quad \mathcal{L}_L^{(u)} = \begin{pmatrix} 1 & 0 \\ 0 & \mathcal{L}_{L,3}^{(u,u)} \end{pmatrix} \text{ and } \mathcal{R}_L^{(u)} = \begin{pmatrix} 1 & 0 \\ 0 & \mathcal{R}_{L,3}^{(u,u)} \end{pmatrix}. \tag{62}$$

Then we have

$$X = \mathcal{D}_L + \mathcal{S}_{\mathcal{L}}\left\{\mathcal{L}_L^{(u)}\mathcal{K}_{\mathrm{df,D}}\frac{1}{1+\mathcal{F}\mathcal{K}_{\mathrm{df,D}}}\mathcal{R}_L^{(u)}\right\}\mathcal{S}_{\mathcal{R}}. \tag{63}$$

Our next step is to determine the result for $\Xi^{(T,T)}$. This lies between factors of B_T, so the two contributions we need to calculate are

$$Y_{22} = B_{32}\Xi_{22}B_{23}, \tag{64}$$

$$Y_{33} = B_{23}\Xi_{33}B_{32}. \tag{65}$$

Y_{22} differs only slightly from X_{22} and is calculated in Appendix C 2, with the result

$$Y_{22} = B_{32}\left[\mathcal{D}_{C,2} - \mathcal{D}_{A',2}F_2\frac{1}{1+\mathcal{K}_{22,D}F_2}\mathcal{D}_{A,2}\right]B_{23}. \tag{66}$$

The volume dependence enters through the factors of F_2. $\mathcal{D}_{C,2}$, $\mathcal{D}_{A',2}$ and $\mathcal{D}_{A,2}$ are infinite-volume integral operators, whose explicit forms are given in Eqs. (C15)-(C17). $\mathcal{D}_{A',2}$ acts to the left, $\mathcal{D}_{A,2}$ to the right, while $\mathcal{D}_{C,2}$ acts in both directions. We refer to them collectively as decoration operators.

Turning now to Y_{33}, we note that this is similar to X_{33}, as can be seen by comparing Eq. (49) to the following:

$$Y_{33} = B_{23}\sum_{n=0}^{\infty}\left[\mathcal{C}_3^H B_{33}\right]^n\mathcal{C}_3^H B_{32}. \tag{67}$$

The major difference is that Y_{33} has factors of B_{23} or B_{32} on the ends, while X_{33} has factors of B_{33}. This is an important difference because B_{23} and B_{32} do not have disconnected parts, while B_{33} does. This means that Y_{33} is analogous to the correlation function studied in Ref. [29], in which there are three-particle connected operators at the ends (called σ and $\sigma^\dagger$ in that work). We thus need to repeat the analysis of Ref. [29] using the TOPT decomposition of the correlation function. This is a subset of the work already done for X_{33} (where the presence of a disconnected component in the kernels on the ends leads to additional complications, as studied in Ref. [30]). The result is that we can simply read off the answer from Eq. (250) of Ref. [29]:

$$Y_{33} = B_{23}\left[\mathcal{D}_{C,3} - \mathcal{D}_{A',3}F_3\frac{1}{1+\mathcal{K}_{\mathrm{df},33,\mathrm{D}}F_3}\mathcal{D}_{A,3}\right]B_{32}. \tag{68}$$

Here $\mathcal{D}_{C,3}$, $\mathcal{D}_{A',3}$ and $\mathcal{D}_{A,3}$ are decoration operators, whose definition can be reconstructed from Ref. [29] taking into account the difference between the Feynman-diagram analysis used there and the TOPT used here. We will, in fact, not need the definitions and so do not reproduce them here. F_3 and $\mathcal{K}_{\mathrm{df},33,\mathrm{D}}$ are the same quantities as appearing in Eq. (53).

We observe that the form of the result is very similar to that for Y_{22}, Eq. (66). The two can be combined into a matrix equation

$$\Xi^{(T,T)} = \mathcal{D}_C - \mathcal{D}_{A'}\mathcal{F}\frac{1}{1+\mathcal{K}_{\mathrm{df},33,\mathrm{D}}\mathcal{F}}\mathcal{D}_A\,, \tag{69}$$

if we use the definitions

$$\mathcal{D}_C = \begin{pmatrix} \mathcal{D}_{C,2} & 0 \\ 0 & \mathcal{D}_{C,3} \end{pmatrix}\,, \quad \mathcal{D}_{A'} = \begin{pmatrix} \mathcal{D}_{A',2} & 0 \\ 0 & \mathcal{D}_{A',3} \end{pmatrix}\,, \quad \mathcal{D}_A = \begin{pmatrix} \mathcal{D}_{A,2} & 0 \\ 0 & \mathcal{D}_{A,3} \end{pmatrix}\,. \tag{70}$$

The final quantities we need to determine are $\Xi^{(D,T)}$ and its "reflection" $\Xi^{(T,D)}$. This requires that we calculate

$$Z_{23} = B_{22}\Xi_{22}B_{23}\,, \tag{71}$$

$$Z_{32} = B_{33}\Xi_{33}B_{32}\,, \tag{72}$$

and their reflections. The former is obtained in Appendix C 2 by a simple extension of the analysis for X_{22} and Y_{22}. The result is

$$Z_{23} + B_{23} = \left[\frac{1}{1+\mathcal{K}_{22,D}F_2}\mathcal{D}_{A,2}\right]B_{23}\,. \tag{73}$$

The calculation of Z_{32} requires a more nontrivial extension of the analysis for X_{33} and Y_{33}. This is because Ξ_{33} connects a kernel with a disconnected component (B_{33}) to one without (B_{32}), and such correlators were not explicitly considered in Refs. [29, 30]. We work out the extension in Appendix C 4, finding

$$Z_{32} + B_{32} = \mathcal{S}_{\mathcal{L},3}\left\{\mathcal{L}^{(u,u)}_{L,3}\frac{1}{1+\mathcal{K}_{\mathrm{df},33,\mathrm{D}}F_3}\mathcal{D}_{A,3}B_{32}\right\}\,. \tag{74}$$

Combining Eqs. (73) and (74) into matrix form yields

$$B_D\Xi^{(D,T)} = \mathcal{S}_{\mathcal{L}}\left[\mathcal{L}^{(u)}_L\frac{1}{1+\mathcal{K}_{\mathrm{df,D}}\mathcal{F}}\mathcal{D}_A\right] - 1\,. \tag{75}$$

A similar analysis leads to the following result for the reflected quantity:

$$\Xi^{(T,D)}B_D = \left[\mathcal{D}_{A'}\frac{1}{1+\mathcal{F}\mathcal{K}_{\mathrm{df},33,\mathrm{D}}}\mathcal{R}^{(u)}_L\right]\mathcal{S}_R - 1\,, \tag{76}$$

We have now determined the volume dependence of all factors of Ξ appearing in the expression (46) for $\mathcal{M}_L$. Substituting Eqs. (63), (69), (75) and (76) into this expression, expanding and rearranging, we find the final result of this subsection:

$$\mathcal{M}_L = \mathcal{D}_L + \mathcal{S}_{\mathcal{L}}\left[\mathcal{L}^{(u)}_L\mathcal{K}_{\mathrm{df}}\frac{1}{1+\mathcal{F}\mathcal{K}_{\mathrm{df}}}\mathcal{R}^{(u)}_L\right]\mathcal{S}_{\mathcal{R}}\,. \tag{77}$$

Here the modified matrix of K-matrices is given by

$$\mathcal{K}_{\mathrm{df}} = \mathcal{K}_{\mathrm{df},D} + \mathcal{D}_A\sum_{n=0}^{\infty}[B_T\mathcal{D}_C]^nB_T\mathcal{D}_{A'}\,. \tag{78}$$

We stress that the second term in $\mathcal{K}_{\mathrm{df}}$, which is induced by the presence of $2\to3$ and $3\to2$ transitions, contains both diagonal and off-diagonal parts (the former having an even number of factors of B_T and the latter an odd number).

It is worth noting that, given the notation we use, the form of $\mathcal{M}_L$ in Eq. (77) qualitatively resembles that of the three-particle sector in the presence of the $\mathbb{Z}_2$ symmetry.

D. Quantization condition

The result (77) allows us to determine the energy levels of the theory in a finite volume. This is because $\mathcal{M}_L$ is simply a (conveniently chosen) matrix of correlation functions through which four-momentum $(E, \vec{P})$ flows. It will thus diverge whenever E equals the energy of a finite-volume state.[10] In general, such a divergence cannot come from $\mathcal{D}_L$, because this quantity depends only on the two-particle K-matrix, while the spectrum should depend on both two- and three-particle channels. Since symmetrization will not produce a divergence, it must be that the quantity in square brackets in Eq. (77) diverges. For the same reason as for $\mathcal{D}_L$, divergences in $\mathcal{L}_L^{(u)}$ and $\mathcal{R}_L^{(u)}$ cannot correspond to finite-volume energies. A divergence in the matrix $\mathcal{K}_{\text{df}}$ will not lead to a divergent $\mathcal{M}_L$, since the former appears in both numerator and denominator. Thus a divergence in $\mathcal{M}_L$ can come, in general, only from the factor $(1+\mathcal{F}\mathcal{K}_{\text{df}})^{-1}$. Since this is a matrix, it will diverge whenever $\det(1 + \mathcal{F}\mathcal{K}_{\text{df}})$ vanishes. Thus we find the quantization condition

$$\det\left[\begin{pmatrix}1 & 0\\ 0 & 1\end{pmatrix} + \begin{pmatrix}F_2 & 0\\ 0 & F_3\end{pmatrix}\begin{pmatrix}\mathcal{K}_{22} & \mathcal{K}_{23}\\ \mathcal{K}_{32} & \mathcal{K}_{\text{df},33}\end{pmatrix}\right] = 0\,, \tag{79}$$

where $\mathcal{K}_{22}$, $\mathcal{K}_{23}$, $\mathcal{K}_{32}$ and $\mathcal{K}_{\text{df},33}$ are entries in the matrix $\mathcal{K}_{\text{df}}$ defined in Eq. (78).

We stress that each of the entries in Eq. (79) is itself a matrix, containing angular-momentum indices and (for the three-particle cases) also a spectator-momentum index. The angular momentum indices run over an infinite number of values, so the quantization condition involves an infinite-dimensional matrix. To use it in practice one must truncate the angular momentum space. This will be discussed further in Sec. IV. We also emphasize that Eq. (79) separates finite-volume dependence, contained in F_2 and F_3, from infinite-volume quantities, contained in $\mathcal{K}_{\text{df}}$.

The generalized quantization condition has a form that is a relatively simple generalization of those that hold separately for two and three particles in the case that there is a $\mathbb{Z}_2$ symmetry. Indeed, this case can be recovered simply by setting $\mathcal{K}_{23} = \mathcal{K}_{32} = 0$. However, we recall that, in the absence of the $\mathbb{Z}_2$ symmetry, the elements of $\mathcal{K}_{\text{df}}$ are complicated quantities, as can be seen from Eq. (78). They are also unphysical, as they depend on the cutoff functions. In particular, $\mathcal{K}_{22}$ is *not* equal to the physical two-particle K-matrix. In fact, all we know about the elements of $\mathcal{K}_{\text{df}}$ is that they are smooth functions of their arguments. In a practical application they would need to be parametrized in some way.

By contrast, we do know F_2—it is given in Eq. (51)—and F_3 can be determined from the spectrum of two-particle states below the three-particle threshold, $E^* < 3m$. Thus it can be determined first, before applying the full quantization condition in the regime $3m < E^* < 4m$. This means that by determining enough energy levels, both in the two- and three-particle regimes, one can in principle use the quantization condition to determine the parameters in any smooth ansatz for $\mathcal{K}_{\text{df}}$. How to go from these parameters to a result for the physical two- and three-particle scattering amplitudes is the topic of the next section.

III. RELATING $\mathcal{K}_{\text{df}}$ TO THE SCATTERING AMPLITUDE

In this section we derive the relation between $\mathcal{K}_{\text{df}}$ and the physically-observable scattering amplitude in the coupled two- and three-particle sector. The quantization condition derived in the previous section depends on $\mathcal{K}_{\text{df}}$ and also on the finite-volume quantities F_2 and F_3. The two-particle finite-volume factor, F_2, is a known kinematic function whereas its three-particle counterpart, F_3, depends on kinematic factors as well as the two-to-two scattering amplitude at two-particle energies below three-particle threshold. Thus, if one uses the standard Lüscher approach to determine the two-to-two scattering amplitude in the elastic region, then both F_2 and F_3 are known functions and each finite-volume energy above three-particle threshold gives a constraint on $\mathcal{K}_{\text{df}}$.

It follows that one can, in principle, use LQCD, or other finite-volume numerical techniques, to determine the divergence-free K-matrix via Eq. (79). As we have already stressed, this infinite-volume quantity is unphysical in several ways. First, the $i\epsilon$ pole prescription is replaced by the modified principal value prescription. Second, the K-matrix depends on the cutoff functions H_2 and H_3. And, finally, the physical singularities that occur at all above-threshold energies in the three-to-three scattering amplitude are subtracted to define a divergence-free quantity.

To relate $\mathcal{K}_{\text{df}}$ to physical scattering amplitudes, we take a carefully defined infinite-volume limit of the result for $\mathcal{M}_L$ given in Eq. (77) such that $\mathcal{M}_L$ goes over into the matrix of infinite-volume scattering amplitudes. This is the approach taken in Ref. [29] to derive a relation between $\mathcal{K}_{\text{df},3}$ and the three-particle scattering amplitude in theories

[10] In general, this means that all elements of the matrix will diverge, unless there are symmetry constraints.

with a $\mathbb{Z}_2$ symmetry preventing two-to-three transitions. The extension here is the need to consider a coupled set of equations with both two- and three-particle channels.

As a warm up, we briefly review the procedure for determining the two-particle scattering amplitude, $\mathcal{M}_{22}$, below three-particle threshold, from its finite-volume analogue, $\mathcal{M}_{L,22}$. The latter has the same function form as X_{22} appearing in Eq. (50), if the unphysical $\mathcal{K}_{22,D}$ is replaced by the physical two-body K-matrix below the three-body threshold, $\mathcal{K}_2$,

$$\mathcal{M}_{L,22}(E,\vec{P}) = \mathcal{K}_2(E,\vec{P})\frac{1}{1+F_2(E,\vec{P})\mathcal{K}_2(E,\vec{P})}\,, \qquad (E^* < 3m)\,, \tag{80}$$

To obtain $\mathcal{M}_{22}$, we first make the replacement $E \to E + i\epsilon$ in the poles that appear in the finite-volume sum contained in F_2, Eq. (51). Then we send $L \to \infty$ with ϵ held fixed and positive, and finally send $\epsilon \to 0$. This converts the finite-volume Feynman diagrams into infinite-volume diagrams with the $i\epsilon$ prescription, which are exactly those diagrams building up $\mathcal{M}_{22}$. The result is

$$\mathcal{M}_{22}(E,\vec{P}) = \lim_{L\to\infty}\Big|_{i\epsilon}\, \mathcal{M}_{L,22}(E,\vec{P}) = \mathcal{K}_2(E,\vec{P})\frac{1}{1+\rho_2(E,\vec{P})\mathcal{K}_2(E,\vec{P})}\,, \qquad (E^* < 3m), \tag{81}$$

where we have used [30]

$$\lim_{L\to\infty}\Big|_{i\epsilon}\, F_2(E,\vec{P}) = \rho_2(E,\vec{P})\,, \tag{82}$$

$$\rho_{2;\ell',m';\ell,m}(E,\vec{P}) \equiv \delta_{\ell',\ell}\delta_{m',m}\tilde{\rho}(E^*)\,, \tag{83}$$

$$\tilde{\rho}(E^*) \equiv \frac{1}{16\pi E^*} \times \begin{cases} -i\sqrt{E^{*2}/4-m^2} & (2m)^2 < E^{*2}\,, \\ |\sqrt{E^{*2}/4-m^2}| & 0 < E^{*2} \le (2m)^2\,. \end{cases} \tag{84}$$

Equation (81) is just the standard relation between the two-particle K-matrix and scattering amplitude.

A. Expressing $\mathcal{M}$ in terms of $\mathcal{K}_{\rm df}$

To relate the generalized divergence-free K-matrix to the scattering amplitudes we take the infinite-volume limit of Eq. (77) using the same prescription as that given in Eq. (81),

$$\begin{pmatrix} \mathcal{M}_{22} & \mathcal{M}_{23} \\ \mathcal{M}_{32} & \mathcal{M}_{33} \end{pmatrix} = \lim_{\epsilon\to 0}\lim_{L\to\infty}\left\{\mathcal{D}_L + \mathcal{S}_{\mathcal{L}}\left[\mathcal{L}_L^{(u)}\mathcal{K}_{\rm df}\frac{1}{1+F\mathcal{K}_{\rm df}}\mathcal{R}_L^{(u)}\right]\mathcal{S}_{\mathcal{R}}\right\}\,. \tag{85}$$

We stress that one must replace $E \to E + i\epsilon$ in all two- and three-particle poles appearing in finite-volume sums. In principle this expression gives the desired relation but in very compact notation. The remainder of this section is dedicated to explicitly displaying the integral equations encoded in this result. In doing so, we take over several results from Ref. [30].

We begin by studying the infinite-volume limit of $\mathcal{D}_L$, which is given in Eq. (61), and whose only nonzero element is $\mathcal{D}_{3,L}$. The latter, defined in Eq. (54), is the symmetrized form of $\mathcal{D}_{L,3}^{(u,u)}$, given in Eq. (55). The infinite volume limit of the latter quantity,

$$\lim_{L\to\infty}\Big|_{i\epsilon}\, \mathcal{D}^{(u,u)}_{L,3;p\ell'm';k\ell m} \equiv \mathcal{D}^{(u,u)}_{3;\ell'm;\ell m}(\vec{p},\vec{k})\,, \tag{86}$$

satisfies the integral equation [30]

$$\mathcal{D}_3^{(u,u)}(\vec{p},\vec{k}) = -\mathcal{M}_{22}(\vec{p})G^{\infty}(\vec{p},\vec{k})\mathcal{M}_{22}(\vec{k}) - \int_{\vec{r}\,'}\frac{1}{2\omega_{r'}}\mathcal{M}_{22}(\vec{p})G^{\infty}(\vec{p},\vec{r}\,')\mathcal{D}_3^{(u,u)}(\vec{r}\,',\vec{k})\,, \tag{87}$$

where

$$G^{\infty}_{\ell'm';\ell m}(\vec{p},\vec{k}) \equiv \left(\frac{k^*}{q_p^*}\right)^{\ell'}\frac{4\pi Y_{\ell'm'}(\hat{k}^*)H_3(\vec{p},\vec{k})Y^*_{\ell m}(\hat{p}^*)}{2\omega_{Pkp}(E-\omega_k-\omega_p-\omega_{Pkp}+i\epsilon)}\left(\frac{p^*}{q_k^*}\right)^{\ell}\,. \tag{88}$$

Note that in Eq. (87) we are following the compact notation of Ref. [30], in which the dependence on the spectator momenta is made explicit but the angular momentum indices are suppressed. Each element appearing in Eq. (87) is a matrix in angular momentum space with two sets of ℓm indices, contracted in the standard way. For example, the first term is explicitly given by

$$\mathcal{D}^{(u,u)}_{3;\ell' m';\ell m}(\vec{p},\vec{k}) \supset -\mathcal{M}_{22;\ell' m';\ell_1 m_1}(\vec{p})\, G^{\infty}_{\ell_1 m_1;\ell_2 m_2}(\vec{p},\vec{k})\, \mathcal{M}_{22;\ell_2 m_2;\ell m}(\vec{k})\,. \tag{89}$$

We next evaluate the infinite-volume limits of the three-particle endcap functions $\mathcal{L}^{(u,u)}_{3,L}$ and $\mathcal{R}^{(u,u)}_{3,L}$, defined, respectively, in Eqs. (56) and (57). These are the only nontrivial elements of the matrices $\mathcal{L}^{(u)}_{L}$ and $\mathcal{R}^{(u)}_{L}$ [see Eq. (62)]. Defining

$$\lim_{L\to\infty}\Big|_{i\epsilon}\, \mathcal{L}^{(u,u)}_{3,L;p\ell' m';k\ell m} \equiv \mathcal{L}^{(u,u)}_{3;\ell' m';\ell m}(\vec{p},\vec{k})\,, \tag{90}$$

$$\lim_{L\to\infty}\Big|_{i\epsilon}\, \mathcal{R}^{(u,u)}_{3,L;p\ell' m';k\ell m} \equiv \mathcal{R}^{(u,u)}_{3;\ell' m';\ell m}(\vec{p},\vec{k})\,, \tag{91}$$

we find [30]

$$\mathcal{L}^{(u,u)}_{3}(\vec{p},\vec{k}) = \left(\frac{1}{3} - \mathcal{M}_{22}(\vec{p})\rho_3(\vec{p})\right)(2\pi)^3\delta^3(\vec{p}-\vec{k}) - \mathcal{D}^{(u,u)}_{3}(\vec{p},\vec{k})\frac{\rho_3(\vec{k})}{2\omega_k}\,, \tag{92}$$

$$\mathcal{R}^{(u,u)}_{3}(\vec{p},\vec{k}) = \left(\frac{1}{3} - \rho_3(\vec{p})\mathcal{M}_{22}(\vec{p})\right)(2\pi)^3\delta^3(\vec{p}-\vec{k}) - \frac{\rho_3(\vec{p})}{2\omega_p}\mathcal{D}^{(u,u)}_{3}(\vec{p},\vec{k}\,)\,. \tag{93}$$

Here we have used[11]

$$\lim_{L\to\infty}\Big|_{i\epsilon}\, F = \rho_3\,, \tag{94}$$

$$\rho_{3;\ell',m';\ell,m}(\vec{k}) \equiv \delta_{\ell',\ell}\;\delta_{m',m}\; H(\vec{k})\tilde{\rho}(E^*_{2,k})\,. \tag{95}$$

We also reiterate that, in Eqs. (92) and (93), $\mathcal{M}_{22}$ is needed only below the three-particle threshold, so that, according to our assumptions, it is a known quantity.

These endcaps must be combined with the infinite-volume limit of the middle factor in Eq. (85),

$$\mathcal{T} \equiv \lim_{L\to\infty}\Big|_{i\epsilon}\, \mathcal{T}_L \tag{96}$$

$$\mathcal{T}_L = \mathcal{K}_{\rm df}\frac{1}{1+\mathcal{F}\mathcal{K}_{\rm df}}\,. \tag{97}$$

Here both $\mathcal{T}_L$ and its infinite-volume counterpart, $\mathcal{T}$, are matrices in the space of two- and three-particle channels

$$\mathcal{T}_L \equiv \begin{pmatrix} \mathcal{T}_{22,L;\ell_2' m_2';\ell_2 m_2} & \mathcal{T}_{23,L;\ell_2' m_2';k\ell_3 m_3} \\ \mathcal{T}_{32,L;k'\ell_3' m_3';\ell_2 m_2} & \mathcal{T}_{33,L;k'\ell_3' m_3';k\ell_3 m_3} \end{pmatrix}\,, \tag{98}$$

$$\mathcal{T} \equiv \begin{pmatrix} \mathcal{T}_{22;\ell_2' m_2';\ell_2 m_2} & \mathcal{T}_{23;\ell_2' m_2';\ell_3 m_3}(\vec{k}) \\ \mathcal{T}_{32;\ell_3' m_3';\ell_2 m_2}(\vec{k}') & \mathcal{T}_{33;\ell_3' m_3';\ell_3 m_3}(\vec{k}';\vec{k}) \end{pmatrix}\,. \tag{99}$$

We have given different labels for the angular-momentum indices on the two- and three-particle states to stress that these are independent quantities. To take the infinite-volume limit of $\mathcal{T}_L$, it is more convenient to use one of the following two matrix equations:

$$\mathcal{T}_L = \mathcal{K}_{\rm df} - \mathcal{K}_{\rm df}\mathcal{F}\mathcal{T}_L \tag{100}$$

$$= \mathcal{K}_{\rm df} - \mathcal{T}_L\mathcal{F}\mathcal{K}_{\rm df}\,. \tag{101}$$

---

[11] What we call ρ_3 here is denoted simply ρ in Ref. [30].

These go over to integral equations for $\mathcal{T}$ in the infinite-volume limit.

The nonzero components of the matrix $\mathcal{F}$ are F_2 and F_3 [see Eq. (61)]. The infinite-volume limit of F_2 is given in Eq. (82), while to obtain that for F_3 it is convenient to rewrite it as [30]

$$F_3 = \frac{F}{2\omega L^3}\left[\frac{1}{3} - \mathcal{M}_{22,L}F - \mathcal{D}_L^{(u,u)}\frac{F}{2\omega L^3}\right], \tag{102}$$

which allows the limit to be constructed from those for F, $\mathcal{M}_{22,L}$ and $\mathcal{D}_L^{(u,u)}$ given above.

We now have all the components to proceed. Taking the infinite-volume limits of Eqs. (100), (101) and (102), expanding out the 2×2 matrices, and performing some simple algebraic manipulations, we find

$$\mathcal{T}_{22} = [1+\mathcal{K}_{22}\,\rho_2\,]^{-1}\left[\mathcal{K}_{22} - \int_{\vec{r}\,'}\int_{\vec{r}}\mathcal{K}_{23}(\vec{r}\,')\,\frac{\rho_3(\vec{r}\,')}{2\omega_{r'}}\,\mathcal{L}_3^{(u,u)}(\vec{r}\,',\vec{r})\,\mathcal{T}_{32}(\vec{r})\right], \tag{103}$$

$$\mathcal{T}_{23}(\vec{k}\,) = [1+\mathcal{K}_{22}\,\rho_2]^{-1}\left[\mathcal{K}_{23}(\vec{k}\,) - \int_{\vec{r}\,'}\int_{\vec{r}}\mathcal{K}_{23}(\vec{r}\,')\,\frac{\rho_3(\vec{r}\,')}{2\omega_{r'}}\,\mathcal{L}_3^{(u,u)}(\vec{r}\,',\vec{r})\mathcal{T}_{33}(\vec{r},\vec{k}\,)\right], \tag{104}$$

$$\mathcal{T}_{32}(\vec{k}\,') = \left[\mathcal{K}_{32}(\vec{k}\,') - \int_{\vec{r}\,'}\int_{\vec{r}}\mathcal{T}_{33}(\vec{k}\,',\vec{r}\,')\,\mathcal{R}_3^{(u,u)}(\vec{r}\,',\vec{r})\,\frac{\rho_3(\vec{r})}{2\omega_r}\,\mathcal{K}_{32}(\vec{r})\right][1+\rho_2\,\mathcal{K}_{22}]^{-1}, \tag{105}$$

$$\mathcal{T}_{33}(\vec{k}\,',\vec{k}\,) = \mathcal{K}_{\mathrm{df},33}(\vec{k}\,',\vec{k}\,) - \mathcal{K}_{32}(\vec{k}\,')\,\rho_2\,\mathcal{T}_{23}(\vec{k}\,) - \int_{\vec{r}\,'}\int_{\vec{r}}\mathcal{K}_{\mathrm{df},3}(\vec{k}\,',\vec{r}\,')\,\frac{\rho_3(\vec{r}\,')}{2\omega_{r'}}\,\mathcal{L}_3^{(u,u)}(\vec{r}\,',\vec{r})\mathcal{T}_{33}(\vec{r},\vec{k}\,). \tag{106}$$

Substituting Eq. (104) in Eq. (106), and performing some further manipulations, we arrive at an integral equation for $\mathcal{T}_{33}$ alone

$$\mathcal{T}_{33}(\vec{k}\,',\vec{k}\,) = V_{33}(\vec{k}\,',\vec{k}\,) - \int_{\vec{r}\,'}\int_{\vec{r}}V_{33}(\vec{k}\,',\vec{r}\,')\,\frac{\rho_3(\vec{r}\,')}{2\omega_{r'}}\,\mathcal{L}_3^{(u,u)}(\vec{r}\,',\vec{r})\mathcal{T}_{33}(\vec{r},\vec{k}\,), \tag{107}$$

where

$$V_{33}(\vec{k}\,',\vec{k}\,) = \mathcal{K}_{\mathrm{df},33}(\vec{k}\,',\vec{k}\,) - \mathcal{K}_{32}(\vec{k}\,')\,\rho_2\,[1+\mathcal{K}_{22}\,\rho_2]^{-1}\,\mathcal{K}_{23}(\vec{k}\,). \tag{108}$$

Given $\mathcal{T}_{33}$ we can then perform the integrals in Eqs. (104) and (105) to obtain $\mathcal{T}_{23}$ and $\mathcal{T}_{32}$, respectively, and finally perform the integral in Eq. (103) to obtain $\mathcal{T}_{22}$. We emphasize that all these equations involve on shell quantities evaluated at fixed total energy and momentum, $(E,\vec{P})$.

Finally, we can combine the results for $\mathcal{T}$, the endcaps, and $\mathcal{D}_3$, to read off the results for the four components of the scattering amplitude from Eq. (85):

$$\mathcal{M}_{22}(\hat{p}'^*;\hat{p}^*) = \mathcal{T}_{22}(\hat{p}'^*;\hat{p}^*), \tag{109}$$

$$\mathcal{M}_{23}(\hat{p}'^*;\vec{k},\hat{a}^*) = \left\{\int_{\vec{r}}\mathcal{T}_{23}(\vec{r})\,\mathcal{R}_3^{(u,u)}(\vec{r},\vec{k}\,)\right\}\mathcal{S}_{\mathcal{R}}, \tag{110}$$

$$\mathcal{M}_{32}(\vec{k}\,',\hat{a}'^*;\hat{p}^*) = \mathcal{S}_{\mathcal{L}}\left\{\int_{\vec{r}\,'}\mathcal{L}_3^{(u,u)}(\vec{k}\,',\vec{r}\,')\mathcal{T}_{32}(\vec{r}\,')\right\}, \tag{111}$$

$$\mathcal{M}_{33}(\vec{k}\,',\hat{a}'^*;\vec{k},\hat{a}^*) = \mathcal{D}_3(\vec{k}\,',\hat{a}'^*;\vec{k},\hat{a}^*) + \mathcal{S}_{\mathcal{L}}\left\{\int_{\vec{r}}\int_{\vec{r}\,'}\mathcal{L}_3^{(u,u)}(\vec{k}\,',\vec{r})\mathcal{T}_{33}(\vec{r},\vec{r}\,')\,\mathcal{R}_3^{(u,u)}(\vec{r}\,',\vec{k}\,)\right\}\mathcal{S}_{\mathcal{R}}. \tag{112}$$

In these expressions we have contracted the external harmonic indices with spherical harmonics to reach functions of momenta with no implicit indices.

To summarize, given $\mathcal{K}_{\mathrm{df}}$ at a given value of $(E,\vec{P})$, together with knowledge of $\mathcal{M}_{22}$ below the three-particle threshold, we can obtain $\mathcal{M}_L$ at this same total four-momentum by solving the integral equations (87) for $\mathcal{D}_3^{(u,u)}$ and (107) for $\mathcal{T}_{33}$, and then doing integrals, matrix multiplications and symmetrizations. All the integrals are of finite range due to the presence of the UV cutoff $H(\vec{k})$ in ρ_3. The matrices have infinite size, and thus for practical applications one must truncate them, as will be discussed in Sec. IV.

We see from Eqs. (103) and (109) that the two-body scattering amplitude no longer satisfies Eq. (81) above the three-particle threshold.[12] It is reassuring to apply the $\mathcal{K}_{23}\to 0$ limit to Eq. (103)

$$\lim_{\mathcal{K}_{23}\to 0}\mathcal{M}_{22} = [1+\mathcal{K}_{22}\,\rho_2]^{-1}\,\mathcal{K}_{22}, \tag{113}$$

[12] If we use the full formalism below the three-particle threshold, then it is not obvious from our results how one regains the two-particle form of Eq. (81). We return to this issue in the conclusions.

in which we recover the elastic two-particle unitarity form, Eq. (81).

For theories that are invariant under time-reversal and parity transformations, the two off-diagonal components of the scattering amplitude are not independent. In Appendix D we explore the consequence of these symmetries and conclude that it is sufficient to determine only one of the off-diagonal elements, since the two are simply related.

B. Expressing $\mathcal{K}_{\text{df}}$ in terms of $\mathcal{M}$

In this subsection we give a method for determining $\mathcal{K}_{\text{df}}$ from the scattering amplitude, $\mathcal{M}$. In other words, we invert the expressions derived in the previous subsection. The motivation for doing so is that we can imagine having a parametrization of $\mathcal{M}$, containing a finite number of parameters, from which we want to predict the finite-volume spectrum. To do so, we need first to be able convert from $\mathcal{M}$ to $\mathcal{K}_{\text{df}}$, so as to be able, in a second step, to use the quantization condition, Eq. (79), to calculate the energy levels.

In the two-particle sector, applying the quantization condition in this manner has allowed lattice practitioners to disentangle partial waves that mix due to the reduction of rotational symmetry [15, 35], as well as the different components in coupled-channel scattering [22–26]. This is done by parametrizing the scattering amplitudes, deducing how the finite-volume energy levels depend on a given parametrization and then performing global fits of the energy levels extracted from various volumes, boosts, and irreducible representations of the various little groups associated with the different total momenta. This technique was proposed and tested in Ref. [36] for the study of coupled-channel two-particle systems. Given the parallels between coupled-channel systems with only two-particle states and the coupled two-to-three system considered here, this approach is likely to be required in an implementation of the present formalism as well.

We again follow closely the derivation of Ref. [30] and use results from that work. We begin by defining the divergence-free three-to-three scattering amplitude

$$\mathcal{M}_{\text{df},33}(\vec{k}',\hat{a}'^*;\vec{k},\hat{a}^*) \equiv \mathcal{M}_{33}(\vec{k}',\hat{a}'^*;\vec{k},\hat{a}^*) - \mathcal{D}_3(\vec{k}',\hat{a}'^*;\vec{k},\hat{a}^*)\,, \tag{114}$$

and expressing this in terms of building blocks introduced in the previous subsection

$$\mathcal{M}_{\text{df},33}(\vec{k}',\hat{a}'^*;\vec{k},\hat{a}^*) = \mathcal{S}_{\mathcal{L}} \left\{ \int_{\vec{r}} \int_{\vec{r}'} \mathcal{L}_3^{(u,u)}(\vec{k}\,',\vec{r}\,')\mathcal{T}_{33}(\vec{r}\,',\vec{r})\,\mathcal{R}_3^{(u,u)}(\vec{r},\vec{k}\,') \right\} \mathcal{S}_{\mathcal{R}}, \tag{115}$$

$$\begin{aligned} &= \int_{\vec{r}} \int_{\hat{b}^*} \int_{\vec{r}'} \int_{\hat{b}'^*} \left\{ (2\pi)^3\delta^3(\vec{k}\,'-\vec{r}\,')4\pi\delta^2(\hat{a}'^*-\hat{b}'^*) + \Delta_{\mathcal{L}}(\vec{k}\,',\hat{a}'^*;\vec{r}\,',\hat{b}'^*) \right\} \\ &\qquad \times \mathcal{T}_{33}(\vec{r}\,',\hat{b}'^*;\vec{r},\hat{b}^*) \left\{ (2\pi)^3\delta^3(\vec{k}-\vec{r})4\pi\delta^2(\hat{a}^*-\hat{b}^*) + \Delta_{\mathcal{R}}(\vec{r},\hat{b}^*;\vec{k},\hat{a}^*) \right\}. \end{aligned} \tag{116}$$

In the second form of the result we have written $\mathcal{T}_{33}$ in terms of on-shell momenta rather than the spherical harmonic indices used in the first form. The kernels $\Delta_{\mathcal{R}}$ and $\Delta_{\mathcal{L}}$ are taken from Ref. [30] and their definition can be inferred by comparing Eqs. (115) and (116). Here and below, all angular integrals are normalized to unity, i.e. $\int_{\hat{a}^*} = \int d\Omega_{\hat{a}^*}/(4\pi)$.

Similar relations hold for $\mathcal{M}_{23}$ and $\mathcal{M}_{32}$

$$\mathcal{M}_{23}(\hat{p}'^*;\vec{k},\hat{a}^*) = \int_{\vec{r}} \int_{\hat{b}^*} \mathcal{T}_{23}(\vec{r}) \left\{ (2\pi)^3\delta^3(\vec{k}-\vec{r})4\pi\delta^2(\hat{a}^*-\hat{b}^*) + \Delta_{\mathcal{R}}(\vec{r},\hat{b}^*;\vec{k},\hat{a}^*) \right\}, \tag{117}$$

$$\mathcal{M}_{32}(\vec{k}\,',\hat{a}'^*;\hat{p}^*) = \int_{\vec{r}'} \int_{\hat{b}'^*} \left\{ (2\pi)^3\delta^3(\vec{k}\,'-\vec{r}\,')4\pi\delta^2(\hat{a}'^*-\hat{b}'^*) + \Delta_{\mathcal{L}}(\vec{k}\,',\hat{a}'^*;\vec{r}\,',\hat{b}'^*) \right\} \mathcal{T}_{32}(\vec{r}\,'). \tag{118}$$

Now, using the kernels $I_{\mathcal{L}}$ and $I_{\mathcal{R}}$ defined in Ref. [30] via the integral equations,

$$I_{\mathcal{L}}(\vec{k}\,',\hat{a}'^*;\vec{k},\hat{a}^*) = (2\pi)^3\delta(\vec{k}\,'-\vec{k})4\pi\delta^2(\hat{a}'^*-\hat{a}^*) - \int_{r'} \int_{\hat{b}^*} I_{\mathcal{L}}(\vec{k}\,',\hat{a}'^*;\vec{r}\,',\hat{b}^*)\Delta_{\mathcal{L}}(\vec{r}\,',\hat{b}^*;\vec{k},\hat{a}^*)\,, \tag{119}$$

$$I_{\mathcal{R}}(\vec{k}\,',\hat{a}'^*;\vec{k},\hat{a}^*) = (2\pi)^3\delta(\vec{k}\,'-\vec{k})4\pi\delta^2(\hat{a}'^*-\hat{a}^*) - \int_{r'} \int_{\hat{b}^*} \Delta_{\mathcal{R}}(\vec{k}\,',\hat{a}'^*;\vec{r}\,',\hat{b}^*)I_{\mathcal{R}}(\vec{r},\hat{b}^*;\vec{k},\hat{a}^*)\,, \tag{120}$$

we derive the following expressions for $\mathcal{T}_{23}$, $\mathcal{T}_{32}$, and $\mathcal{T}_{33}$ in terms of $\mathcal{M}_{23}$, $\mathcal{M}_{32}$, and $\mathcal{M}_{\text{df},33}$ respectively:

$$4\pi Y^*_{\ell'm'}(\hat{p}'^*)\mathcal{T}_{23;\ell'm';\ell m}(\vec{k}\,')Y_{\ell m}(\hat{a}^*) = \int_r \int_{\hat{b}^*} \mathcal{M}_{23}(\hat{p}'^*;\vec{r},\hat{b}^*)I_{\mathcal{R}}(\vec{r},\hat{b}^*;\vec{k},\hat{a}^*)\,, \tag{121}$$

$$4\pi Y^*_{\ell'm'}(\hat{a}'^*)\mathcal{T}_{32;\ell'm';\ell m}(\vec{k}\,')Y_{\ell m}(\hat{p}^*) = \int_r \int_{\hat{b}^*} I_{\mathcal{L}}(\vec{k}\,',\hat{a}'^*;\vec{r},\hat{b}^*)\mathcal{M}_{32}(\vec{r},\hat{b}^*;\hat{p}^*)\,, \tag{122}$$

$$4\pi Y^*_{\ell'm'}(\hat{a}'^*)\mathcal{T}_{33;\ell'm';\ell m}(\vec{k}\,';\vec{k}\,')Y_{\ell m}(\hat{a}^*) = \int_{r'} \int_{\hat{b}'^*} \int_r \int_{\hat{b}^*} I_{\mathcal{L}}(\vec{k}\,',\hat{a}'^*;\vec{r}\,',\hat{b}'^*)\mathcal{M}_{\text{df},33}(\vec{r}\,',\hat{b}'^*;\vec{r},\hat{b}^*)I_{\mathcal{R}}(\vec{r},\hat{b}^*;\vec{k},\hat{a}^*)\,, \tag{123}$$

while $\mathcal{T}_{22} = \mathcal{M}_{22}$ from Eq. (109).

These expressions allow one to obtain the various components of $\mathcal{T}$ from the scattering amplitude. The final task is to invert Eqs. (103), (104) and (106), to determine $\mathcal{K}_{\text{df}}$ given $\mathcal{T}$. One simple way to do this is to start with the inverted finite-volume relation and again take the infinite-volume limit, as in Eqs. (100) and (101). This gives

$$\mathcal{K}_{22} = [1 - \mathcal{T}_{22}\,\rho_2\,]^{-1} \left[\mathcal{T}_{22} + \int_{r'}\int_{r} \mathcal{T}_{23}(\vec{r}\,')\,\frac{\rho_3(\vec{r}\,')}{2\omega_{r'}}\,\mathcal{L}_3^{(u,u)}(\vec{r}\,',\vec{r})\,\mathcal{K}_{32}(\vec{r})\right], \tag{124}$$

$$\mathcal{K}_{23}(\vec{k}\,) = [1 - \mathcal{T}_{22}\,\rho_2\,]^{-1} \left[\mathcal{T}_{23} + \int_{r'}\int_{r} \mathcal{T}_{23}(\vec{r}\,')\,\frac{\rho_3(\vec{r}\,')}{2\omega_{r'}}\,\mathcal{L}_3^{(u,u)}(\vec{r}\,',\vec{r})\,\mathcal{K}_{\text{df},33}(\vec{r},\vec{k}\,)\right], \tag{125}$$

$$\mathcal{K}_{32}(\vec{k}\,') = \left[\mathcal{T}_{32} + \int_{r'}\int_{r} \mathcal{K}_{\text{df},33}(\vec{k}\,';\vec{r}\,')\,\mathcal{R}_3^{(u,u)}(\vec{r}\,',\vec{r})\,\frac{\rho_3(\vec{r})}{2\omega_{r}}\,\mathcal{T}_{32}(\vec{r})\right][1 - \rho_2\,\mathcal{T}_{22}\,]^{-1}, \tag{126}$$

$$\mathcal{K}_{\text{df},33}(\vec{k}\,',\vec{k}\,) = W_{33}(\vec{k}\,',\vec{k}\,) + \int_{r'}\int_{r} W_{33}(\vec{k}\,',\vec{r}\,')\,\frac{\rho_3(\vec{r}\,')}{2\omega_{r'}}\,\mathcal{L}_3^{(u,u)}(\vec{r}\,',\vec{r})\,\mathcal{K}_{\text{df},33}(\vec{r},\vec{k}\,), \tag{127}$$

where

$$W_{33}(\vec{k}\,',\vec{k}\,) = \mathcal{T}_{33}(\vec{k}\,',\vec{k}\,) + \mathcal{T}_{32}(\vec{k}\,')\,\rho_2\,[1 - \mathcal{T}_{22}\,\rho_2]^{-1}\,\mathcal{T}_{23}(\vec{k}\,). \tag{128}$$

This completes the expression for $\mathcal{K}_{\text{df}}$ in terms of $\mathcal{M}$.

In summary, given $\mathcal{M}$, one can determine the finite-volume energies as follows:

- Using $\mathcal{M}_{22}$ below three-particle threshold, solve the integral equation (87) to determine $\mathcal{D}_3^{(u,u)}(\vec{p},\vec{k})$.
- Substitute this into Eqs. (92) and (93) to determine $\mathcal{L}_3^{(u,u)}(\vec{p},\vec{k})$ and $\mathcal{R}_3^{(u,u)}(\vec{p},\vec{k})$ and from these infer $\Delta_{\mathcal{L}}$ and $\Delta_{\mathcal{R}}$ via Eqs. (115) and (116).
- Using $\Delta_{\mathcal{L}}$ and $\Delta_{\mathcal{R}}$ as inputs, solve the integral equations (119) and (120) and thereby determine $I_{\mathcal{L}}$ and $I_{\mathcal{R}}$.
- Use these, in turn, in Eqs. (121)-(123) to deduce the two-by-two matrix $\mathcal{T}$ from the scattering amplitude.
- Inserting $\mathcal{T}$, $\mathcal{L}_3^{(u,u)}$ and $\mathcal{R}_3^{(u,u)}$ into Eqs. (124)-(127), calculate the generalized divergence-free K-matrix, $\mathcal{K}_{\text{df}}$, corresponding to the input scattering amplitude.
- Substitute $\mathcal{K}_{\text{df}}$ into Eq. (79) and solve for all roots in E at fixed values of $\vec{P}$ and L.

Up to neglected terms that scale as e^{-mL}, these solutions correspond to the unique finite-volume energies associated with the input scattering amplitudes. Performing this procedure for a particular parametrization of $\mathcal{M}$, one may fit the parameter set to a large number of finite-volume energies and thereby determine the coupled two- and three-particle scattering amplitudes from Euclidean finite-volume calculations.

IV. APPROXIMATIONS

In order to use Eq. (79) in practice, it is necessary to truncate the matrices appearing inside the determinant.

To systematically understand the various truncations that one might apply it is useful to "subduce" the quantization quantization, i.e. to block diagonalize $1 + \mathcal{K}_{\text{df}}\mathcal{F}$ and identify the quantization conditions associated with each sector. The divergence-free K-matrix is an infinite-volume quantity and is thus diagonal in the total angular momentum of the system. By contrast the finite-volume quantities F_2 and F_3 couple different angular-momentum states, a manifestation of the reduced rotational symmetry of the box. At the same time, the residual symmetry of the finite volume still provides important restrictions on form of F_2 and F_3. For a given boost, these can be blocked diagonalized, with each block corresponding to an irreducible representation of the symmetry group. One can then truncate each block by assuming that all partial waves above some ℓ_{max} do not contribute. This subduction procedure is well understood for the two-particle system [35], and is expected to carry through to three-particle systems.

In this work we do not further discuss the subduction of the quantization condition but instead consider two simple approximations applied directly to the main result. These approximations were also discussed in Refs. [29, 30]. First, we consider the case of $\ell_{2,\text{max}} = \ell_{3,\text{max}} = 0$, in which all two-particle angular momentum components beyond the s-wave are assumed to vanish. In the two-particle sector, this implies that all quantities that were previously matrices in angular momentum are replaced with single numbers. The three-particle states, by contrast, still carry dependence

on the spectator momentum so that the index space is reduced from k, ℓ, m to k. We refer to this as the s-wave approximation.

Using the same arguments as in Ref. [29], one can show that the presence of the cutoff function H_3 in F and G^H implies that only a finite number of spectator momenta contribute to the quantization condition. Labeling the set of allowed momenta $\{k_1, k_2, \ldots, k_N\}$, we can write the condition out explicitly in the s-wave approximation:

$$\det \begin{pmatrix} 1+F_2^s\mathcal{K}_2^s & [F_2^s\mathcal{K}_{23}^s]_{k_1} & [F_2^s\mathcal{K}_{23}^s]_{k_2} & & [F_2^s\mathcal{K}_{23}^s]_{k_N} \\ [F_3^s\mathcal{K}_{32}^s]_{k_1} & 1+[F_3^s\mathcal{K}_{\mathrm{df},33}^s]_{k_1;k_1} & [F_3^s\mathcal{K}_{\mathrm{df},33}^s]_{k_1;k_2} & \cdots & [F_3^s\mathcal{K}_{\mathrm{df},33}^s]_{k_1;k_N} \\ [F_3^s\mathcal{K}_{32}^s]_{k_2} & [F_3^s\mathcal{K}_{\mathrm{df},33}^s]_{k_2;k_1} & 1+[F_3^s\mathcal{K}_{\mathrm{df},33}^s]_{k_2;k_2} & & [F_3^s\mathcal{K}_{\mathrm{df},33}^s]_{k_2;k_N} \\ & \vdots & & \ddots & \\ [F_3^s\mathcal{K}_{32}^s]_{k_N} & [F_3^s\mathcal{K}_{\mathrm{df},33}^s]_{k_N;k_1} & [F_3^s\mathcal{K}_{\mathrm{df},33}^s]_{k_N;k_2} & & 1+[F_3^s\mathcal{K}_{\mathrm{df},33}^s]_{k_N;k_N} \end{pmatrix} = 0\,. \tag{129}$$

The "s" superscripts indicate that $\ell = 0$ for the two-particle states and also for one of the particle pairs within the three-particle states. The explicit definitions are

$$\mathcal{K}_{22}^s \equiv \mathcal{K}_{22;00;00}\,, \tag{130}$$

$$\mathcal{K}_{23;k}^s \equiv \mathcal{K}_{23;00;k00}\,, \tag{131}$$

$$\mathcal{K}_{32;k'}^s \equiv \mathcal{K}_{32;k'00;00}\,, \tag{132}$$

$$\mathcal{K}_{\mathrm{df},33;k';k}^s \equiv \mathcal{K}_{\mathrm{df}33;k'00;k00}\,, \tag{133}$$

$$F_2^s \equiv F_2^s(E,\vec{P}) \equiv \frac{1}{2}\left[\frac{1}{L^3}\sum_{\vec{a}} - \mathrm{PV}\int \frac{d^3a}{(2\pi)^3}\right]\frac{h(\vec{a})}{2\omega_a 2\omega_{Pa}(E-\omega_a-\omega_{Pa})}\,, \tag{134}$$

$$F_{k';k}^s \equiv \delta_{k'k}H(\vec{k})F_2^s(E-\omega_k, \vec{P}-\vec{k})\,, \tag{135}$$

$$G_{k';k}^s \equiv \frac{H_3(\vec{k}', \vec{k}\,)}{2\omega_{Pkk'}(E-\omega_k-\omega_{k'}-\omega_{Pkk'})}\frac{1}{2\omega_k L^3}\,, \tag{136}$$

$$F_{3;k';k}^s \equiv \left[\frac{F^s}{2\omega L^3}\left(-\frac{2}{3} + \frac{1}{1+[1+\mathcal{K}_{22}^s G^s]^{-1}\mathcal{K}_{22}^s F^s}\right)\right]_{k';k}\,. \tag{137}$$

Thus in this approximation, there are $(N+1)^2$ unknown elements of $\mathcal{K}_{\mathrm{df}}$, a complete determination of which would require determining the same number of energy levels. Assuming this has been achieved, the relations of Sec. III A that give $\mathcal{M}$ in terms of $\mathcal{K}_{\mathrm{df}}$ still hold, except that now all the previously implicit spherical harmonic indices are all set to zero.

Secondly, we consider the simplest possible case, referred to in Refs. [29, 30] as the isotropic approximation. In this approximation all components of $\mathcal{K}_{\mathrm{df}}$ are constant functions of the momenta of the incoming and outgoing particles. Compared to the s-wave-only limit discussed above, here we make the additional assumption that $\mathcal{K}_{23}$, $\mathcal{K}_{32}$ and $\mathcal{K}_{\mathrm{df},33}$ have the same values for all choices of the spectator momentum, i.e. are constant functions of these coordinates

$$\mathcal{K}_{23}^{\mathrm{iso}} = \mathcal{K}_{23;00;k00}\,, \tag{138}$$

$$\mathcal{K}_{32}^{\mathrm{iso}} = \mathcal{K}_{32;k'00;00}\,, \tag{139}$$

$$\mathcal{K}_{\mathrm{df},33}^{\mathrm{iso}} = \mathcal{K}_{\mathrm{df},33;k'00;k00}\,, \tag{140}$$

for all spectator momenta. Within this approximation, Eq. (129) simplifies further to

$$(1+F_2^s\mathcal{K}_2^s)(1+F_3^{\mathrm{iso}}\mathcal{K}_{\mathrm{df},33}^{\mathrm{iso}}) = F_2^s F_3^{\mathrm{iso}}\mathcal{K}_{32}^{\mathrm{iso}}\mathcal{K}_{23}^{\mathrm{iso}}\,, \tag{141}$$

where

$$F_3^{\mathrm{iso}} \equiv \sum_{k',k} F_{3;k';k}^s\,. \tag{142}$$

Additional simplifications to the relation between $\mathcal{K}_{\mathrm{df}}$ and $\mathcal{M}$ also occur, but we do not give these explicitly as they are simple generalizations of those derived in Ref. [30].

It is worth noting that Eq. (141) resembles the expression for two coupled two-particle channels each projected to a single partial wave [7, 12, 13]. In the limit that the $\mathbf{2} \leftrightarrow \mathbf{3}$ coupling vanishes, one recovers the spectrum for s-wave two-particle states together with that obtained in Ref. [29] for three-particle states in the isotropic approximation. Turning on the two-to-three coupling then shifts the levels and also splits the degeneracies between two- and three-particle states for volumes where they happen degenerate, as is qualitatively illustrated in the rightmost panel of Fig. 2.

V. CONCLUSIONS AND OUTLOOK

In this paper we have obtained the finite-volume quantization condition for a general theory of identical scalar particles, in the regime where both two- and three-particle states contribute ($3m < E^* < 4m$). At this stage, the most important remaining restriction is that the two-particle K-matrix, $\mathcal{K}_2$, cannot have a singularity on the real axis in our kinematic regime. This is an important limitation as there are many examples of interesting three-particle systems in particle and nuclear physics where $\mathcal{K}_2$ does have such poles, due to the presence of a narrow resonance. Nevertheless, the extension to allow both two- and three-particle channels simultaneously is a necessary advance, as $\mathbf{2} \leftrightarrow \mathbf{3}$ transitions occur in many phenomenologically interesting systems.

Significant work is still required in order to make the formalism into a practical tool for numerical lattice QCD. In addition to the inclusion of singularities in $\mathcal{K}_2$, the quantization condition must be generalized to nonidentical particles, and to particles with intrinsic spin. This will then allow the application to the Roper resonance, for example, which has a significant branching fraction into $N\pi\pi$. We expect that the latter two generalizations will be relatively straightforward, based on the experience with two particles. For the same reason, we also expect the generalization to multiple two- and three-particle channels to be straightforward. We are working on all of these generalizations.

The methodology adopted here differs from that used in previous field-theoretic derivations of quantization conditions (e.g. that of Ref. [29]) because it relies on time-ordered perturbation theory in an essential way. This approach has the advantage that it appears to naturally generalize to four or more particles. While such a generalization seems quite ambitious at present, it is our ultimate goal as it will allow us to completely establish the relation between finite-volume energies and scattering observables. This in turn will allow us to study a large variety of hadronic resonances that decay into many-particle final states.

One result that we find surprising concerns the transformation, under time-reversal, of the auxiliary amplitude $\mathcal{K}_{\text{df}}$. As shown in Appendix D, $\mathcal{K}_{\text{df}}$ has exactly the same transformation properties as $\mathcal{M}$. The complicated construction of $\mathcal{K}_{\text{df},3}$, described in Ref. [29] for the case of no mixing with two-particle channels, and carried over here to the case where two-to-three mixing does occur, includes a choice of ordering of loop integrals that seems to violate time-reversal. Nevertheless, any such violation must be canceled by the "decorations" that must be applied to obtain the final form. Thus $\mathcal{K}_{\text{df}}$ has properties that are closer to those of $\mathcal{M}$ than previously expected.

One property that $\mathcal{K}_{\text{df}}$ does not share with $\mathcal{M}$ is Lorentz invariance. Our derivation violates manifest Lorentz invariance since it uses time-ordered perturbation theory. Nevertheless, as in the case of time-reversal symmetry, it could have been the case that, at the end of the analysis, $\mathcal{K}_{\text{df}}$ turned out to be Lorentz invariant. In fact, it nearly does. Looking at the relations in Sec. III, one finds that the only violation of Lorentz invariance comes from the denominator in G^∞ [see Eq. (88)]. The factor of $\omega_{Pkp}(E - \omega_k - \omega_p - \omega_{Pkp} + i\epsilon)$ is manifestly noninvariant.[13] We are investigating an alternative, Lorentz-invariant definition of $\mathcal{K}_{\text{df},3}$, but save the details for a future publication.

Finally, we highlight another feature of our formalism that deserves to be better understood. This concerns what happens when E^* passes through the three-particle threshold at $E^* = 3m$. When we are sufficiently far below this threshold, the two-particle analysis should be valid leading to the quantization condition $\det(1 + F_2\mathcal{K}_2) = 0$. However, as stressed earlier, we can also use our more general approach in this regime, and it should lead to the same answer. This equality is not, however, manifest. The issue is that $\mathcal{K}_{22}$ does not coincide with the standard two-particle K-matrix, even below three-particle threshold. To study the subthreshold behavior of $\mathcal{K}_{22}$ one must use its relation to the standard two-particle scattering amplitude given by Eqs. (103) and (109). It should then be possible to express the quantization condition as the vanishing of $\det(1 + F_2\mathcal{K}_2)$, up to corrections that vanish in the infinite-volume limit. We expect the latter to scale as $e^{-c\kappa_3 L}$ where κ_3 is a momentum scale related to the distance to three-particle threshold and c a constant of $\mathcal{O}(1)$.

Acknowledgments

RAB acknowledges support from U.S. Department of Energy contract DE-AC05-06OR23177, under which Jefferson Science Associates, LLC, manages and operates Jefferson Lab. SRS was supported in part by the United States Department of Energy grant DE-SC0011637.

---

[13] The remaining factors in G^∞ are invariant as they always refer to the CM frame of the nonspectator pair. Were it not for the form of the denominator, $\mathcal{L}_3^{(u,u)}(\vec{p},\vec{k})2\omega_k$ and $2\omega_p\mathcal{R}_3^{(u,u)}(\vec{p},\vec{k})$ would be Lorentz invariant, as would $\mathcal{D}_3^{(u,u)}$, and this would carry over to $\mathcal{K}_{\text{df}}$, because all integrals would then be over Lorentz invariant phase space.

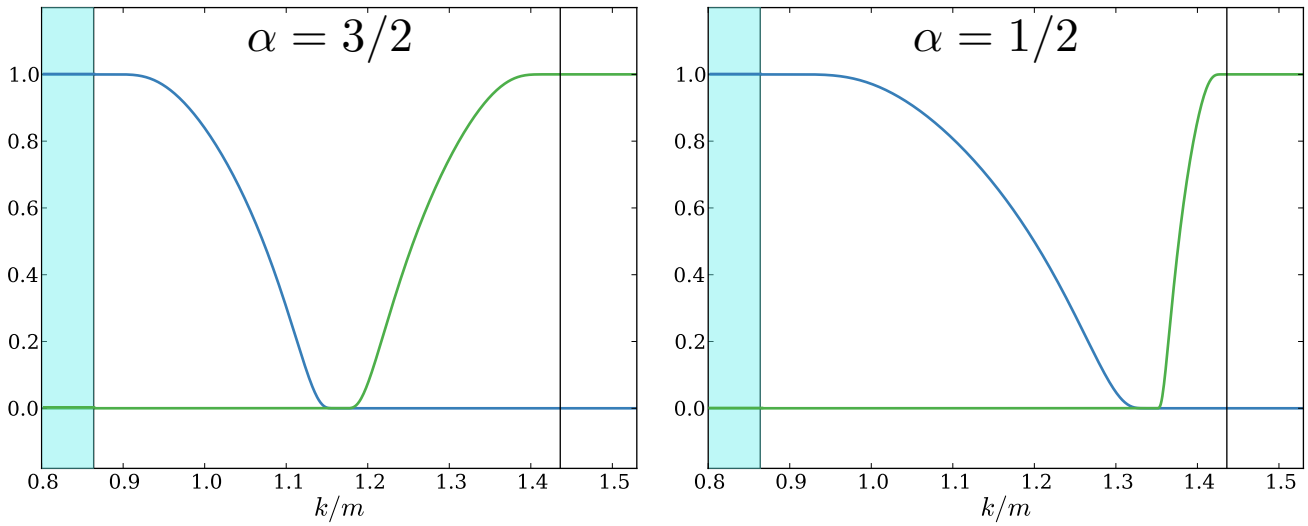

FIG. 6: $H(\vec{k})$ (falling, blue) and $H_2(\vec{k})$ (rising, green) as a function of $k = |\vec{k}|$ for $\vec{P} = 0$ and $E = E^* = 3.5m$. (For $\vec{P} = 0$, H and H_2 depend only on the magnitude of $\vec{k}$.) The shaded region on the left and the vertical line on the right indicate where on-shell states can occur. (The vertical lines indicate where on-shell states can occur.) For all of the shaded region on the left, k is small enough that the non-spectator pair in the three particle state can be on shell $[E^*_{2,k} \geq 2m \implies H(\vec{k}) = 1]$. Similarly, the right line indicates the k value for which $E = 2\omega_k$, i.e. the value where the two-particle state goes on-shell $[2\omega_k \geq E^* \implies H_2(\vec{k}) = 1]$. In the left plot we see that $\alpha = 3/2$ gives the same characteristic width to both cutoff functions (and thus similar finite-volume effects). In the right plot $\alpha = 1/2$ broadens $H(\vec{k})$, but at the expense of narrowing $H_2(\vec{k})$, leading to enhanced finite-volume effects from the latter.

Appendix A: Details of the smooth cutoff functions

In this appendix we give an explicit example of the smooth cutoff functions used in the main text. These must satisfy the symmetry properties of Eqs. (33) and (34), the "non-overlap" property of Eq. (35), and must equal unity when the particles are on shell.

Our example uses the interpolating function $J(x)$ introduced in Ref. [37]. This vanishes for $x \leq 0$, equals unity for $x \geq 1$, and interpolates smoothly in between. A specific example of such a function is

$$J(x) \equiv \begin{cases} 0\,, & x \leq 0\,; \\ \exp\left(-\frac{1}{x}\exp\left[-\frac{1}{1-x}\right]\right)\,, & 0 < x < 1\,; \\ 1\,, & 1 \leq x\,, \end{cases} \tag{A1}$$

but our formalism works for any J that satisfies the key property of being smooth for all x.

Our example for the three-particle cutoff function is then given by

$$H_3(\vec{k}, \vec{a}) = H(\vec{k})H(\vec{a})H(\vec{b}_{ka})\,, \tag{A2}$$

where $\vec{b}_{ka} = \vec{P} - \vec{k} - \vec{a}$, and

$$H(\vec{k}) = J(z_3)\,, \qquad z_3 = \frac{E^{*2}_{2,k} - (1+\alpha)m^2}{(3-\alpha)m^2}\,. \tag{A3}$$

Here α is a parameter satisfying $-1 < \alpha < 3$ that we discuss in more detail below. The value $\alpha = -1$ corresponds to the cutoff used in Refs. [31, 37], but here we need a more general form.

To understand Eqs. (A2) and (A3), recall that $E^{*2}_{2,k} = (E - \omega_k)^2 - (\vec{P} - \vec{k})^2$ is the energy of the nonspectator pair in their CM frame, assuming that the spectator is on shell. If all three particles are on shell, it follows that $E^{*2}_{2,k} \geq 4m^2$. In this case, $z_3 \geq 1$ (with $z_3 = 1$ at threshold for the nonspectator pair, $E^{*2}_{2,k} = 4m^2$) and so $H(\vec{k}) = 1$. Similarly, the

other two H functions equal unity. Thus $H_3 = 1$ if all three particles are on shell.[14] Now consider changing $\vec{k}$ (with E and $\vec{P}$ fixed) such that $E^{*2}_{2,k}$ drops below $4m^2$. Then z_3 drops below unity, and $H(\vec{k})$ falls smoothly, vanishing when $E^{*2}_{2,k}$ reaches $(1+\alpha)\,m^2$, and staying zero thenceforth. Because of the symmetric product in Eq. (A2) it follows that H_3 vanishes when any nonspectator pair has a CM squared energy that lies $(3-\alpha)\,m^2$ below threshold. We stress that H_3 will also vanish when, with fixed E and $\vec{P}$, any of the three momenta becomes sufficiently large. Thus H_3 acts as a UV cutoff.

We next describe our example for the two-particle cutoff function, $H_2(\vec{p})$. This depends only on a single momentum, since the momentum of the second particle is fixed to $\vec{b}_p \equiv \vec{P} - \vec{p}$. The aim of H_2 is to ensure that, if either $\vec{p}$ or $\vec{b}_p$ is equal to one of the three-particle momenta $\vec{k}$, $\vec{a}$ or $\vec{b}_{ka}$, then $H_2(\vec{p})H_3(\vec{k},\vec{a}) = 0$. The motivation for this condition is discussed in the main text. We also need $H_2(\vec{p})$ to equal unity if both particles are on shell.

A solution to these conditions is

$$H_2(\vec{p}) = J(z_p)J(z_b)\,, \qquad z_p = \frac{E^{*,2}_{2,p} - (1+\alpha)m^2}{(-\alpha m^2)}\,, \qquad z_b = \frac{E^{*,2}_{2,b_p} - (1+\alpha)m^2}{(-\alpha m^2)}\,. \tag{A4}$$

Here α the same parameter as above, except now satisfying $0 < \alpha < 3$. In the two-particle case, $E^{*2}_{2,p}$ (given by the same expression as $E^{*2}_{2,k}$ except with k replaced with p) is the invariant mass-squared of the particle with momentum $\vec{b}_p$, assuming that with momentum $\vec{p}$ is on shell. Similarly, E^{*2}_{2,b_p} is the invariant mass-squared of the particle with momentum $\vec{p}$ if that with momentum $\vec{b}_p$ is on shell. In general these two invariant masses are different. One case when they are the same is if both particles are on shell, in which case $E^{*2}_{2,p} = E^{*2}_{2,b_p} = m^2$. Then $z_p = z_b = 1$, so that $H_2 = 1$, as required.

Now we consider what happens to H_2 as we vary $\vec{p}$ away from a value leading to two on-shell particles. If $E^{*2}_{2,p}$ decreases below m^2, then $J(z_p)$ remains equal to unity. If, instead, $E^{*2}_{2,p}$ increases above m^2, then $J(z_p)$ decreases, vanishing for $E^{*2}_{2,p} \geq (1+\alpha)m^2$. Thus H_2 vanishes when either $E^{*2}_{2,p}$ or E^{*2}_{2,b_p} reaches $(1+\alpha)m^2$, i.e. when one of these invariant mass-squareds lies αm^2 or more *above* threshold.

We can now see why $H_2H_3 = 0$ if one of the two-particle momenta equals one of the three-particle momenta. Consider first $\vec{k} = \vec{p}$, so that $E^{*2}_{2,k} = E^{*2}_{2,p}$. If $E^{*2}_{2,k} \leq (1+\alpha)m^2$ we have $H_2(\vec{p}) > 0$ and $H(\vec{k}) = 0$, while if $E^{*2}_{2,k} \geq (1+\alpha)m^2$ we have $H_2(\vec{p}) = 0$ and $H(\vec{k}) > 0$. $H_2H_3 \propto H_2(\vec{p})H(\vec{k})$ vanishes in either case. The symmetries of H_2 and H_3 ensure that this holds also if any other pair of two- and three-particle momenta are equal.

Finally, we argue that $\alpha = 3/2$ is a reasonable choice in order to minimize exponentially-suppressed finite-volume effects. Such effects are generated by the difference between a sum and an integral over the loop momenta with the integrand given by the cutoff functions multiplied by other smooth functions. Generically, from the Poisson summation formula, we know that the suppression falls as $\exp(-\Delta L)$, where Δ characterizes the size of the region over which the summand/integrand varies. Thus we want the cutoff functions to change from 0 to 1 over as large a region as possible. Here this leads to two conflicting conditions. From H_3, we want $(3-\alpha)m^2$ [the range of $E^{*2}_{2,k}$ over which the variation in $H(\vec{k})$ occurs] to be as large as possible, while from H_2 we want αm^2 to be maximized. The choice $\alpha = 3/2$ sets these two distances from threshold equal. We illustrate this optimization in Fig. 6.

We close this appendix by stressing that the forms we have given for H_2 and H_3 are far from unique. We think that these are reasonable, somewhat optimized choices, but in a practical application it would be worthwhile investigating other choices.

Appendix B: Detailed derivation of Eq. (42)

In this appendix we give the details of the derivation of the result Eq. (42) for the finite-volume correlator, $\mathcal{M}_L$. This replaces the naive analysis of Sec. II A. The outline of the new derivation has been sketched in Sec. II B. We break the derivation into seven steps.

---

[14] We note that the converse does not hold: $H_3 = 1$ does not imply that all three particles are on shell, as can be seen from the simple example of $\vec{P} = \vec{k} = \vec{a} = 0$ with $E > 3m$.

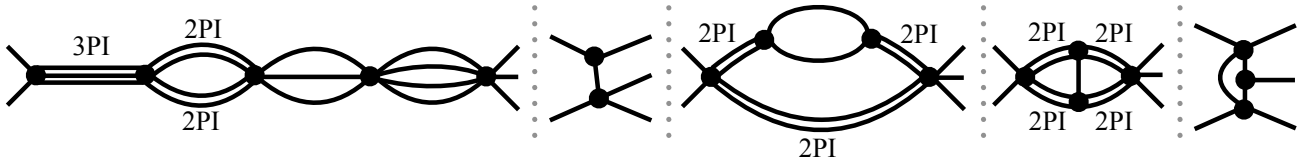

FIG. 7: Examples of diagrams contributing to $\mathcal{M}_{L,23}$, showing the three different types of dressed propagators, and the notation we use for them in subsequent diagrams. The details of the vertices are not specified—they are drawn from the interactions in Eq. (B1) having the appropriate number of fields. External propagators are amputated, and unlabeled propagators are fully dressed.

1. Diagramatic Expansion

The first step is the same as in the naive approach, namely to write out a perturbative expansion in Feynman diagrams for $\mathcal{M}_L$. This has been described in some detail in Sec. II A, and here we add a few further details.

We work with a general effective field theory (EFT) for our scalar field, with Lagrange density

$$\mathcal{L}(x) = \frac{1}{2}\phi(x)(\partial^2 + m^2)\phi(x) + \sum_{n=3}^{\infty} \frac{\lambda_n}{n!}\phi(x)^n + \sum_{n=3}^{\infty} \frac{g_n}{(n-1)!}[\partial^2\phi(x)]\phi(x)^{n-1} + \cdots + \frac{1}{2}(\delta Z_\phi)\phi(x)\partial^2\phi(x) + \frac{1}{2}(\delta Z_m m^2)\phi(x)^2 + \frac{\lambda_3}{3!}(\delta Z_{\lambda_3})\phi(x)^3 + \cdots . \quad \text{(B1)}$$

The first ellipsis indicates additional interactions containing more derivatives, and the second indicates the counterterms corresponding to all included vertices. We imagine regulating Feynman diagrams using, for example, dimensional regularization, and choose the counterterms so that, in the limit that the UV regulator is removed, all correlation functions are finite functions of the mass, m, and the coupling constants, $\lambda_n, g_n, \cdots$. We define δZ_ϕ and δZ_m so that m is the physical pole mass of the particle interpolated by ϕ and the pole has unit residue:

$$\frac{1}{i}\lim_{p^2\to m^2}(p^2 - m^2)\int d^4x\, e^{-ipx}\langle 0|\phi(x)\phi(0)|0\rangle = 1\,. \quad \text{(B2)}$$

We do not need to specify the precise definitions of the remaining counterterms—any scheme may be used, e.g. the $\overline{\text{MS}}$ scheme.

$\mathcal{M}_{L,ij}$ is formally defined as the sum of all connected finite-volume Feynman diagrams with j incoming and i outgoing legs, amputated and put on shell. As described in the main text, we use a diagram-by-diagram renormalization scheme in which the appropriate counterterm is combined with each divergent diagram. This implies, in particular, that the combination of each self-energy Feynman diagram with its counterterm satisfies the renormalization conditions of Eq. (14). How this generalizes when using TOPT will be discussed later.

As noted in the main text, we sum self energy insertions into dressed propagators of three different types, shown in Fig. 4. Here we describe in more detail where we use each type of dressed propagator. The underlying rule is simple: all cuts in which two or three particles can go on shell must be kept explicit. Here a cut must separate the diagram into two parts in the s-channel and pass through at least one propagator that is not external. If a particular propagator appears only in cuts with three or more particles, it can be fully dressed, i.e. composed of 1PI self-energies. This is because any cut through the self-energy loops would contain at least four particles. Similarly, if the propagator can appear in cuts with two particles, then it must be composed of 2PI self-energies (and thus be 2PI-dressed). Finally, if the propagator can appear in cuts with a single particle, then it must be composed of 3PI self-energies (and thus be 3PI-dressed).[15] These three cases are illustrated in Fig. 7. Further examples appear in Figs. 9(a) and 9(b) below.

An important observation is that all three types of dressed propagator have only exponentially suppressed volume dependence and thus can be replaced by their infinite-volume counterparts. This is because the loops appearing (implicitly) in these propagators lead to four- or higher cuts of the overall diagram, and thus do not have singularities in the kinematic range of interest. Thus the summands are smooth and the sum-integral difference is exponentially suppressed [see Eq. (17)].

---

[15] Note that it is not possible for a given propagator to appear in both two- and one-particle s-channel cuts, so that our classification here is unambiguous.

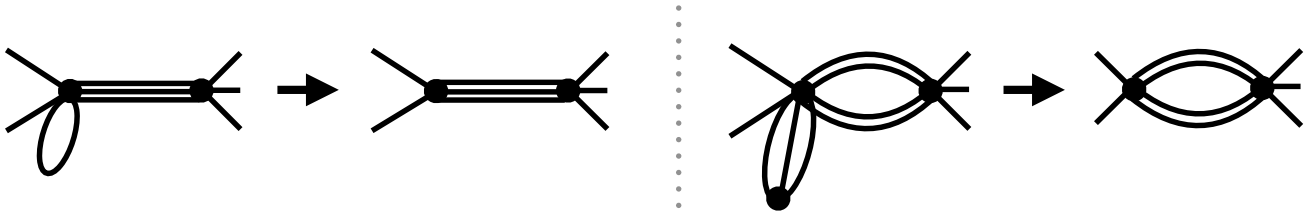

FIG. 8: Examples of tadpole diagrams and their absorption into the adjoining vertices, as described in the text. Notation for propagators is as in Fig. 7.

A final comment concerns "tadpole loops", i.e. loops through which no external four-momentum flows. Examples are shown in Fig. 8. Such loops do not lead to on-shell intermediate states precisely because no external momentum flows through the subdiagrams. They are thus uncuttable according to our rules. This is equivalent to the observation that the summands are nonsingular, so that the momentum sums can be replaced with integrals. In fact, from the point of view of determining finite-volume effects, we can simply absorb these loops (along with their [implicitly] associated counterterms) into the adjoining vertices. This reduction is illustrated in the figure.

2. Partial reduction of two-particle self-energy bubbles

We now depart from the approach used in Sec. II A. Rather than use TOPT immediately, we first sum up a class of Feynman diagrams. These are the diagrams that contain at least one 2PI-dressed propagator on which there is a self-energy insertion that is two-particle reducible. Examples are shown in Fig. 9(a), and we refer to them collectively as diagrams of class 2PI+. The challenge here is that all such diagrams have three-particle cuts that lead to finite-volume effects. We stress that diagrams containing 2PI-dressed propagators without additional self-energy insertions, such as those in Fig. 9(b), are not included in the 2PI+ class of diagrams. However diagrams containing at least one two-particle loop with a self-energy insertion, as well as some number of two-particle loops without insertions, are included in 2PI+.

We next use the function $H_2(\vec{p})$ (defined in Appendix A). For each diagram in class 2PI+, we multiply each two-particle loop containing at least one explicit two-particle self-energy insertion by

$$1 = H_2(\vec{p}) + [1 - H_2(\vec{p})]\,, \tag{B3}$$

and consider separately the H_2 and $1-H_2$ parts. Here $\vec{p}$ is the momentum of one of the propagators—we can use either of the two momenta in the loop as H_2 is symmetric. It is important that only one such factor is inserted in a given loop, irrespective of how many self-energy insertions are present. To illustrate these rules, we note that all of the diagrams of Fig. 9(a) except the last are multiplied by $H_2(\vec{p}) + [1-H_2(\vec{p})]$, while the last diagram is multiplied by $(H_2(\vec{p}) + [1-H_2(\vec{p})])(H_2(\vec{q}) + [1-H_2(\vec{q})])$. We stress that, in the latter case, the momenta $\vec{p}$ and $\vec{q}$ are independent.

For the remainder of this subsection we consider two-particle loops that have been multiplied by the H_2 part of Eq. (B3). The presence of H_2 leads to a key simplification: the sums inside all of the self-energies on the 2PI-dressed propagators can be replaced with integrals. This result holds because the function $H_2(\vec{p})$ only has support when the momenta in the three-particle state are far from going on-shell. To explain this, we consider the first diagram in Fig. 9(a). The three particles under consideration are are those with momenta labeled $\vec{a}$, $\vec{p}-\vec{a}$ and $\vec{b}_p = \vec{P} - \vec{p}$. We recall that the function $H_3(\vec{b}_p, \vec{a})$ has support in a region around the on-shell manifold (those values of $\vec{b}_p$ and $\vec{a}$ for which all three particles can go on shell) of characteristic width m. But, by construction, $H_2(\vec{p})H_3(\vec{b}_p, \vec{a}) = H_2(\vec{b}_p)H_3(\vec{b}_p, \vec{a}) = 0$, implying that $H_2(\vec{p})$ vanishes everywhere in this near-on-shell region. Thus $H_2(\vec{p})$ forces the momentum in the self-energy loops to be well away from their on-shell values, and thus well away from the $\mathcal{C}_3$ pole associated with a three-particle intermediate state.[16] The difference between momentum sums and integrals for such loops is therefore exponentially suppressed.

The self-energy insertions on the 2PI-dressed propagators can also contain loops with more than two particles. An example is the third diagram in Fig. 9(a). Since particles in such loops cannot go on shell (requiring an intermediate

[16] We stress that this is not a direct constraint on the momentum in the self-energy loop, i.e. on $\vec{a}$ in our example. This momenta is freely summed/integrated. The point is that, in the presence of $H_2(\vec{p})$, the summand does not come close to the three-particle singularity.

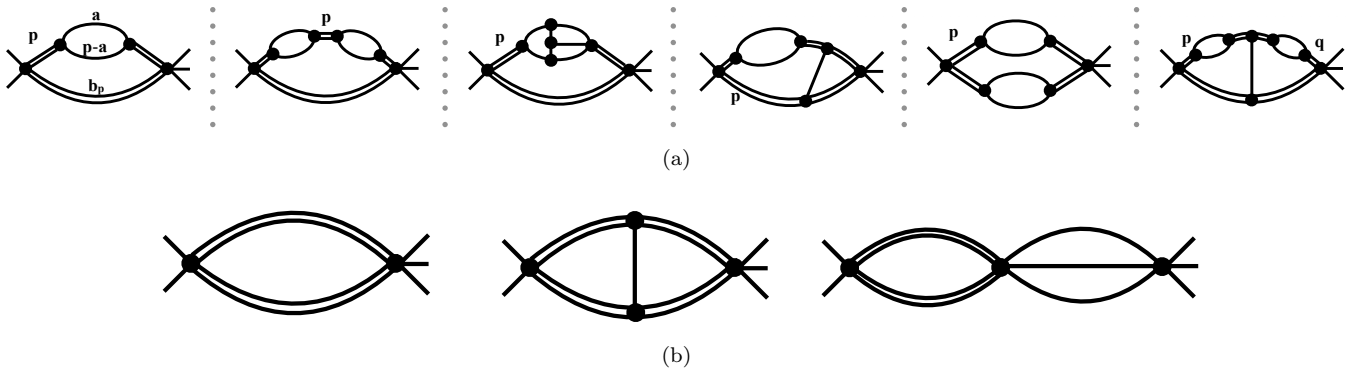

(a)

(b)

FIG. 9: (a) Examples of diagrams contained in the class 2PI+. 2PI-dressed propagators are shown by double lines, fully-dressed propagators by single lines. For each two-particle loop containing at least one self-energy insertion on a 2PI-dressed propagator, we multiply the loop by $H_2 + [1 - H_2]$, as described in the text. (b) Examples of diagrams not included in the set 2PI+.

state containing four or more particles for the complete diagram) the momentum sums in these loops can be also be replaced with integrals. Thus we find the result claimed above: the entire self-energy can be evaluated in infinite volume.

The resulting integrated self-energies are just particular examples of the quantities $D_i^R(p^2)$ discussed in the main text. In particular, since the diagrams are accompanied by counterterms that enforce the conditions of Eq. (14), we know that they vanish quadratically as one goes on shell:

$$D_i^R(p^2) \underset{p^2 \to m^2}{\longrightarrow} c(p^2 - m^2)^2 \,. \tag{B4}$$

Thus each self-energy cancels the poles from the 2PI-dressed propagators on either side. If there is a chain of self-energies then the poles are "overcanceled" leading to factors of $(p^2 - m^2)$ in the numerator. As a result, each 2PI-dressed propagator with self-energy insertions, in a cut that is accompanied by a factor of H_2, gives only short-distance contributions. We can implement this diagrammatically by shrinking the propagator to a new effective vertex, as shown in Fig. 10. This vertex is complicated—possibly involving non-analytic functions of momenta and containing $H_2(\vec{p})$—but it satisfies the key property that it is "uncuttable". In other words, it is a smooth function of real three-momenta and thus cannot lead to important finite-volume effects, which is also true for vertices in general.

As shown in Fig. 10, shrinking propagators often leads to tadpole loops. These loops can then be absorbed into vertices, as discussed in the previous subsection.

The conclusion of this analysis is that we can effectively ignore self-energy insertions on 2PI propagators when the factor H_2 is present. They give rise to additional vertices, which are special in that they occur only in certain topologies of diagrams and contain factors of H_2. But since we are at no stage actually calculating the Feynman diagrams, the presence of new vertices does not lead to any change in the diagrams to be considered.[17]

In summary, the analysis of this subsection allows us to avoid one of the problems with the naive result (39), namely the fact that the quantity $\widetilde{A}$ does not contain all time-orderings needed to build up the full self-energy, and so the result behaves as $(p^2 - m^2)$ rather than the quadratic dependence of Eq. (B4). By working at this stage with Feynman diagrams we are, in effect, summing all the time-orderings, rather than the restricted set contained in $\widetilde{A}$.

---

[17] The only exception to the statement that no new diagrams need to be considered is that, after applying the shrinking procedure, there are diagrams in which some of the propagators are 2PI-dressed, whereas, if one applied the rules discussed in Appendix B 1, they would be fully dressed. An example is shown by the lower-left diagram in Fig. 10, where the bottom propagator in the left-most loop would be fully dressed according to the general rules, but is in fact 2PI-dressed. This exception has, however, no impact on determining finite-volume effects, as both types of propagator have the same pole and residue.

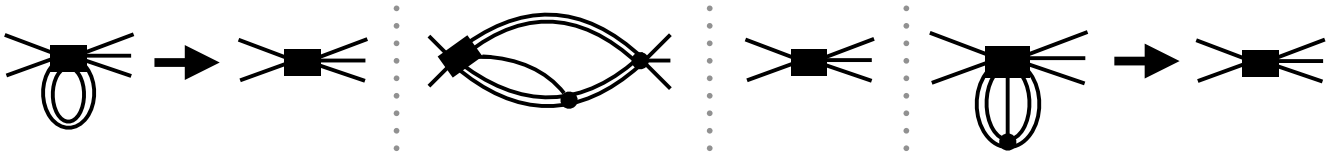

FIG. 10: Simplification of the class 2PI+ diagrams shown in Fig. 9(a) when the loops containing two 2PI-dressed propagators with self-energy insertions are multiplied by H_2. Propagators containing self-energy insertions are shrunk to new vertices, shown by the filled rectangles. The detailed form of the vertex represented by the rectangle depends on the diagram. The first three diagrams in Fig. 9(a) are all simplified to the same form, and thus only one diagram is shown. The remaining three are simplified in different ways. In a second step, indicated by the arrows, tadpole diagrams are absorbed into the vertices.

3. Shrinking 3PI-dressed propagators

The second problem mentioned at the end of Sec. II A in the main text concerned contributions to $\mathcal{M}_L$ that involve 3PI-dressed propagators. In this section we describe the problem in more detail and then explain how it can be avoided by shrinking all 3PI-dressed propagators down to local vertices.

The problem arises once we switch from working with Feynman diagrams to using TOPT (a change that is discussed more extensively in Appendix B 5 below). We then discover that certain time-orderings of diagrams containing 3PI-dressed propagators have spurious three-particle intermediate states. Two examples are shown in Fig. 11. These are contributions to TOPT that have poles of the form $(E - \sum_{i=1,3} \omega_i)^{-1}$ and thus, in general, contribute to the kernels A introduced in Sec. II A. These poles are spurious, however, because they cancel in the full Feynman diagrams. This is clear in the examples shown because one can factorize the corresponding Feynman diagrams into a product of loops and propagators and the singularities arise only from these individual factors, and not from overlapping cuts such as those shown.

In principle one could continue with the TOPT analysis, keeping track of these spurious contributions until they cancel in the end. This is difficult, however, as they contain disconnected contributions involving Kronecker-deltas. A better solution is to avoid these contributions from the beginning. This is possible due to the fact that there are no on-shell intermediate states that involve the 3PI-dressed propagators in our kinematic range. This is apparent from the initial Feynman diagram in which each 3PI-dressed propagator appears factorized from the remainder of the diagram, and has singularities only at $E^* = m$ and $E^* \geq 4m$. Thus the 3PI-dressed propagators are uncuttable. They are also functions only of the fixed external four-momentum, $(E, \vec{P})$, and are thus themselves fixed. It follows that, from the point of view of determining finite-volume dependence, we can shrink them into the adjoining vertices. With this done, none of the spurious cuts remain. In the following we assume that such a procedure has been employed.

4. Classification of remaining loops

At this stage it is useful to take stock of the types of Feynman diagrams that remain after propagators and tadpole diagrams are shrunk as described above. The remaining diagrams contain only fully dressed and 2PI-dressed propagators, and are built from overlapping loops that fall into the four classes:

1. Loops containing a pair of 2PI-dressed propagators, on which there are no self-energy insertions. Examples are shown in Fig. 9(b). These loops are, at this stage, not multiplied by factors containing H_2.

2. Loops containing a pair of 2PI-dressed propagators in which at least one of these propagator has a self-energy insertion. Such loops are contained in diagrams of class 2PI+ (see Fig. 9(a)). All such loops are multiplied by $[1-H_2(\vec{p})]$. The presence of this factor implies that these loops cannot give rise to two on-shell particles, but do give rise to three particles that all go on shell.

3. Loops that include sets of three particles that carry the total energy and momentum $(E, \vec{P})$ (and can thus simultaneously go on shell) but are not included in the previous class. Examples are shown in Fig. 12(a).

4. Loops that give rise to no on-shell intermediate states, either because four or more particles carry the total energy and momentum or because the loops are in a t-channel-like structure and thus do not carry the total energy-momentum that flows through the diagram. Examples are shown in Fig. 12(b).

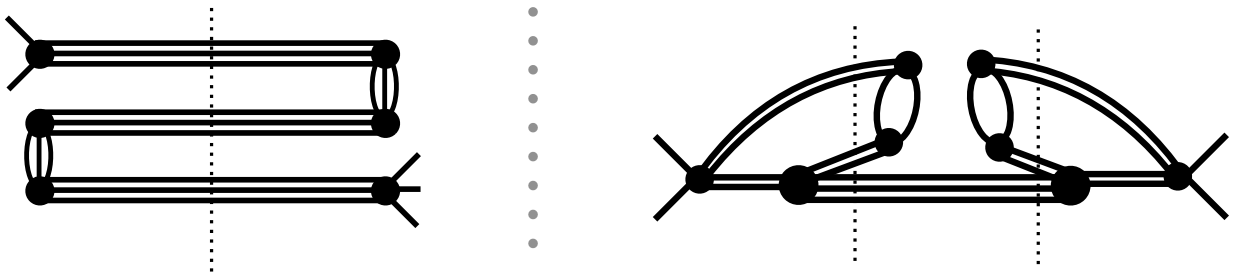

FIG. 11: Examples of spurious three-particle intermediate states arising when applying TOPT to diagrams involving 3PI-dressed propagators.

The overall result is that we have removed all appearances of self-energy diagrams except where they are needed because a physical on-shell cut can run through them, i.e. in loops of class (2).

Finally, we observe that, because loops overlap, there is not a one-to-one correspondence between loops and cuts. This is illustrated in Fig. 13. As a result, we cannot study individual loops, or even finite sets of loops, and determine the important finite-volume effects. Indeed, in general, the singularity structure of a given diagram is quite complicated. Since finite-volume dependence arises from two- and three-particle cuts, what we need is a tool for breaking diagrams into multiple terms that individually contain a specific sequence of cuts. This can be done straightforwardly using TOPT, to which we now turn.

5. Applying time-ordered perturbation theory

At this stage we break up the Feynman diagrams into their component time-orderings. This can be achieved by evaluating all energy integrals, and then partial fractioning the resulting products of poles. A more direct method is to evaluate the Feynman diagrams using a mixed time-momentum representation for the propagators, and then do the time integrals.[18] The result—the TOPT expression—is a sum of terms each of which depend only on spatial momenta. Since we work in finite volume, these momenta are summed over the finite-volume discrete set.

Our application of TOPT is slightly complicated by our use of dressed propagators. We first describe the approach ignoring this complication, i.e. using bare propagators, and then return to the complications introduced by dressing. Consider a Feynman diagram with some number of on-shell, amputated external legs and with total energy-momentum $(E, \vec{P})$ flowing from the initial to the final state. One then enumerates all ordered sequences of vertices in the diagram between the initial and final states.[19] Each individual ordering represents a mathematical expression determined as follows. (1) Route a vertical line (i.e. a "cut", c) between each pair of consecutive vertices in the ordering. (2) Define the factor $\sum_{i\in\{c\}}\omega_i$, given by summing all of the on-shell energies of the propagators intersecting the cut. (3) Calculate the product

$$\mathcal{P}_o = \prod_{c\in\{o\}} \left(\frac{1}{E - \sum_{i\in\{c\}}\omega_i} \right) , \tag{B5}$$

where o denotes a particular ordering, $\{o\}$ denotes the set of cuts within the ordering, and c denotes a particular cut. (4) Multiply $\mathcal{P}_o$ by a factor of $1/(2\omega_j)$ for each internal propagator, and by the expressions arising from each vertex, as well as possible $1-H_2$ and symmetry factors. This leads to the expression for the n-cut factor $\mathcal{C}_n$ given in Eq. (15). Summing over all orderings then gives the value of the Feynman diagram. Examples of time-orderings are shown in Fig. 5.

As noted in the main text, when we apply TOPT in the kinematic range given in Eq. (8), the only singularities that can appear are the poles due to two- and three-particle intermediate states, given in Eq. (16). Finite-volume

---

[18] For a lucid explanation of this method, see Ref. [38].

[19] The requirement that all vertices must lie *between* the inital and final states is a consequence of having on-shell, amputated external propagators. One can think of this as occuring because the initial particles are created at $t = -\infty$ and the final particles destroyed at $t = \infty$.

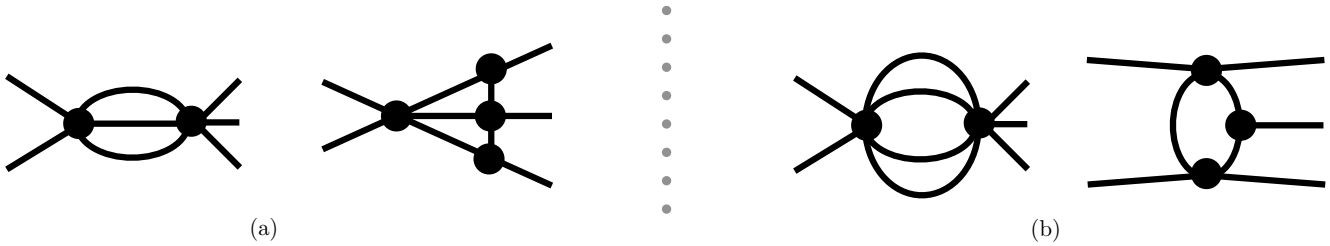

(a) (b)

FIG. 12: Examples of the (a) third and (b) fourth classes of loops that arise after shrinking propagators and tadpole loops. See the numbered list in the text for details.

effects arise only from momentum sums that run over one or both of these poles. All other sums can be converted to integrals.

The above discussion assumes a propagator $i/(p^2 - m^2 + i\epsilon)$, which does not hold for the dressed propagators. Given the renormalization conditions of Eq. (14), however, both types of dressed propagator do have exactly this pole structure, including the residue, for $p^0 \to \omega_p$. The effect of dressing appears only in the constant and in terms of $\mathcal{O}(p^2 - m^2)$, but such terms can be absorbed into the vertices as long as they remain smooth within our kinematic range. Since the vertices are general, this leads to no additional complications. Then it is legitimate to use TOPT ignoring the fact that the propagators are dressed. This means that the distinction between fully- and 2PI-dressed propagators is no longer relevant.

The remaining issue is thus whether there are additional singularities in the dressed propagators within our kinematic range ($E^* < 4m$). The fully dressed propagator has a two-particle cut, while the 2PI-dressed propagator has a three-particle cut. However, by construction, these both correspond to cuts with four or more particles in the full diagram. Thus these singularities do not appear within our kinematic range.

A final technical complication concerns counterterms in TOPT. When we break up a UV divergent loop into its various time-orderings we also need to break up the counterterms accordingly. An example is given by the self-energy loop in the center of the diagrams of Fig. 5: its two vertices have different time-orderings in the two diagrams, and these are separately UV divergent. In fact, in general, since we have broken Lorentz symmetry in TOPT, the individual counterterms needed for the different time-orderings will not be Lorentz invariant. Lorentz invariance is regained only at the end when all time-orderings are recombined. In practice, one can always define the counterterms operationally for each time-ordering by using dimensional regularization and removing the pole with a prescription such as $\overline{\text{MS}}$ (up to finite corrections needed to satisfy renormalization conditions discussed previously).

In summary at this stage we have reduced every Feynman diagram to a sum of terms each given by products of smooth functions and two- and three-particle poles. Thus $\mathcal{M}_L$ can be written in the form given in Eq. (18) of the main text, except that the kernels between two- and three-cuts are now different.[20] These differences are due to the presence of factors of $[1-H_2]$ in diagrams with self-energy insertions, to the absence of 3PI-dressed propagators, and to the alterations in vertices arising from the shrinking procedure and from the tadpole loops and other smooth terms that have been absorbed.

In what follows we denote the coordinates that appear in the two- and three-particle poles as "explicit" whereas all coordinates that are integrated at this stage are buried inside various smooth functions and are thus referred to as "implicit". Note that all $H_2(\vec{p})$ functions at this point are implicit with the exception of the $[1-H_2(\vec{p})]$ factors accompanying the two- and three-particle poles in class (2) loops.

6. Introduction of regulator functions on cuts

The next step is, as in Sec. II A, to multiply each two- and three-cut by unity written, respectively, as Eq. (B3) and

$$1 = H_3(\vec{k}, \vec{a}) + [1-H_3(\vec{k}, \vec{a})]\,. \tag{B6}$$

[20] Strictly speaking, we need to show that kernels that appear are independent of their position in the chain of terms in Eq. (18). We return to this issue below.

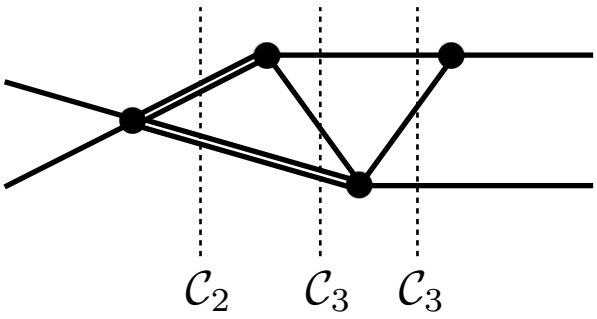

FIG. 13: Example of a diagram with overlapping loops. The possible two- and three-particle cuts are shown. The central cut is not associated uniquely to a single loop.

The momenta here are the explicit summed coordinates appearing in the cut factors. The only difference compared to the main text is that here we do not make this substitution in the two-cuts in class 2 loops, since these loops already come with a factor of $[1-H_2(\vec{p})]$.

Having made these substitutions we then consider the parts containing H_i and $1-H_i$ separately, so that the cuts that arise are $\mathcal{C}_2^H$, $\mathcal{C}_2^\infty$, $\mathcal{C}_3^H$, $\mathcal{C}_3^\infty$ and higher-order cuts. [See Eq. (37) for the definitions of these cuts.] At this stage singularities arise only from factors of $\mathcal{C}_2^H$ or $\mathcal{C}_3^H$. All other possibilities do not have poles within our kinematic regime. This implies that any loop momentum that does not appear in either a $\mathcal{C}_2^H$ or $\mathcal{C}_3^H$ can be integrated rather than summed.

We can now make use of the important result that, whenever a two-cut and a three-cut share a common propagator, then $H_2H_3=0$ (as described in Appendix A). In Sec. II A, we used this result to drop disconnected parts from $\widetilde{A}_{23}$ and $\widetilde{A}_{32}$. Here we apply it at a slightly earlier stage. The aim is to come up with a version of Eq. (39) which does not suffer from the problems described in the main text.

To see how this works we consider three examples, given in Figs. 14 and 15. These show how a particular time-ordering is reduced to a product of smooth kernels and regulated cut factors, $\mathcal{C}_2^H$ and $\mathcal{C}_3^H$. Figure 14(a) shows a diagram containing a class 2 loop. We recall that, although two-cuts appear in the TOPT expression, the factor of $1-H_2$ cancels the poles.[21] Now we insert the identity (B6) on the three-cut, leading to the two diagrams on the right-hand side of the equality. For that containing H_3, we use $H_2(\vec{p})H_3(\vec{p},\vec{a})=0$ to drop the factor of H_2, as shown.[22] In other words, the presence of the H_3 in $\mathcal{C}_3^H$ is sufficient to ensure that there are no on-shell two-cuts. Thus we can decompose this diagram in the form shown on the second line, with two smooth kernels and a single pole factor.

The diagram containing $1-H_3$ is simpler to analyze. Since both two- and three-particle poles are canceled, the two loop sums have smooth summands, and can be converted into integrals. Thus this contribution has no pole, and gives only a smooth kernel. It is important to note that the $1-H_2$ factor, which remains for this time-ordering, is not associated with the left-hand cut, but rather with the entire outer loop.

We now turn to Fig. 14(b), which is a different time-ordering of the diagram in Fig. 14. In this case there are no cuts that require the use of the identities in Eqs. (B3) and (B6). All cuts are nonsingular in our kinematic region (the two-cuts due to the factor of $1-H_2$, and the 5-cut due to the kinematic constraints), and so both loop sums can be replaced by integrals, leading to a contribution to the kernel B_{22}.

Finally, we consider Fig. 15, which is one time-ordering of the diagram with overlapping class 1 and class 3 loops shown in Fig. 13. It thus comes with no explicit factors of H_i, and we must insert the identities of Eqs. (B3) and (B6) on all three cuts. This leads to 2^3 terms, but only the three shown survive. This reduction occurs as follows. Because the rightmost two-particle state is on-shell, we know that the three particles present in the adjacent three-cut cannot all simultaneously go on shell, as they share an unscattered particle. This already tells us that only 2^2 terms will be nonzero. In other words, the right-hand cut cannot have a factor of H_3, so only the $1-H_3$ factor survives for this cut, and furthermore we can set $1-H_3\to 1$.

A further reduction occurs if we choose H_2 for the left-hand cut, for then the middle cut cannot have a factor of H_3. If the left-hand cut has a factor of $1-H_2$, however, then the middle cut can contain either H_3 or $1-H_3$, as

---

[21] A single factor of $1-H_2$ can cancel any number of poles since it has an essential zero at the pole.

[22] The fact that the H_2 can be dropped means that we do not have to worry about distributing the $1-H_2$ factor between the kernels B_{23} and B_{32} on either side of the three-cut. This is important since we want to treat all such kernels in a consistent manner.

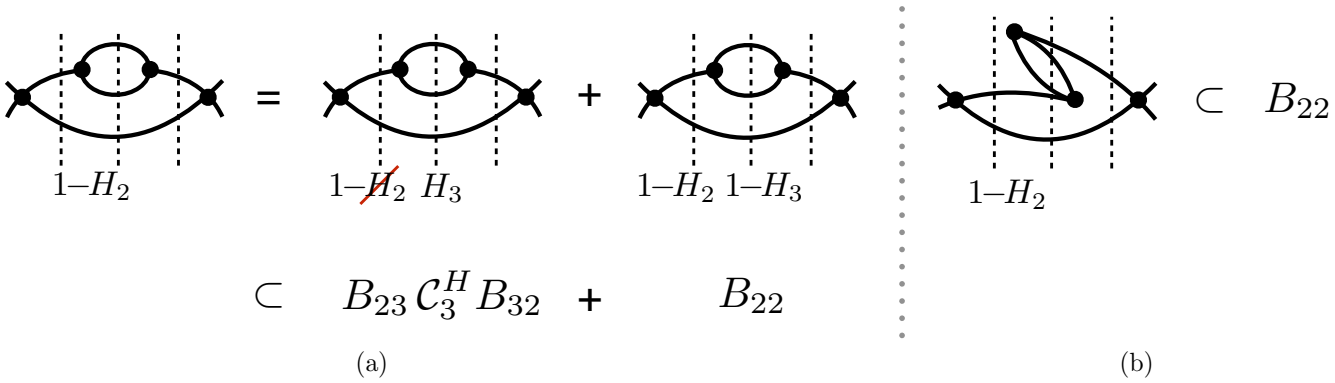

FIG. 14: (a) The reduction procedure for one time-ordering of a diagram with a class 2 loop. Vertical dashed lines indicate n-cuts. Fully dressed and 2PI-dressed propagators are both shown by single lines, because the singularities arise only from the pole parts of these propagators, which are identical. The factor of $1-H_2$ is associated with the entire loop, and not with a particular cut. (b) Shows the reduction procedure for a different time-ordering. See text for detailed discussion.

shown. In the former case, the H_2 in the left-hand cut can be dropped. The net result is that there are only three diagrams. These give the kernel and cut-factors shown in the figure, where all momentum sums within the kernels can be replaced by integrals.

We can make several important general observations from these examples. First, the off-diagonal kernels B_{23} and B_{32} produced by this reduction *do not have disconnected contributions*. This is simply because such contributions necessarily come with a factor of $\mathcal{C}_2^H\mathcal{C}_3^H \propto H_2H_3$ which vanishes when one propagator is unscattered. Thus, unlike in the naive approach of Sec. II A, where $\widetilde{A}_{23}$ and $\widetilde{A}_{32}$ had disconnected contributions that could be dropped, here the corresponding kernels simply do not have such contributions.

The second observation is that *there are no disconnected contributions to B_{22}*. Such contributions arise in the naive method of Sec. II A from diagrams involving self-energy insertions such as Fig. 14. For example, in Fig. 14(b), the loop lying between the two-cuts gives a disconnected contribution to A_{22}. Here, however, all such contributions are avoided because of the presence of the factor of $1-H_2$ (and the renormalization scheme chosen), which cancels the poles in the two-cuts.

The third observation is that *the kernel B_{33}, unlike the other components of B, can have disconnected parts.* An example where this arises is shown in Fig. 16. A disconnected contribution occurs in the first diagram on the right-hand side of the equality, arising from a $2 \leftrightarrow 2$ scattering. The explicit form of the disconnected part is shown in Eq. (C22) below. Note that completely disconnected parts cannot occur because there must be a vertex between the two cuts, and self-energy insertions are not allowed on fully dressed propagators.

The final observation is more technical, but nevertheless important for the following development. This is that *all factors of $1-H_2$ remaining after reduction lie within loops that are integrated.*[23] The observation can be demonstrated simply by noting that the loop momentum running through the $1-H_2$ cannot be shared with either a $\mathcal{C}_2^H$ or $\mathcal{C}_3^H$ cut. The former possibility is ruled out by the construction of Appendix B 2, in which only a single regulator function was applied to each two-particle loop. The latter is ruled out because, if a momentum is shared, then one can use the $H_2H_3 = 0$ identity to replace $1-H_2$ with 1. The importance of this observation can be seen most easily from the middle diagrams on the right-hand side of Fig. 16. Here the $1-H_2$ is not in an integrated loop, so there would be an ambiguity as to which two-cut it is attached. In fact, since $1-H_2$ can be replaced by 1, this problem is absent. In the right-hand diagram, where the $1-H_2$ remains, it can be unambiguously attached to the integrated loop as a whole. This means that there is a well-defined set of rules for assigning factors of $1-H_i$ to the diagrams contributing to the kernels.

---

[23] The same is not true of factors of $1-H_3$, which can appear in tree level contributions to B_{33}.

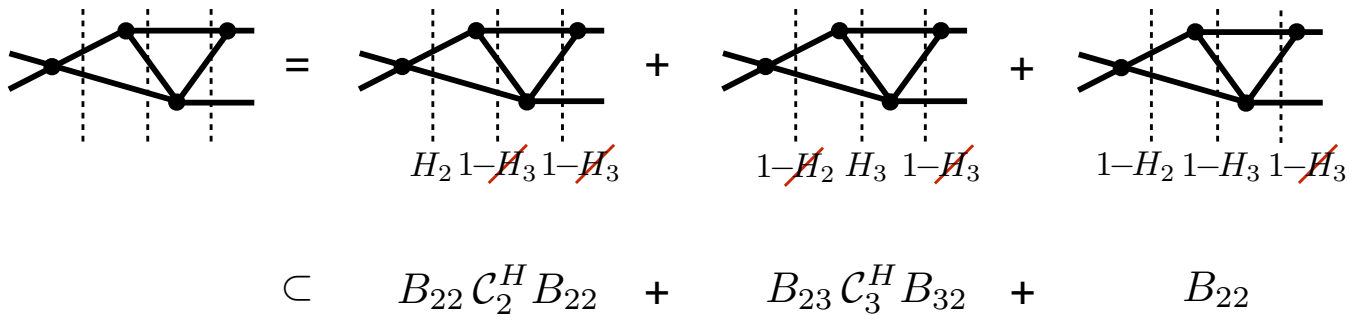

FIG. 15: The reduction procedure for one time-ordering of the diagram of Fig. 13. Notation as in Fig. 14. See text for detailed discussion.

7. Final summation

After following the steps described above we have decomposed $\mathcal{M}_L$ into the following sum of terms

$$\mathcal{M}_L = \sum_{n=1}^{\infty} \mathcal{M}_L^{(n)}, \tag{B7}$$

$$\mathcal{M}_L^{(n)} = \sum_{i\in\text{diagrams}} B^{(n,i;1)}\mathcal{C}^H B^{(n,i;2)}\mathcal{C}^H \cdots \mathcal{C}^H B^{(n,i;n-1)}\mathcal{C}^H B^{(n,i;n)}\,. \tag{B8}$$

Here we have reverted to the 2×2 matrix notation. The sum over i runs over all contributions (coming from the different time-orderings of all Feynman diagrams with all possible appearances of regulator factors after the reduction described above) containing $n-1$ factors of $\mathcal{C}^H$. From the previous section we know that the kernels $B_{22}^{(n,i;j)}$, $B_{23}^{(n,i;j)}$ and $B_{32}^{(n,i;j)}$ are connected, smooth, infinite-volume (L-independent) functions. The $B_{33}^{(n,i;j)}$, however, consist of a connected, smooth, infinite-volume part plus a term involving a Kronecker-delta and factor of L^3 multiplying a two-to-two smooth, infinite-volume kernel [as in Eq. (C22)].

The construction of the $B^{(n,i;j)}$ follows the rather involved steps described in the previous sections of this Appendix. What we show in this final section is that the sum over i in Eq. (B8) leads to the simple form[24]

$$\mathcal{M}_L^{(n)} + I^{(n)} = \underbrace{B\,\mathcal{C}^H B\,\mathcal{C}^H \cdots \mathcal{C}^H B\,\mathcal{C}^H B}_{n\ \text{kernels}}\,. \tag{B9}$$

Here $I^{(n)}$ contains only disconnected contributions. The key claim in this result is that the same kernels appear in all positions and for all values of n. Summing over n then leads to the claimed result, Eq. (42), with the full subtraction given by $I = \sum_{n=1}^{\infty} I^{(n)}$.

Before demonstrating Eq. (B9) we recall the need for the subtraction term $I^{(n)}$. We know from diagrams such as Fig. 16 that the kernel B must contain disconnected parts in the 33 component. If there were no subtraction in Eq. (B9), then $\mathcal{M}_L^{(1)}$ would equal B, and thus contain a disconnected part, which is inconsistent with its definition. In other words, in order for the same kernel B to appear in $\mathcal{M}_L^{(n)}$ for all n, a subtraction is required.

Before demonstrating Eq. (B9) we recall the need for the subtraction. This arises from a mismatch between the kernels appearing in $\mathcal{M}_L^{(1)}$ and those in the higher-order terms. The former must be connected (since $\mathcal{M}_L$ is) while those appearing in higher order terms must contain disconnected parts in the 33 component (in order to accommodate diagrams such as that in Fig. 16). In order to have a uniform definition of the kernel a subtraction is required.

To proceed we next give a precise definition of the kernel B. This is done by following exactly the same steps as described in the preceding subsections, but instead of starting with the fully connected $\mathcal{M}_L$, we allow also diagrams

[24] As discussed in the main text, this is a slight oversimplification, in that the matrix indices at the end of the chain are slightly different from those in the middle. As reiterated below, however, all the kernels B can be obtained from a single master function, analogous to that in Eq. (27).

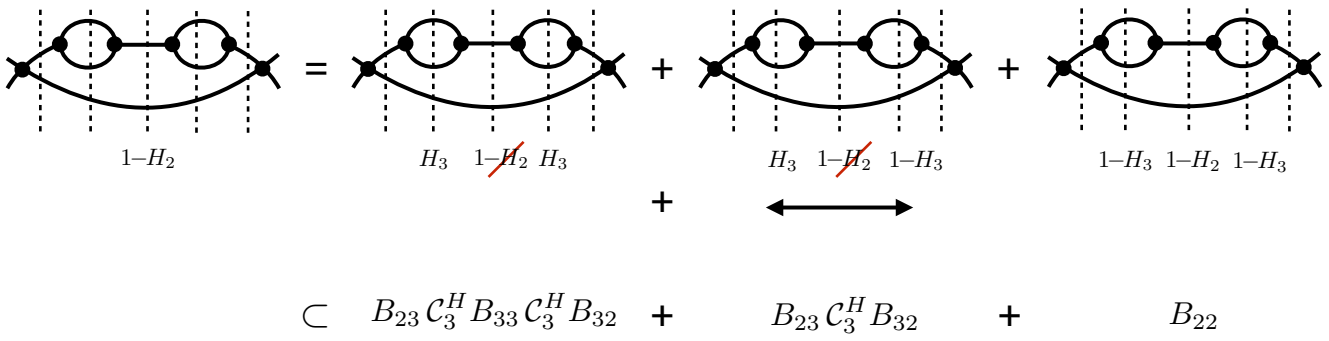

FIG. 16: The reduction procedure for one time-ordering of a diagram with a class 2 loop containing two self-energy insertions. Notation as in Fig. 14. There are four diagrams on the right-hand side of the equality, with the middle two related by a horizontal reflection. Both contribute to $B_{23}\,\mathcal{C}_3^H\,B_{32}$.

with $2 \to 2$ scattering and a single disconnected propagator in $\mathcal{M}_{L,33}$. Fully disconnected diagrams are not included, nor are those involving a $1 \leftrightarrow 2$ subprocess in the 32 or 23 components. We call this extended quantity $\mathcal{M}_{L,\text{ext}}$. It can be expanded in powers of the number of pole factors $\mathcal{C}^H$, just as in Eq. (B7). By construction, we then have that

$$\mathcal{M}_{L,\text{ext}}^{(n)} = \mathcal{M}_L^{(n)} + I^{(n)}\,, \tag{B10}$$

where $I^{(n)}$ is simply the disconnected part of the left-hand side (which can be unambiguously identified). B is simply defined as the part of $\mathcal{M}_{L,\text{ext}}$ without factors of $\mathcal{C}^H$:

$$B \equiv \mathcal{M}_{L,\text{ext}}^{(1)}\,. \tag{B11}$$

Using the new extended $\mathcal{M}_L$, we can reformulate the result Eq. (B9) in the simpler form

$$\mathcal{M}_{L,\text{ext}}^{(n)} = B\left(\mathcal{C}^H B\right)^{n-1}\,. \tag{B12}$$

We now recall that, when we say that all factors of B are equal in (B12), we mean aside from the different momenta at which they are sampled. In particular, we define a master kernel

$$B(\vec{p}\,',\vec{k}\,',\vec{a}\,';\vec{p},\vec{k},\vec{a}) = \begin{pmatrix} B_{22}(\vec{p}\,';\vec{p}) & B_{23}(\vec{p}\,';\vec{k},\vec{a}) \\ B_{32}(\vec{k}\,',\vec{a}\,';\vec{p}) & B_{33}(\vec{k}\,',\vec{a}\,';\vec{k},\vec{a}) \end{pmatrix}\,, \tag{B13}$$

by extending the on-shell definition of B to general momenta $\vec{p}\,',\vec{k}\,',\vec{a}\,';\vec{p},\vec{k},\vec{a}$. Then the kernel in Eq. (B12) is given by restricting the momenta in the master kernel appropriately: external momenta are set on shell, while internal coordinates (those contracted with $\mathcal{C}^H$) are restricted to the finite-volume set. This is identical to the description given for the naive kernel A in the main text following Eq. (27).

By definition, Eq. (B12) holds true for $n = 1$, so we begin by considering the $n = 2$ case. We know that, using the procedure of previous subsections, we can bring the contributions to $\mathcal{M}_{L,\text{ext}}$ with a single $\mathcal{C}^H$ into the form

$$\mathcal{M}_{L,\text{ext}}^{(2)} = B'\,\mathcal{C}^H B'\,, \tag{B14}$$

with B' a matrix of kernels having the same properties as B (smooth and connected except for B'_{33}). These kernels are constructed of all possible time-orderings of the allowed Feynman diagrams lying between the external states and the cut $\mathcal{C}^H$, with appropriate factors of $1 - H_i$ inserted, and all loops integrated. Since the same set of orderings can occur on both sides of the $\mathcal{C}^H$, the two kernels are equal.[25] What we need to show is that $B' = B$, i.e. that all contributions to B' are contained in B and *vice versa*. The former property is clear—any diagram connecting an external state to a cut $\mathcal{C}^H$ can also serve to connect two external states (or, as needed below, two cut factors). The latter property follows because every contribution contained in $B\mathcal{C}^H B$ will occur in $\mathcal{M}_{L,\text{ext}}^{(2)}$, simply by gluing the two halves together and inserting the cut factor.

This argument extends straightforwardly to arbitrary n, and completes the demonstration of Eq. (B12).

---

[25] This relies on the fact that the cut factors $\mathcal{C}^H$ act just like amputation on the external legs: removing the factors associated with the cut propagators from the kernels, and only allowing time-orderings in which the vertices lie between the external states.

Appendix C: Finite-volume dependence from the TOPT results

In this appendix we sketch the derivations of various results quoted in the main text. We first discuss quantities involving only two-cuts, and then consider those containing three-cuts.

1. Derivation of result for X_{22}

The analysis of Refs. [8, 29, 30] uses a skeleton expansion applied to standard relativistic Feynman diagrams. This is in contrast to the analysis in the main text, which uses TOPT, leading to the expression Eq. (48) for $\mathcal{M}_L$. While the two approaches lead to the same poles, as they must, they differ in the way that various non-pole parts are allocated to non-singular kernels. For example, the quantity B_{22} in Eq. (48) differs from the Bethe-Salpeter kernel $\widetilde{B}_2$ that appears in the analogous expression from the Feynman diagram analysis (as discussed further in Appendix C 3 below). Because of this, there is no simple way to recast the TOPT expression for X_{22} back into a Feynman-diagram form. Thus we cannot directly apply the results obtained in Refs. [8, 29, 30]. Instead, we apply the methodology developed in those references directly to the TOPT expression.

Starting from Eq. (48), we focus on one of the two-cuts, and make the matrix multiplications explicit, leading to

$$\left[B_{22}\,\mathcal{C}_2^H B_{22}\right]_{p;k} = \sum_{\vec{p},\vec{r}} B_{22;p'';p}\,\mathcal{C}_{2;p;r}\,H_2(\vec{r})\;B_{22;r;p'} \tag{C1}$$

$$= -\frac{1}{L^3}\sum_{\vec{p}} B_{22;p'';p}\frac{1}{2}\frac{1}{2\omega_p 2\omega_{Pp}(E-\omega_p-\omega_{Pp})}H_2(\vec{p})\;B_{22;p;p'}\,. \tag{C2}$$

The factor of -1 coming with $\mathcal{C}^H$ arises from the product of the i associated with the energy denominator and that associated with one of the adjacent vertices. We now recall that the key property of B_{22} for our purposes is that it is a smooth function of its momentum arguments. Thus the only singularity in the summand is that from the explicit pole in $\mathcal{C}^H$.

We now write the sum over $\vec{p}$ as an integral plus a sum-integral difference to reach

$$\left[B_{22}\,\mathcal{C}_2^H B_{22}\right]_{p;k} = -\mathrm{PV}\int_{\vec{p}} B_{22;p'';p}\frac{H_2(\vec{p})}{8\omega_p\omega_{Pp}(E-\omega_p-\omega_{Pp})}\;B_{22;p;p'}$$
$$-\left[\frac{1}{L^3}\sum_{\vec{p}} -\mathrm{PV}\int_{\vec{p}}\right] B_{22;p'';p}\frac{1}{2}\frac{h(\vec{p})}{2\omega_p 2\omega_{Pp}(E-\omega_p-\omega_{Pp})}\;B_{22;p;p'}\,. \tag{C3}$$

Here we have also replaced $H_2(\vec{p})$ with $h(\vec{p})$ in the sum-integral difference, with $h(\vec{p})$ the UV regulator introduced in Eq. (51) above. This substitution is justified because $H_2(\vec{p})-h(\vec{p})$ vanishes at the pole so that the replacement is equivalent to dropping the sum-integral difference of a function that is smooth for all real $\vec{p}$, i.e. dropping a contribution that is exponentially suppressed. Here and below we keep implicit the fact that we are dropping exponentially suppressed terms.

From here we follow the steps outlined in Ref. [8], to rewrite the second term in terms of the zeta-function F_2, defined in Eq. (51). Given that B_{22} is a smooth function, the dominant finite-volume corrections from the second term above are due to the explicit propagator pole. As a result, one can replace B_{22} with its value when the internal momentum p is projected on shell. This is effected by setting the CM frame magnitude to equal q^*. This fixes the magnitude but not the direction and this remaining degree of freedom motivates us to decompose B_{22} in spherical harmonics

$$B_{22;p'';p}\Big|_{p^*=q^*} = \sqrt{4\pi}\,Y_{\ell' m'}(\hat{p}^*)B_{22;p'';\ell' m'}, \qquad B_{22;p;p'}\Big|_{p^*=q^*} = \sqrt{4\pi}\,Y^*_{\ell,m}(\hat{p}^*)B_{22;\ell m;p'}\,. \tag{C4}$$

Using the sum-integral-difference identity of Ref. [8], as expressed in Appendix A of Ref. [29], we find

$$\left[B_{22}\,\mathcal{C}_2^H B_{22}\right]_{p;k} = -\mathrm{PV}\int_{q} B_{22;p'';q}\frac{H_2(\vec{q})}{8\omega_q\omega_{Pq}(E-\omega_q-\omega_{Pq})}\;B_{22;q;p'} - B_{22;p';\ell' m'}F_{2;\ell' m';\ell m}B_{22;\ell m;p'}\,. \tag{C5}$$

We summarize this result in shorthand notation as

$$B_{22}\,\mathcal{C}_2^H B_{22} = -B_{22}I_C B_{22} - B_{22}F_2 B_{22}\,, \tag{C6}$$

with I_C an integral operator. We note that this identity holds for any choice of kernels on the left- and right-hand sides, as long as they are smooth functions of momenta. We can thus condense the notation even further and write

$$\mathcal{C}_2^H = -I_C - F_2\,. \tag{C7}$$

Using this identity, we can reorganize the sum in Eq. (48) into a series in powers of F_2 (following the method of Ref. [8])

$$X_{22} = B_{22}\sum_{n=0}^{\infty}\left[(-I_C - F_2)B_{22}\right]^n \tag{C8}$$

$$= \mathcal{K}_{22,D}\sum_{n=0}^{\infty}\left[-F_2\mathcal{K}_{22,D}\right]^n\,, \tag{C9}$$

where

$$\mathcal{K}_{22,D} = \sum_{n=0}^{\infty} B_{22}[-I_C B_{22}]^n\,. \tag{C10}$$

Summing the geometric series in Eq. (C9) leads to the result quoted in the main text, Eq. (50).

2. Derivation of results for Y_{22} and Z_{23}

The determination of the volume dependence of Y_{22}, defined in Eq. (64), follows similar steps to those described in Appendix C 1 for X_{22}. We can use the identity (C7) for all two-cuts, since the kernels on either side of the cut involve the smooth functions B_{22}, B_{23} or B_{32}. Collecting terms according to the number of factors of F_2, we find

$$Y_{22} = B_{32}\left[C_2^H + \mathcal{C}_2^H B_{22}\mathcal{C}_2^H + \cdots\right]B_{23} \tag{C11}$$

$$= B_{32}\left[-I_C + I_C B_{22} I_C - \cdots\right]B_{23} - B_{32}\left[1 - I_C B_{22} + \cdots\right]F_2\left[1 - B_{22}I_C + \cdots\right]B_{23} \tag{C12}$$

$$+ B_{32}\left[1 - I_C B_{22} + \cdots\right]F_2\left[B_{22} - B_{22}I_C B_{22} + \cdots\right]F_2\left[1 - B_{22}I_C + \cdots\right]B_{23} + \cdots \tag{C13}$$

$$= B_{32}\mathcal{D}_{C,2}B_{23} - B_{32}\mathcal{D}_{A',2}F_2\mathcal{D}_{A,2}B_{23} + B_{32}\mathcal{D}_{A',2}F_2\mathcal{K}_{22,D}F_2\mathcal{D}_{A,2}B_{23} - \cdots\,, \tag{C14}$$

where in the last step we have used Eq. (C10) and defined the integral operators

$$\mathcal{D}_{C,2} = \left[-I_C + I_C B_{22} I_C - \cdots\right]\,, \tag{C15}$$

$$\mathcal{D}_{A',2} = \left[1 - I_C B_{22} + \cdots\right]\,, \tag{C16}$$

$$\mathcal{D}_{A,2} = \left[1 - B_{22}I_C + \cdots\right]\,. \tag{C17}$$

Summing the geometric series in Eq. (C14) leads to the result quoted in the main text, Eq. (66).

This derivation applies also for Z_{23}, the only change being the replacement of B_{32} on the left with B_{22}. Thus from Eq. (66) we obtain

$$Z_{23} = B_{22}\left[\mathcal{D}_{C,2} - \mathcal{D}_{A',2}F_2\frac{1}{1+\mathcal{K}_{22,D}F_2}\mathcal{D}_{A,2}\right]B_{23}\,. \tag{C18}$$

This can be simplified using the identities

$$B_{22}\mathcal{D}_{A',2} = \mathcal{K}_{22,D}\,, \tag{C19}$$

$$B_{22}\mathcal{D}_{C,2} = \mathcal{D}_{A,2} - 1\,, \tag{C20}$$

leading to

$$Z_{23} = \left[\mathcal{D}_{A,2} - 1 - \mathcal{K}_{22,D}F_2\frac{1}{1+\mathcal{K}_{22,D}F_2}\mathcal{D}_{A,2}\right]B_{23}\,. \tag{C21}$$

The result for Z_{23} in the main text, Eq. (73), follows immediately.

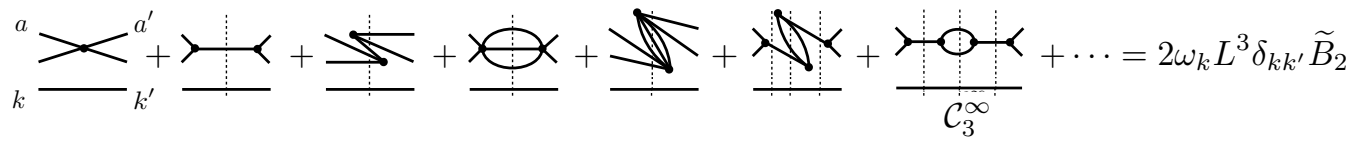

FIG. 17: Examples of TOPT diagrams contributing to $B_{33}^{\rm disc}$, and thus to $\widetilde{B}_2$, in a general EFT. The external three-particle state is either on shell or has a factor of $\mathcal{C}_3^H$. The vertical dashed lines indicate intermediate states, which come with factors of $1/(E - \sum_i \omega_i)$. Three-particle intermediate states also include a factor of $(1 - H_3)$, as indicated by the $\mathcal{C}_3^\infty$ in the last diagram. Two-particle intermediate states do not contain factors of H_2, and there are no H_i factors in intermediate states containing four or more particles. No vertices are allowed before the initial time or after the final time. All loop momenta are integrated rather than summed (since there are no physical cuts).

3. Comments on the derivation of the result for X_{33}

As explained in the main text, to determine X_{33} we must repeat the analysis of Refs. [29, 30] starting from the TOPT decomposition of Eq. (49) instead of the skeleton expansion of Feynman diagrams. To do so, we use the decomposition of B_{33} into connected and disconnected parts, Eq. (52). $B_{33}^{\rm conn}$ is the analog in the present analysis of the three-particle Bethe-Salpeter amplitude B_3 in the analysis of Refs. [29, 30]. The disconnected part can be written

$$B_{33;k'a';ka}^{\rm disc} = 2\omega_k L^3 \delta_{k'k} \widetilde{B}_2(\vec{k})_{a';a} + \text{permutations}\,, \tag{C22}$$

where $\widetilde{B}_2$ plays the role here of the two-to-two Bethe-Salpeter kernel B_2 appearing in Ref. [29], with some important distinctions that we discuss below. "Permutations" refers to the inclusion of all possible choices of incoming and outgoing spectator momenta. There are nine terms in total, corresponding to the three different choices of the momentum of the noninteracting particle in both initial and final states (e.g. $\vec{k}$, $\vec{a}$ or $\vec{P} - \vec{k} - \vec{a}$ in the initial state). Thus we can rewrite the result using the symmetrization operators introduced in the main text:

$$B_{33;k'a';ka}^{\rm disc} = \mathcal{S}_{\mathcal{L}} \left\{ 2\omega_k L^3 \delta_{k'k} \widetilde{B}_2(\vec{k})_{a';a} \right\} \mathcal{S}_{\mathcal{R}}\,. \tag{C23}$$

The factor of $2\omega_k$ is needed to cancel the $1/(2\omega_k)$ contained in the adjacent three-cut, $\mathcal{C}_3^H$, sinceeach disconnected propagator should come with only one overall factor of $1/(2\omega_k)$, and this factor is provided by the first $\mathcal{C}_3^H$. Similarly, the factor of L^3 is introduced to assure that diagrams with insertions of $B_{33}^{\rm disc}$ have the correct powers of L.

It is important to understand in some detail the differences between the Bethe-Salpeter kernel, B_2, and the quantity appearing here, $\widetilde{B}_2$. B_2 consists of all amputated two-to-two Feynman diagrams that are two-particle irreducible in the s-channel. $\widetilde{B}_2$ contains all the time-orderings arising from these Feynman diagrams, except those in which any vertex lies before the initial three-cut or after the final three-cut. In addition, because of the definition of B described in Sec. II A, $\widetilde{B}_2$ includes time-orderings (constrained as above) from two-to-two diagrams that are two-particle *reducible* in the s-channel. These, however, are weighted by a factor of $1 - H_3$, so that there is no physical cut. (The weight involves H_3 and not H_2 because this is part of a three-particle kernel.) These features are illustrated in Fig. 17. Because of the appearance of $1 - H_3$ in some intermediate states, $\widetilde{B}_2$ is an unconventional quantity.

We now proceed through the steps of the derivation in Refs. [29, 30]. We recall that Ref. [30] studied the quantity of interest, $\mathcal{M}_L$, but made heavy use of the work in Ref. [29], so we need to repeat the steps from both references. We stress that the steps we need to take using the TOPT decomposition are in one-to-one correspondence with those using the skeleton expansion. To illustrate this correspondence we consider the following contributions to X_{33}:

$$X_{33} \supset B_{33}^{\rm conn} \left[\mathcal{C}_3^H + \mathcal{C}_3^H B_{33}^{\rm disc} \mathcal{C}_3^H + \mathcal{C}_3^H B_{33}^{\rm disc} \mathcal{C}_3^H B_{33}^{\rm disc} \mathcal{C}_3^H + \cdots \right] B_{33}^{\rm conn}\,. \tag{C24}$$

If we keep the subset of these contributions in which the spectator meson remains the same for all factors of B_{33} then we obtain the diagrams shown in Fig. 18. These correspond to the "no switch" diagrams considered in Sec. IVA of Ref. [29], and shown in Fig. 7 of that work. The differences between the expressions represented by the diagrams are as follows: First, while here the "end caps" are provided by factors of $B_{33}^{\rm conn}$, in Ref. [29] they are given by the external operators σ and $\sigma^\dagger$. As noted in Ref. [29], however, as long as they are nonsingular, the choice of end caps has no impact on the form of the result. Second, as already described, $\widetilde{B}_2$ here is replaced by B_2 in Ref. [29]. Last, the expression for $\mathcal{C}_3^H$ differs from the "cut" that arises in Ref. [29]. The key point, however, is that the residue of the pole is the same in both cases, with the differences appearing in nonsingular terms. This can be seen, for example,

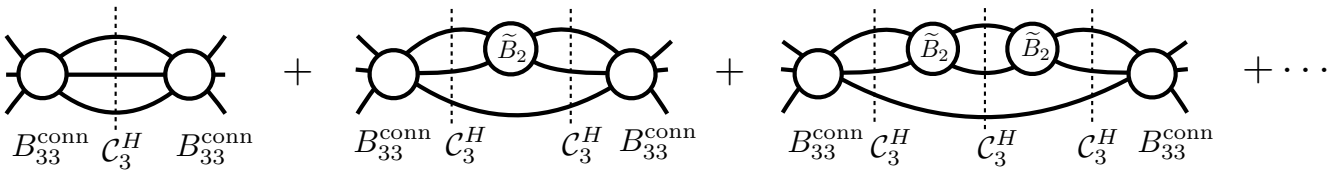

FIG. 18: Contributions to X_{33} in TOPT that correspond to the "no switch" diagrams considered in Ref. [29].

from Eq. (56) of Ref. [29], which is proportional to $\mathcal{C}_3^H$. Indeed, the essential difference between the TOPT analysis and that using Feynman diagrams is that non-singular terms are reshuffled between the kernels.

In the expression represented by the diagrams of Fig. 18, the three-momentum sums associated with each $\mathcal{C}_3^H$ factor are replaced by integrals and a zeta function, using a generalization of the identity given in Eq. (C6). Following the steps of Ref. [29], we find that this class of diagrams leads to the following volume-dependent terms

$$\mathcal{M}_L \supset -B_{33}^{\rm conn}(1+\mathcal{D}_{A',3}^{(1,u)})\frac{F}{2\omega L^3}\frac{1}{1+\mathcal{K}_{22}F}(1+\mathcal{D}_{A,3}^{(1,u)})B_{33}^{\rm conn} + B_{33}^{\rm conn}\frac{F}{2\omega L^3}B_{33}^{\rm conn}\,. \tag{C25}$$

Here F is defined in Eq. (59), $\mathcal{K}_{22}$ is given by

$$\mathcal{K}_{22;k'\ell'm';k\ell m} = \delta_{k'k}\left[\widetilde{B}_2(\vec{k}) + {\rm PV}\!\int \widetilde{B}_2(\vec{k})6\omega_k L^6\,\mathcal{C}_3^H\,\widetilde{B}_2(\vec{k}) + \cdots\right]_{\ell'm';\ell m}\,, \tag{C26}$$

(where the integral runs over the implicit $\vec{a}$ dependence of the two $\widetilde{B}_2$ factors and of $\mathcal{C}_3^H$), and $\mathcal{D}_{A',3}^{(1,u)}$ and $\mathcal{D}_{A,3}^{(1,u)}$ are the first contributions to the decoration operators $\mathcal{D}_{A',3}$ and $\mathcal{D}_{A,3}$ discussed in the main text. The result (C25) has the same form as Eq. (90) of Ref. [29].

We have checked that all subsequent steps in the lengthy derivations of Refs. [29, 30] go through, and we do not present further details. The conclusion is that we can read off the final result for X_{33} from that for $\mathcal{M}_L$ given in Eq. (68) of Ref. [30], as long as we change the meaning of the symbols appropriately. This is what we have done in Eqs. (53)-(58).

There are, however, two features of the result that deserve further mention. The first concerns the matrix G^H. This arises from diagrams involving switches, the simplest of which is shown in Fig. 19. The corresponding diagram is analyzed in Sec. IVB of Ref. [29]. In one of the volume-dependent contributions, the two outer $\mathcal{C}_3^H$ factors are replaced by F factors, while the central factor gives rise to a switch matrix G^H:

$$G^H_{p\ell'm';k\ell m} = \left(\frac{k^*}{q_p^*}\right)^{\ell'}\frac{4\pi Y_{\ell'm'}(\hat{k}^*)H_3(\vec{p},\vec{k})Y^*_{\ell m}(\hat{p}^*)}{2\omega_{Pkp}(E-\omega_k-\omega_p-\omega_{Pkp})}\left(\frac{p^*}{q_k^*}\right)^{\ell}\frac{1}{2\omega_k L^3}\,. \tag{C27}$$

This switches the interacting pair from the upper two to the lower two particles. The key point here is that G^H inherits the cutoff $H_3 = H(\vec{p})H(\vec{k})H(\vec{b}_{kp})$ from $\mathcal{C}_3^H$. By contrast, in Ref. [29], where the switch matrix is first introduced in Eq. (116), there is some freedom in the choice of the cutoff function, and the choice made there is $H(\vec{p})H((\vec{k})$. Thus G^H and G differ by a factor of $H(\vec{b}_{kp})$. We note, however, that in Ref. [29] one could equally well have included the full H_3 in the definition of G without changing the derivation. In other words, the form of G that is forced on us here is a completely viable option in Ref. [29] as well.

The second feature of the result for X_{33} concerns $\mathcal{K}_{22}$, Eq. (C26). We find that

$$\mathcal{K}_{22;k'\ell'm';k\ell m} = \delta_{k'k}\mathcal{K}_{2;\ell'm';\ell m}(E-\omega_k,\vec{P}-\vec{k})\,, \tag{C28}$$

i.e. $\mathcal{K}_{22}$ in fact contains the *physical* two-particle K-matrix. To show this requires two further results: the unphysical dependence of $\widetilde{B}_2$ on H_3 must cancel, and the missing time-orderings in $\widetilde{B}_2$ must become irrelevant. To explain the cancelation of H_3 dependence, we rewrite B_{22} to make its dependence on H_3 explicit:

$$\widetilde{B}_2 = \overline{B}_{22} + {\rm PV}\int \overline{B}_2 6\omega_k L^6 \mathcal{C}_3^\infty \overline{B}_2 + \cdots\,. \tag{C29}$$

Here $\overline{B}_2$ is the result obtained when all diagrams containing $\mathcal{C}_3^\infty$ are dropped, and thus is independent of H_3. For example, in Fig. 17, the last diagram would be dropped. Thus $\overline{B}_2$ differs from the Bethe-Salpeter amplitude B_2 only

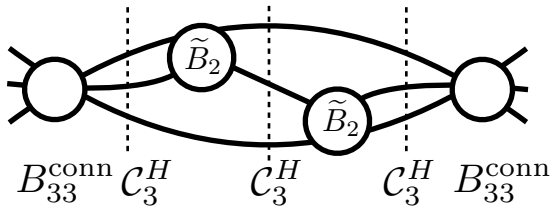

FIG. 19: Example of one-switch diagram contributing to X_{33} in TOPT.

in that certain time-orderings are not included in the former. The H_3 dependence of $\widetilde{B}_{22}$ is then reintroduced by the terms involving integrals in Eq. (C29), corresponding to adding back in diagrams like the last one in Fig. 17. Substituting this result into Eq. (C26), and rearranging terms, we find that

$$\mathcal{K}_{22;k'\ell'm';k\ell m} = \delta_{k'k}\left[\overline{B}_2(\vec{k}) + \mathrm{PV}\int \overline{B}_2(\vec{k}) 6\omega_k L^6\, \mathcal{C}_3 \overline{B}_2(\vec{k}) + \cdots\right]_{\ell'm';\ell m} . \tag{C30}$$

The H_3 dependence has canceled because $\mathcal{C}_3^H + \mathcal{C}_3^\infty = \mathcal{C}_3$. Thus $\mathcal{K}_{22}$ receives contributions from all amputated two-to-two TOPT diagrams, with two-particle loops integrated using the PV prescription, except that no time-orderings are allowed in which vertices lie before the initial cut or after the final cut. However, as indicated by the spherical harmonic indices in Eq. (C30), these diagrams are evaluated on shell assuring that diagrams with the missing time-orderings vanish. Thus we find the result (C28).

4. Derivation of result for Z_{32}

The final quantity we consider in this Appendix is $Z_{32} = B_{33}\Xi_{33}B_{32}$. As noted in the main text, this is not a quantity for which a result can simply be read off from Refs. [29, 30], since it has disconnected parts on one end but not the other. Nevertheless, by a small extension of Eq. (64) in Ref. [30] the relevant result can be found. This equation gives a result for $\mathcal{M}_{3,L}^{(u,u)}$, the unsymmetrized three-particle finite-volume amplitude, with all factors of B_3 (the fully connected three-particle Bethe-Salpeter amplitude) explicit. To obtain Z_{32} we must (a) drop any contribution in which there is no B_3, (b) replace the rightmost B_3 with B_{32}, (c) replace all other factors of B_3 with $B_{33}^{\rm conn}$, and (d) symmetrize on the left. The result is

$$Z_{32} = \mathcal{S}_{\mathcal{L},3}\left\{\mathcal{L}_{L,3}^{(u,u)}\widetilde{\mathcal{Z}}\mathcal{D}_{A,3}^{[B_2,\rho]}\sum_{n=0}^{\infty}\left(B_{33}^{\rm conn}M^{[B_2,\rho]}\right)^n B_{32}\right\} - B_{32}\,, \tag{C31}$$

where $\mathcal{L}_{L,3}^{(u,u)}$ is defined in Eq. (56), while

$$\widetilde{\mathcal{Z}} = \frac{1}{1+\mathcal{K}_{\mathrm{df},33,D}^{[B_2,\rho]}F_3}\,, \tag{C32}$$

$$M^{[B_2,\rho]} = \mathcal{D}_{C,3}^{[B_2,\rho]} - \mathcal{D}_{A',3}^{[B_2,\rho]}F_3\widetilde{\mathcal{Z}}\mathcal{D}_{A,3}^{[B_2,\rho]}\,. \tag{C33}$$

The superscript $[B_2,\rho]$, which is defined in Ref. [29], indicates the parts of the integral operators that do not contain factors of $B_{33}^{\rm conn}$. The relation between these parts and the full integral operators can be read off from Eqs. (247)-(249)

of Ref. [29], and is[26]

$$\mathcal{D}_{C,3} = \mathcal{D}_{C,3}^{[B_2,\rho]} \sum_{n=0}^{\infty} \left(B_{33}^{\text{conn}} \mathcal{D}_{C,3}^{[B_2,\rho]} \right)^n , \tag{C34}$$

$$\mathcal{D}_{A,3} = \mathcal{D}_{A,3}^{[B_2,\rho]} \sum_{n=0}^{\infty} \left(B_{33}^{\text{conn}} \mathcal{D}_{C,3}^{[B_2,\rho]} \right)^n , \tag{C35}$$

$$\mathcal{D}_{A',3} = \sum_{n=0}^{\infty} \left(\mathcal{D}_{C,3}^{[B_2,\rho]} B_{33}^{\text{conn}} \right)^n \mathcal{D}_{A',3}^{[B_2,\rho]} . \tag{C36}$$

These operators appear in the expression for Y_{33}, Eq. (68).

Our final comment about Eq. (C31) concerns the subtraction of B_{32} on the right-hand side. This is required to cancel the leading contribution from the first term on the right-hand side, which comes from the symmetrization of the product of the 1/3 term in $\mathcal{L}_{L,3}^{(u,u)}$ [Eq. (56)], the 1 in $\widetilde{Z}$, the 1 in $\mathcal{D}_{A,3}^{[B_2,\rho]}$, and the $n = 0$ term in the sum. This B_{32} term is absent in Z_{32}.

The next step is to substitute the result (C33) into Eq. (C31) and collect terms according the number of F_3 factors. This leads to

$$Z_{32} + B_{32} = \mathcal{S}_{\mathcal{L},3} \left\{ \mathcal{L}_{L,3}^{(u,u)} \widetilde{\mathcal{Z}} \left[1 - B_{33}^{\text{conn},CA} F_3 \widetilde{Z} + \left(B_{33}^{\text{conn},CA} F_3 \widetilde{Z} \right)^2 + \cdots \right] \mathcal{D}_{A,3} B_{32} \right\} , \tag{C37}$$

where

$$B_{33}^{\text{conn},CA} = \mathcal{D}_{A,3}^{[B_2,\rho]} \sum_{n=0}^{\infty} \left(B_{33}^{\text{conn}} \mathcal{D}_{C,3}^{[B_2,\rho]} \right)^n B_{33}^{\text{conn}} \mathcal{D}_{A',3}^{[B_2,\rho]} , \tag{C38}$$

is the analog here of the quantity $B_3^{[B_2,\rho]}$ in Ref. [30]. Finally, summing the geometric series in Eq. (C37), performing some algebraic manipulations, and using

$$\mathcal{K}_{\text{df},33,\text{D}} = \mathcal{K}_{\text{df},33}^{[B_2,\rho]} + B_{33}^{\text{conn},CA} \tag{C39}$$

[the analog of Eq. (65) of Ref. [30]], leads to the claimed result, Eq. (74).

Appendix D: Time-reversal and parity invariance

In this section we investigate the implications for $\mathcal{K}_{\text{df}}$ of assuming that time-reversal and parity invariance hold in the underlying theory. We first discuss the consequences of time-reversal invariance; the consequences of parity invariance can then be inferred by a straightforward modification.

Naïvely, one might expect that, since $\mathcal{K}_{\text{df}}$ is an infinite-volume scattering quantity, it should transform under time reversal in the same way as $\mathcal{M}$. However, upon closer inspection, this result is far from obvious. In particular, the definition of $\mathcal{K}_{\text{df},33}$, the three-to-three component of $\mathcal{K}_{\text{df}}$, involves a choice of ordering of loop integrals that is not manifestly time-reversal invariant [29]. Nevertheless, as we show in this Appendix, given the relations between $\mathcal{K}_{\text{df}}$ and $\mathcal{M}$ derived in Sec. III B, the transformation properties of $\mathcal{M}$ are indeed inherited by $\mathcal{K}_{\text{df}}$.

Time-reversal invariance implies that the components of the scattering amplitude satisfy

$$\mathcal{M}_{22;\vec{P}}(\hat{p}'^*; \hat{p}^*) = \mathcal{M}_{22;-\vec{P}}(-\hat{p}^*; -\hat{p}'^*) , \tag{D1}$$

$$\mathcal{M}_{23;\vec{P}}(\hat{p}'^*; \vec{k}, \hat{a}^*) = \mathcal{M}_{32;-\vec{P}}(-\vec{k}, -\hat{a}^*; -\hat{p}'^*) , \tag{D2}$$

$$\mathcal{M}_{\text{df},33;\vec{P}}(\vec{k}', \hat{a}'^*; \vec{k}, \hat{a}^*) = \mathcal{M}_{\text{df},33;-\vec{P}}(-\vec{k}, -\hat{a}^*; -\vec{k}', -\hat{a}'^*) , \tag{D3}$$

---

[26] We comment that the decoration operator $\mathcal{D}_{C,3}$ used here and the analog used in Ref. [29], denoted D_C, differ by a trivial relative phase. In particular, in the limit where the two-to-three coupling is set to zero, the operators are related by $\mathcal{D}_{C,3} = iD_C$.

where we have denoted dependence on the total momentum, $\vec{P}$, as a subscript.[27] Decomposing using spherical harmonics, one finds that the various components satisfy

$$\mathcal{M}_{22;\ell m;\ell' m';\vec{P}} = (-1)^{\ell+m+\ell'+m'}\, \mathcal{M}_{22;\ell'-m';\ell-m;-\vec{P}}\,, \tag{D4}$$

$$\mathcal{M}_{23;\ell m;\ell' m';\vec{P}}(\vec{k}) = (-1)^{\ell+m+\ell'+m'}\, \mathcal{M}_{32;\ell'-m';\ell-m;-\vec{P}}(-\vec{k}), \tag{D5}$$

$$\mathcal{M}_{\mathrm{df},33;\ell m;\ell' m';\vec{P}}(\vec{k}';\vec{k}) = (-1)^{\ell+m+\ell'+m'}\, \mathcal{M}_{\mathrm{df},33;\ell'-m';\ell-m;-\vec{P}}(-\vec{k};-\vec{k}')\,. \tag{D6}$$

To obtain these results we have used standard properties of the spherical harmonics under complex conjugation and parity transformation. Note that, since we are considering the divergence-free form of $\mathcal{M}_{33}$, we can decompose in spherical harmonics. From these results we conclude that it is sufficient to determine $\mathcal{M}_{22}$, $\mathcal{M}_{23}$, and $\mathcal{M}_{\mathrm{df},33}$, since $\mathcal{M}_{32}$ then follows trivially from Eq. (D5).

In the following, we will say that a quantity has "standard time-reversal transformation properties" if Eqs. (D4)-(D6) hold with the quantity substituted for $\mathcal{M}$. We recall from Sec. III B that $\mathcal{K}_{\mathrm{df}}$ is obtained from $\mathcal{M}$ in two steps. First, the intermediate quantity $\mathcal{T}$ is obtained from $\mathcal{M}$ using Eqs. (121)-(123), and, second, $\mathcal{K}_{\mathrm{df}}$ is obtained from $\mathcal{T}$ using Eqs. (124)-(127). In what follows we first show that $\mathcal{T}$ has standard time-reversal transformation properties and then show that the same holds for $\mathcal{K}_{\mathrm{df}}$.

$\mathcal{T}$ is obtained from $\mathcal{M}$ by integrating with the kernels $I_{\mathcal{R}}$ and $I_{\mathcal{L}}$, which are themselves obtained from $\Delta_{\mathcal{L}}$ and $\Delta_{\mathcal{R}}$ by solving the integral equations (119) and (120), respectively. The latter kernels are essentially the symmetrized forms of $\mathcal{L}_3^{(u,u)}$ and $\mathcal{R}_3^{(u,u)}$, as shown by Eqs. (115) and (116). Thus, to proceed, we need to understand the time-reversal transformation properties of $\mathcal{L}_3^{(u,u)}$ and $\mathcal{R}_3^{(u,u)}$, which are defined, respectively, in Eqs. (92) and (93). These are built using $\mathcal{D}_3^{(u,u)}$, which, as shown in Eq. (87), involves the kernel G^{∞} of Eq. (88).

Thus we begin by studying the transformation properties of G^{∞}. It follows from its definition that

$$G^{\infty}_{\ell m;\ell' m';\vec{P}}(\vec{k}';\vec{k}) = (-1)^{\ell+m+\ell'+m'}\, G^{\infty}_{\ell'-m';\ell-m;-\vec{P}}(-\vec{k};-\vec{k}')\,, \tag{D7}$$

where we have used $H_{3;\vec{P}}(\vec{k}',\vec{k}) = H_{3;-\vec{P}}(-\vec{k},-\vec{k}')$. Using the definition of $\mathcal{D}_3^{(u,u)}$, Eq. (87), and substituting the symmetry relations for $\mathcal{M}_{22}$, Eq. (D4), and G^{∞}, Eq. (D7), we find

$$\mathcal{D}^{(u,u)}_{3;\ell m;\ell' m';\vec{P}}(\vec{k}';\vec{k}) = (-1)^{\ell+m+\ell'+m'}\mathcal{D}^{(u,u)}_{3;\ell'-m';\ell-m;-\vec{P}}(-\vec{k};-\vec{k}')\,, \tag{D8}$$

i.e. $\mathcal{D}_3^{(u,u)}$ transforms in the same way as G^{∞}. It is now straightforward to use the definitions, Eqs. (92) and (93), to show that the components of $\mathcal{L}_3^{(u,u)}$ and $\mathcal{R}_3^{(u,u)}$ satisfy

$$\mathcal{L}^{(u,u)}_{3;\ell m;\ell' m';\vec{P}}(\vec{k}',\vec{k}) = (-1)^{\ell+m+\ell'+m'}\mathcal{R}^{(u,u)}_{3;\ell'-m';\ell-m;-\vec{P}}(-\vec{k},-\vec{k}')\,. \tag{D9}$$

We further note that $\mathcal{L}_3^{(u,u)}$ and $\mathcal{R}_3^{(u,u)}$ satisfy

$$\frac{\rho_3(\vec{k}')}{2\omega_{k'}}\,\mathcal{L}_3^{(u,u)}(\vec{k}',\vec{k}) = \mathcal{R}_3^{(u,u)}(\vec{k}',\vec{k})\,\frac{\rho_3(\vec{k})}{2\omega_k}\,, \tag{D10}$$

and from this and Eq. (116), we deduce

$$\Delta_{\mathcal{L};\ell m;\ell' m';\vec{P}}(\vec{p},\vec{k}) = (-1)^{\ell+m+\ell'+m'}\,\Delta_{\mathcal{R};\ell'-m';\ell-m;-\vec{P}}(-\vec{k},-\vec{p}). \tag{D11}$$

Inserting this into Eq. (119) and solving for $I_{\mathcal{L}}$ iteratively then gives

$$I_{\mathcal{L};\ell m;\ell' m';\vec{P}}(\vec{p},\vec{k}) = (-1)^{\ell+m+\ell'+m'}\,I_{\mathcal{R};\ell'-m';\ell-m;-\vec{P}}(-\vec{k},-\vec{p}). \tag{D12}$$

Substituting these properties of $I_{\mathcal{L}}$ and $I_{\mathcal{R}}$ along with the standard time-reversal transformation properties of $\mathcal{M}$ into Eqs. (121)-(123), it then follows immediately that $\mathcal{T}$ has standard transformation properties. Finally, using these

---

[27] Previously the dependence on $\vec{P}$ has been implicit. We make it explicit throughout this appendix.

properties of $\mathcal{T}$ in Eqs. (124)-(127), we find the claimed result that $\mathcal{K}$ also has standard transformation properties, i.e.

$$\mathcal{K}_{22;\ell m;\ell' m';\vec{P}} = (-1)^{\ell+m+\ell'+m'}\, \mathcal{K}_{22;\ell' -m';\ell -m;-\vec{P}}\,, \tag{D13}$$

$$\mathcal{K}_{23;\ell m;\ell' m';\vec{P}}(\vec{k}) = (-1)^{\ell+m+\ell'+m'}\, \mathcal{K}_{32;\ell' -m';\ell -m;-\vec{P}}(-\vec{k})\,, \tag{D14}$$

$$\mathcal{K}_{\mathrm{df},33;\ell m;\ell' m';\vec{P}}(\vec{k}';\vec{k}) = (-1)^{\ell+m+\ell'+m'}\, \mathcal{K}_{\mathrm{df},33;\ell' -m';\ell -m;-\vec{P}}(-\vec{k};-\vec{k}'). \tag{D15}$$

We conclude that the K-matrix appearing in the quantization condition, Eq. (79), satisfies the same time-reversal transformation properties as a standard K-matrix. This implies that only three of the four components of the K-matrix must be determined from the finite-volume spectrum.

We can extend this result if we also assume parity invariance. Since there is nothing in the construction of $\mathcal{K}_{\mathrm{df}}$ that violates parity, it transforms in the same way as $\mathcal{M}$ under parity, namely by flipping the sign of all vectors and multiplying spherical harmonics by $(-1)^\ell$. We thus arrive at the following relations in a theory that is invariant under both time-reversal and parity transformations:

$$\mathcal{K}_{22;\ell m;\ell' m';\vec{P}} = (-1)^{m+m'}\, \mathcal{K}_{22;\ell' -m';\ell -m;\vec{P}}, \tag{D16}$$

$$\mathcal{K}_{23;\ell m;\ell' m';\vec{P}}(\vec{k}) = (-1)^{m+m'}\, \mathcal{K}_{32;\ell' -m';\ell -m;\vec{P}}(\vec{k}), \tag{D17}$$

$$\mathcal{K}_{\mathrm{df},33;\ell m;\ell' m';\vec{P}}(\vec{k}';\vec{k}) = (-1)^{m+m'}\, \mathcal{K}_{\mathrm{df},33;\ell' -m';\ell -m;\vec{P}}(\vec{k};\vec{k}'). \tag{D18}$$

These relations are more useful since the same value of the total three-momentum appears on both sides. In particular, the second relations shows that $\mathcal{K}_{23}$ is not independent of $\mathcal{K}_{32}$.

[1] S. Prelovsek, *Proceedings, 32nd International Symposium on Lattice Field Theory (Lattice 2014): Brookhaven, NY, USA, June 23-28, 2014*, PoS **LATTICE2014**, 015 (2014), arXiv:1411.0405 [hep-lat] .
[2] A. Portelli, *Proceedings, 32nd International Symposium on Lattice Field Theory (Lattice 2014): Brookhaven, NY, USA, June 23-28, 2014*, PoS **LATTICE2014**, 013 (2015), arXiv:1505.07057 [hep-lat] .
[3] C. Liu, in *Proceedings, 34th International Symposium on Lattice Field Theory (Lattice 2016): Southampton, UK, July 24-30, 2016* (2016) arXiv:1612.00103 [hep-lat] .
[4] M. Lüscher, Commun.Math.Phys. **105**, 153 (1986).
[5] M. Lüscher, Nucl.Phys. **B354**, 531 (1991).
[6] K. Rummukainen and S. A. Gottlieb, Nucl. Phys. **B450**, 397 (1995), arXiv:hep-lat/9503028 .
[7] S. He, X. Feng, and C. Liu, JHEP **0507**, 011 (2005), arXiv:hep-lat/0504019 [hep-lat] .
[8] C. Kim, C. Sachrajda, and S. R. Sharpe, Nucl.Phys. **B727**, 218 (2005), arXiv:hep-lat/0507006 [hep-lat] .
[9] N. H. Christ, C. Kim, and T. Yamazaki, Phys.Rev. **D72**, 114506 (2005), arXiv:hep-lat/0507009 [hep-lat] .
[10] M. Lage, U.-G. Meißner, and A. Rusetsky, Phys.Lett. **B681**, 439 (2009), arXiv:0905.0069 [hep-lat] .
[11] V. Bernard, M. Lage, U.-G. Meißner, and A. Rusetsky, JHEP **1101**, 019 (2011), arXiv:1010.6018 [hep-lat] .
[12] M. T. Hansen and S. R. Sharpe, Phys.Rev. **D86**, 016007 (2012), arXiv:1204.0826 [hep-lat] .
[13] R. A. Briceño and Z. Davoudi, Phys. Rev. D. 88, **094507**, 094507 (2013), arXiv:1204.1110 [hep-lat] .
[14] R. A. Briceño, Phys.Rev. **D89**, 074507 (2014), arXiv:1401.3312 [hep-lat] .
[15] J. J. Dudek, R. G. Edwards, and C. E. Thomas (Hadron Spectrum), Phys. Rev. **D87**, 034505 (2013), [Erratum: Phys. Rev.D90,no.9,099902(2014)], arXiv:1212.0830 [hep-ph] .
[16] C. B. Lang, D. Mohler, S. Prelovsek, and R. M. Woloshyn, Phys. Lett. **B750**, 17 (2015), arXiv:1501.01646 [hep-lat] .
[17] C. B. Lang, L. Leskovec, D. Mohler, S. Prelovsek, and R. M. Woloshyn, Phys. Rev. **D90**, 034510 (2014), arXiv:1403.8103 [hep-lat] .
[18] X. Feng, K. Jansen, and D. B. Renner, Phys. Rev. **D83**, 094505 (2011), arXiv:1011.5288 [hep-lat] .
[19] S. Prelovsek, L. Leskovec, C. B. Lang, and D. Mohler, Phys. Rev. **D88**, 054508 (2013), arXiv:1307.0736 [hep-lat] .
[20] S. Aoki *et al.* (CP-PACS), Phys. Rev. **D76**, 094506 (2007), arXiv:0708.3705 [hep-lat] .
[21] R. A. Briceno, J. J. Dudek, R. G. Edwards, and D. J. Wilson, Phys. Rev. Lett. **118**, 022002 (2017), arXiv:1607.05900 [hep-ph] .
[22] G. Moir, M. Peardon, S. M. Ryan, C. E. Thomas, and D. J. Wilson, JHEP **10**, 011 (2016), arXiv:1607.07093 [hep-lat] .
[23] J. J. Dudek, R. G. Edwards, and D. J. Wilson (Hadron Spectrum), Phys. Rev. **D93**, 094506 (2016), arXiv:1602.05122 [hep-ph] .
[24] D. J. Wilson, R. A. Briceño, J. J. Dudek, R. G. Edwards, and C. E. Thomas, Phys. Rev. **D92**, 094502 (2015), arXiv:1507.02599 [hep-ph] .
[25] D. J. Wilson, J. J. Dudek, R. G. Edwards, and C. E. Thomas, Phys. Rev. **D91**, 054008 (2015), arXiv:1411.2004 [hep-ph] .
[26] J. J. Dudek, R. G. Edwards, C. E. Thomas, and D. J. Wilson (Hadron Spectrum), Phys. Rev. Lett. **113**, 182001 (2014), arXiv:1406.4158 [hep-ph] .

[27] K. Polejaeva and A. Rusetsky, Eur.Phys.J. **A48**, 67 (2012), arXiv:1203.1241 [hep-lat] .
[28] R. A. Briceño and Z. Davoudi, Phys.Rev. **D87**, 094507 (2013), arXiv:1212.3398 [hep-lat] .
[29] M. T. Hansen and S. R. Sharpe, Phys.Rev. **D90**, 116003 (2014), arXiv:1408.5933 [hep-lat] .
[30] M. T. Hansen and S. R. Sharpe, Phys. Rev. **D92**, 114509 (2015), arXiv:1504.04248 [hep-lat] .
[31] M. T. Hansen and S. R. Sharpe, Phys. Rev. **D93**, 096006 (2016), arXiv:1602.00324 [hep-lat] .
[32] M. T. Hansen and S. R. Sharpe, (2016), arXiv:1609.04317 [hep-lat] .
[33] X. Liu, Chin. Sci. Bull. **59**, 3815 (2014), arXiv:1312.7408 [hep-ph] .
[34] H.-X. Chen, W. Chen, X. Liu, and S.-L. Zhu, Phys. Rept. **639**, 1 (2016), arXiv:1601.02092 [hep-ph] .
[35] J. J. Dudek, R. G. Edwards, and C. E. Thomas, Phys. Rev. **D86**, 034031 (2012), arXiv:1203.6041 [hep-ph] .
[36] P. Guo, J. Dudek, R. Edwards, and A. P. Szczepaniak, Phys. Rev. **D88**, 014501 (2013), arXiv:1211.0929 [hep-lat] .
[37] M. T. Hansen and S. R. Sharpe, Phys. Rev. **D93**, 014506 (2016), arXiv:1509.07929 [hep-lat] .
[38] G. Sterman, *An Introduction to Quantum Field Theory* (Cambridge University Press, 1993).